Antenna fabrication using 3D printing technologies

A Thesis Submitted to

The University of Kent at Canterbury

In the Subject of Electronic Engineering

For the Degree of

Masters of Science by Research

By

Ahmed Elibiary

September 2017

To my Family…

… especially to my parents who have given me undivided love and educated me my entire life and who continue to love and support me and my ambitions.

Abstract

This thesis focuses to explore the use of additive manufacturing (AM) techniques to fabricate various radio frequency (RF) devices. 3D printing, a term used for AM has evolved to the point where it is being introduced into various industries, one of these, discussed in this thesis is the fabrication of antennas for the aim to reduce manufacturing costs and time.

The aim is to investigate the performance and reliability of a modified low-cost 3D printer to print plastic and metal simultaneously. Accordingly, this thesis will explore the use of two specific AM technologies employed in the fabrication of several types of antennas and surfaces: i.e. the Fused Deposition Modelling (FDM) method and a pneumatic micro dispensing technique for the conductive ink. The variety of antenna and surfaces that will be fabricated using this technique are a collection of patch antennas, dipole antenna and frequency selective surfaces. In addition, this thesis will address the design, fabrication and testing of the stated antennas covering a range of frequencies and their applications. Nonetheless, it is worth mentioning that this paper is not solely limited to the analysis of the two previously mentioned methods but also other addictive manufacturing technologies will be used and discussed in this project to reach a better understanding of the antennas fabrication process.

In conclusion, the thesis aims to demonstrate the efficient performance and successful integration of economical 3D printing methods to design and produce antennas, which are one of the most important gateways to communication.

Ahmed Elibiary

September 2017

Acknowledgements

Throughout my long time spent at Kent undergoing my undergraduate and Masters degree, I was fortunate enough to meet many people that helped and supported me along this journey. For all of them I would like to give them my deepest thanks and cherish the vast memories shared together.

I would like to give my biggest thanks and gratitude towards my supervisor Dr. Benito Sanz for his consistent advice, guidance and continuous support throughout my research work. He has always pushed me to achieve my best throughout my study at Kent.

I would like to also thank Simon Jakes for all his help in the workshop and the countless hours trying to troubleshoot some of the fabricated antennas. His assistance with operation of the workshop equipment and the immense technical advice, which he always was available to offer. I would also like to thank him and Antonio Mendoza for their excellent assistance and guidance in the measurements of the various antennas.

I want to show my thanks to David Bird, Lee Winchester and Paolo Melgari at CPI for their patience and understanding and their valuable lessons throughout my training course on the various machines at CPI.

Publications from this work

1. **A. Elibiary**, W. Oakey, S. Jun, B. Sanz-Izquierdo, D.Bird, A.Mc.Clelland, " Fully 3D printed GPS Antenna using a Low-cost Open-source 3D Printer," accepted to in *Antennas & Propagation Conference (LAPC*), 2017 Loughborough, Nov. 2017.
2. S. Jun, **A. Elibiary**, B. Sanz-Izquierdo, “Study of Diversity WLAN Antennas for Fully 3D Printed Wrist Worn Applications”, in progress. 2017
3. B.Sanz-Izquierdo, **A. Elibiary**, S. Jun and E.A.Parker, "An approach to full 3D printing metallo-dielectric electromagnetic structures," Invited to *IEEE MTTS Int Microw. Symp.*, 2018

Table of Contents

Table of Figures

Abbreviations

3D	Three Dimensional
ABS	Acrilonitrile Butadiene Stirene
AM	Additive Manufacturing
CAD	Computer Assisted Drawing
CP	Circular Polarization
CPI	Centre for Process Innovations
CPW	Co-Planar Waveguide
dB	Decibels
DPAM	Direct Printing Additive Manufacturing
DC	Direct Current
FDM	Fused Deposition Modelling
FFF	Fused Filament Fabrication
GHz	Giga-Hertz
GPS	Geo Positioning Service
LBM	Laser Beam Melting
MHz	Mega-Hertz
mm	Millimetre
Ω-m	Ohms per metre
PC	Polycarbonate
PCB	Printed Circuit Board
PET	Polyethylene Terephthalate
PLA	Polylactic Acid
PTFE	Polytetrafluoroethylene

PVA	Polyvinyl Acetone
RF	Radio Frequency
RFID	Radio Frequency Identification
RHCP	Right Hand Circular Polarization
RP	Rapid Prototyping
S/m	Siemens per metre
SL	Stereolithography
SLA	Stereolithography Apparatus
SLS	Selective Laser Sintering
SMA	Subminiature version A
STL	Standard Tessellation Language
UV	Ultra-Violet

Chapter 1 – Introduction

1.1 Introduction

The realisation of a fully three-dimensional electronic circuit via the use of traditional fabrication techniques is complex, if not impossible, to achieve. The current techniques are limited to the use of a two-dimensional printed circuit board (PCB), which, along with being expensive, requires multiple processes which are time consuming. Furthermore, a copious and costly production is necessary for electronics to completely function. Nonetheless, thanks to the advancements of Additive Manufacturing (AM) or three-dimensional (3D) printing, these issues have been addressed and - for some - even completely overcome.

3D printing has allowed some parameters to be extended such as a higher range of freedom along conformal surfaces and material customisation (i.e. the ability of embedded circuitry). Before 3D printing, the latter was thought to be unfeasible when compared to more traditional methods. In other words, 3D printing has developed diverse ranges of optimization towards radio frequency (RF) component design and fabrication.

1.2 Three-dimensional printing Overview

The 3D printing is a term that originated from the process called rapid prototyping (RP) which is used to identify the task that quickly fabricates models using 3D computer aided design data (CAD). It is a form of AM, which was created as a way to represent and examine a design of an object before the production stage [1]. Previously, the manufacturing process used to be a subtractive process by using blocks of material and carving away until the desired shape was achieved, but this process was seen to be disadvantageous as it used expensive tools and wasted material in the process [1-2]. Over time, the capabilities to use additive manufacturing became apparent, with some calling that the 3D printing technologies to be the next big innovation of the generation. At the preliminary stages of the technique, the process was particularly expensive and yielded low resolution models but recently the technology has become more affordable and widely available to hobbyist and the public. The term now is widely known as 3D printing, which refers to the equipment used for AM.

The technology has progressed drastically to the extent that the electronic industry has become a big player in integrating 3D components into systems and sub-systems. This has therefore created a competition to manufacture quality products, which especially target the individual consumer along with providing a plethora of functionality. The market required for high-end technology and low-cost electronics, which therefore sparked the development of multifunctional, compact and lightweight devices to be created. This has therefore led to the significant advancements in 3D manufacturing technology for a range of applications, such as electronic sensors and mobile phones, or in aerospace [3-7].

The fabrication process has proved to be economically advantageous in several cases; being an additive manufacturing technique, it therefore drastically reduces the amount of wasted materials, when high value materials, helps reduce the total final cost. It has advanced significantly to the point where 3D fabricated structures can now be adapted to carry out electrical functionality, one area that has proven exciting potential is in the design of antenna structures which can provide an improved

performance as complex 3D structures that are once thought to be unobtainable can be easily fabricated [8-12]. The technology has also made it easier to manufacture millimetre wave passive components [13] there is also a move to the Terahertz band, where the proposal of a hollow core and plasmonic waveguides [14-16].

1.3 Antennas Overview

'Antennas are our electronic eyes and ears on the world, an essential, integral part of our civilisation.' [17]

There are many types of antennas that are used in today's world of communication, from connecting to deep space satellites down to the RFID tags on consumer products, with an increase in the amount of information that needs to be sent, the search for more accurate and cost-effective methods are never ending. Over the past few years, there has been a shift of attention in the communications industry to the development of planar antennas, which are favourable for a number of reasons. To begin with, they are compact and lightweight and can be manufactured at a much lower cost than waveguide-based antennas. Secondly, the planar nature of the antennas allows them to be used in applications where the size and shape are crucial, such as conformal printed antennas on airplanes. It also makes them ideal for large arrays and simplifies the interaction of additional electronics such as phase shifters and amplifiers. This thesis describes and tests a technique using a low-cost 3D printer to fabricate various antennas at RF / microwave frequencies.

1.4 Hypothesis and Aims

The general hypothesis of this thesis is to prove that electronic devices can be fabricated without using traditional expensive processes and that with the advancements in various 3D printing technologies, it can be used in the printing and prototyping of integrated antennas. As technology in our modern societies, plays a vital role in the everyday life and the global economy, there is always a drive for lowering costs.

The ability and the impact of 3D printing has been questioned by some to be able to affect the traditional process of antenna fabrication. The technology is ever-developing and is showing exciting potential and has with new materials and inks being developed constantly.

The aim of the research is to conduct a detailed investigation on various antennas for the fabrication using a variety of additive manufacturing techniques.

1.5 Thesis Outline

The thesis is split up into eight chapters;

In the beginning of the thesis, chapter one is an introduction which provides a brief introduction to the topic at hand. It has two sub heading; 3D printing and antennas covering a quick overview of both areas.

The second chapter entails the researched literature review of the topic. This chapter starts with a brief history of the origin of 3D printing and then covers in depth the various available technologies within the field of 3D printing. The discussion continues to talk about the research under taken in the field of 3D printing and the various companies that have made an impact. Also within this chapter is a detailed theoretical work of antennas and the various analysis characteristics of antennas.

The third chapter of this thesis provides a general theoretical background to antenna technology and electromagnetic theory. This gives some background information to what is covered throughout the thesis. Chapter starts with some basic electromagnetic theories, then several antenna types, and then the wide range of antenna analysis that is required.

In the fourth chapter of the thesis, the design, assembly and calibration of the FDM 3D printer used will be discussed. From the design and fabrication of the extra parts used, to the calibration and proposed improvements to the system will be detailed. This covers a detailed account of the firmware parameters and the integration with the second extruder

In the fifth chapter, the investigation of the designing and printing of Frequency Selective Surfaces (FSS) using a low-cost 3D printer. The substrate and the elements are fabricated using one machine, two different designed were proposed and tested.

Chapter 6 discusses the next antenna in the project, which is a GPS antenna printed on the FDM 3D printer. This chapter covers the design, fabrication and testing of the GPS antenna. Using the same technique as the previous chapter, the performance of the printer is put to the test.

In chapter 7, the design, fabrication and testing of a bracelet antenna will be reported. The simulations and the measured results are also reported. The antenna is a fully 3D printed dipole antenna used as wearable connected device, all the components of the antenna and the frame, including the feed lines and substrate are printed using the modified 3D printer. The antenna performance is then tested with and without the body, along with being tested against a more expensive fabrication process.

In the last chapter, the final antenna is proposed, which is another wearable antenna. This type of antenna is supposed to be placed on the human nail. Due to it being at a higher frequency, the antenna was fabricated using the Aerosol Jet printer available at Centre of Process (CPI). The simulations and measured results are included and discussed.

References

[1] A. Savini and G. G. Savini, "A short history of 3D printing, a technological revolution just started," 2015 ICOHTEC/*IEEE International History of High-Technologies* and their Socio-Cultural Contexts Conference (HISTELCON), Tel-Aviv, 2015, pp. 1-8, 2015

[2] Y. Zhou, H. Chen, Y. Tang, S. Gopinath, X. Xu and Y. F. Zhao, "Simulation and optimization framework for additive manufacturing processes," Proceedings of the 2014 International Conference on Innovative Design and Manufacturing (ICIDM), Montreal, QC, 2014, pp. 34-40, 2014

[3] S. Leigh, R. Bradley, C. Purssell, D. Billson and D. Hutchins, 'A Simple, Low-Cost Conductive Composite Material for 3D Printing of Electronic Sensors', Research article, 2012

[4] J. Muth, D. Vogt and R. Truby, 'Embedded 3D Printing of Strain Sensors within Highly Stretchable Elastomers', Advanced Materials, Vol. 26, 2014

[5] G. Whyte, 'Antennas for Wireless Sensor Network Applications', thesis for Doctor of Philosophy, 2008, University of Glasgow

[6] Sarik, John, et al 'Combining 3D printing and printable electronics', Proceedings of TEI, 2012

[7] Ready, Steven, et al, '3D printed Electronics', NIP and Digital Fabrication Conference. Vol 2013. No 1. Society for Imaging Science and technology, 2013

[8] O. S. Kim, "Rapid Prototyping of Electrically Small Spherical Wire Antennas," in *IEEE Transactions on Antennas and Propagation*, vol. 62, no. 7, pp. 3839-3842, July 2014

[9] J. Floch, B. Jaafari and A. Ahmed, 'New Compact Broadband GSM/UMTS/LTE Antenna Realised by 3D printing' IETR, April 2015

[10] M. Liang, C. Shemely, et al, '3D printed microwave Patch Antenna via Fused Deposition Method and Ultrasonic Wire Mesh Embedding Technique', *IEEE Antennas and Propagation*, Vol. 14, 2015

[11] E. Kohler, S. Rahiminejad and P. Enoksson, 'Evaluation of 3D printed materials used to print WR10 horn antennas', Chalmers University of Technology, Vol 757, 2016

[12] A. Angrish, "A critical analysis of additive manufacturing technologies for aerospace applications," *2014 IEEE Aerospace Conference*, Big Sky, MT, 2014, pp. 1-6.

[13] M. D'Auria, "Low cost fabrication processing for microwave and millimetre-wave passive components" Electrical and electronic engineering in Imperial College London, October 2015

[14] N. Yudasari, D. Vogt, J. Anthony and R. Leonhardt, "Hollow core terahertz waveguide fabricated using a 3D printer," 2014 39th International Conference on Infrared, Millimeter, and Terahertz waves (IRMMW-THz), Tucson, AZ, pp. 1-2, 2014

[15] M. D'Auria et al., "3-D Printed Metal-Pipe Rectangular Waveguides," in IEEE Transactions on Components, Packaging and Manufacturing Technology, vol. 5, no. 9, pp. 1339-1349, Sept. 2015

[16] S. Pandey, B. Gupta and A. Nahata, "Complex geometry plasmonic terahertz waveguides created via 3D printing," CLEO: 2013, San Jose, CA, pp. 1-2, 2013

[17] J. D. Kraus and R. J. Marhefka, "Antennas for All Applications", McGraw-Hill, 2002

Chapter 2 – Literature Review

2.1 3D printing Technologies

Rolling back to the 1980's, a breakthrough technology was officially announced; the first account of a 3D printed model was published by Dr Hideo Kodama in the Nagoya Municipal Industrial Research Institute [1]. The first model was using a photopolymer technology which cured a photopolymer material when exposed to a UV light which later on helped develop a technique known as Stereolithography.

Many years later, there are now a wide variety of 3D printers available on the market with different technologies, although they all share the same principle for building or constructing the model, by adding layer upon layer. 3D printing technologies are ever-growing and each have specific strengths and weaknesses discussed throughout the chapter. The key technologies of various 3D printing techniques are discussed, such as; FDM, SLA, SLS, Aerosol-jet, DPAM, SLM and LBM.

Fused Deposition Modelling (FDM)

One of the technologies out in the market is called Fused Deposition Modelling (FDM) or also known as Fused Filament Fabrication (FFF), it is the most common and populous type of 3D printing method. FDM is a process that uses a continuous

filament of a thermoplastic material, which is melted and layered on top of each other creating strong functional parts [3]. The plastic is pushed through to a heated chamber block with an inner diameter that is around the same size as the filament which melts the filament to a useable temperature, the heated filament is then forced out through a heated nozzle which has a much smaller diameter. The material is extruded onto a room temperature or heated platform while moving to the correct X/Y/Z position. The resolution and surface finish are a compromise when compared to other types like Stereolithography (SL). With a majority of FDM printers being open-source, it allows makers and engineers to modify, experiment and improve the overall mechanical design and performance of the machine.

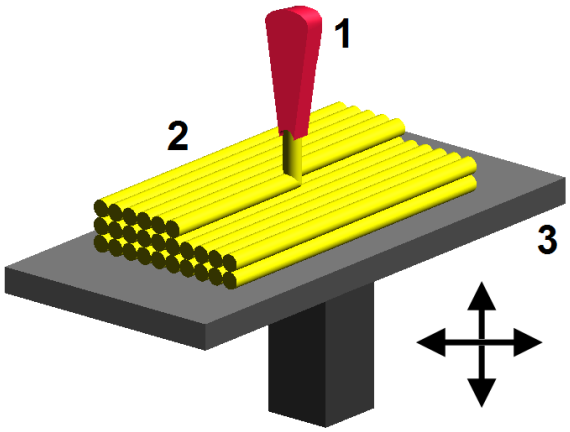

Figure 2-1 Overview of the process of a FDM machine [2]

FDM printing process starts with a 3D computer model which is exported as an industry standard format called Standard Tessellation Language (STL) file, which is a collection of triangles defining the surface of the solid. The STL is then loaded into a slicing software, which is a process that breaks the solid model into horizontal layers. Within each of the layers there is a collection of co-ordinates or set of paths that the head of the printer will follow, these set of instructions are saved as a G-code file. The slicing software controls several variables within the models' characteristics, first the slicer generates the outlines of the model, which controls the surface roughness. Significant amount of time and material can be saved if the outline height is increased. Then generates the infill patterns, which controls the dielectric constant and loss tangent.

Within the 3D printing industry, there are a wide array of different types of materials that are used to print with. FDM printers use thermoplastics as their choice of material, new thermoplastics materials are constantly being discovered and used in filament form for FDM. Within the thermoplastics section, there are several types of plastics that are available and each have different properties and characteristics to suit specific applications. Several factors can influence which type of plastic to choose; the extrusion process, the cost and the application. The most common types are listed below, where most of them have a lower microwave loss compared to the materials used in other printing technologies;

- Polylactic acid (PLA)
- Acrylonitrile butadiene styrene (ABS)
- Polycarbonate (PC)
- Polyvinyl acetate (PVA)
- Aliphatic polyamides (Nylon)
- Polyethylene terephthalate (PET)

The printing nature of FDM objects does not allow the model to come out smooth and accurate. It is known that FDM 3D printing produces a rougher surface finish than to other 3D printing techniques such as SL or DPAM.

Stereolithography Apparatus (SLA)

The next additive manufacturing technique is Stereolithography Apparatus (SLA or SL) which is the next popular method of consumer printing after FDM, even though it was the first technique of additive manufacturing introduced back in the 1980s. Stereolithography uses a light source to cure a resin when it is shunned upon; a computer controlled laser draws the outline of the model onto a liquid resin where it cures it. The model is lowered into the resin and the next layer is drawn, this is repeated until the model is finished. This technique offers the best / highest level of resolution and surface finish as well as material transparency.

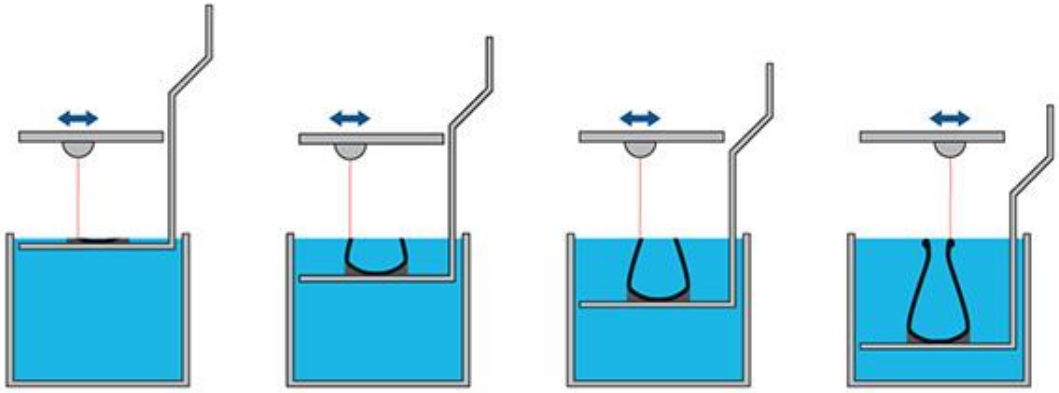

Figure 2-2 Overview of the process of SLA [4]

There are a variety of UV-curable resins giving distinctive characteristics and mechanical properties; there are basic resins that include opaque and transparent, resins that have tensile strength and hardness along with ductile resins for resiliency. As the resins have a low viscosity, the layers must be very thin and therefore the printing time is much greater than to a FDM process. Main manufactures in this field of additive manufacturing include and not limited to; 3D systems, Formlabs, DWS, XYZ Printing and Autodesk.

Selective Laser Sintering (SLS)

Selective Laser Sintering (SLS) is similar to SLA but the key difference is that instead of using a liquid resin this type of printer uses powdered material. A laser is used to sinter selected areas of the powder to form layers of granules, which join to form a solid structure. the object is fully printed, it is left to cool and air is used to remove the surrounding powder. There are wide variety of powdered materials used in SLS from nylon, glass, plastic, ceramics and even metal.

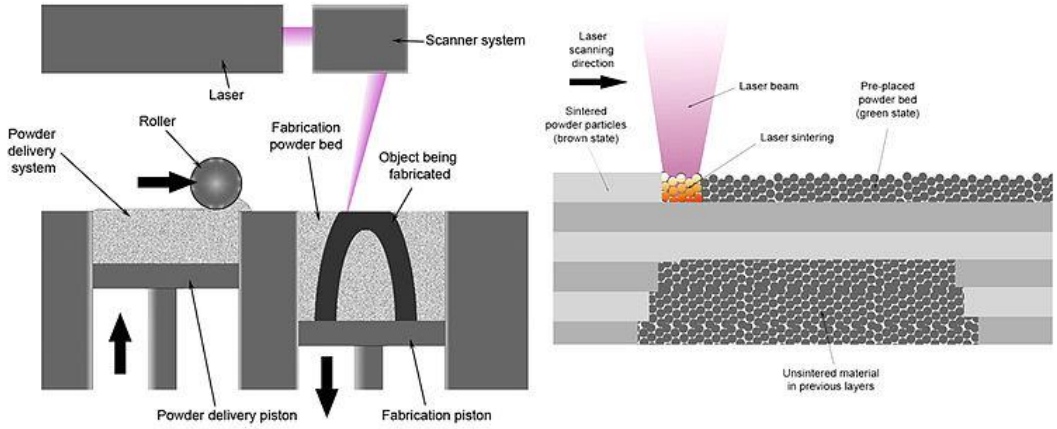

Figure 2-3 Overview of the process of SLA printing [5]

The resolution of this technology is not only determined by the size of the laser spot but also from the powder particle dimensions, this often results to low surface finish and visible roughness. The advantage of this technology is that the printed model will never require support for suspended parts because of the un-sintered powder surrounding the model. This then opens the chances of models with higher geometrical complexity and models with multiple structures (i.e. hinges, bearings and joints) where it was otherwise not possible. SLS is widely used for product development and rapid prototyping in a wide range of commercial industries where large items are needed.

Aerosol jet

A different type of additive manufacturing technique is Aerosol jet printing. This form of printing is a non-contact micro dispensing technique, which allows the deposition of various functional materials such as particle inks and paste like fluids. The materials are dispensed onto a wide variety of substrates without convention adhesion equipment. The process requires the material to first be broken down into its particles to create a mist which is surrounded by a coaxial sheath of air flowing out of an orifice directed at the substrate; which creates features as small as 10 μm in size with a good stable adhesion.

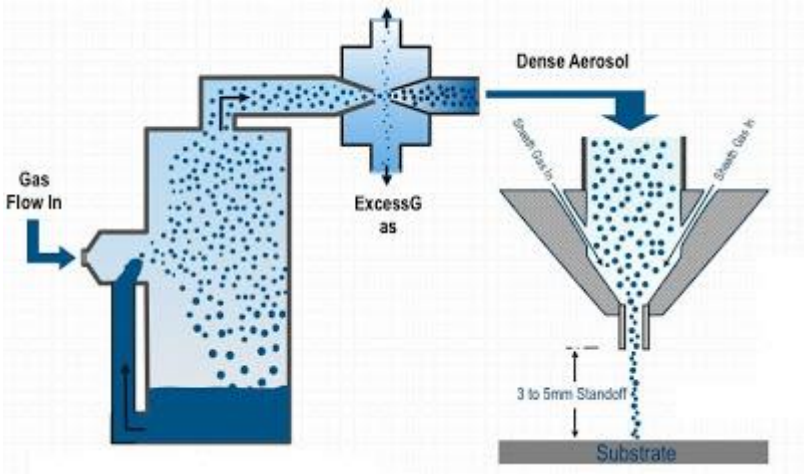

Figure 2-4 Overview of the aerosol jet printing [6]

This technique is especially used when accuracy and repeatability is targeted. On demand manufacturing is offered with the ability to produce patterns of conductive and resistive pastes. Micro dispensing companies include Optomec, nScrypt, Novacentrix, Envision Tech and Precision Valve and Automation.

With several different abilities presented by different techniques, the manufacturing industries have taken 3D printing to a whole new level. As the initial idea was to use it for creating a prototype of a model before it was manufactured to find out its functionality, however now the area of 3D printing has been developed to produce consumer end products. This jump in technology has opened up a vast spectrum of applications in a variety of industries.

2.2 3D printing in research

Over the years, electronic devices have continued to decrease in size approaching the limits of the silicon technology. While the evolution of 3D printing of circuits has evolved from concept to adoption, with some companies and researchers are experimenting with the limits of the innovative technology to take electronics to a new dimension. The advantages of seeking this industry can benefit many; engineering designers of printed circuit boards (PCBs) can attain faster prototypes in-house and have the ability to work in complex three

dimensions [3]. Moreover, this can save time and additional cost for the fabrication of boards that they do not use. 3D printing is not only capable of fabricating structurally functional parts, the technique can be integrated into several industries; currently there are several companies in the market that have proven the ability to print 3D print sensors, circuit boards and more.

Nano Dimension Ltd.

The company Nano Dimensions have been focusing on the research and development of the world 3D printing to print electronics. They have developed a printer with their proprietary conductive silver ink to print advanced multi-layer PCBs on multiple substrates. They are able to achieve this by developing a process using the inkjet technology for pico-liter deposition of silver and dielectric Nano inks allowing them to have ridged or flexible circuits.

Figure 2-5 Nano Dimensions electronics printer [7]

The DragonFly 2020 3D printer process uses two print heads which deposit a 3-micron height of the material at the exact location specified by the design file, the printer has a print area of 20 x 20 x 0.3cm with an accuracy of 0.001mm. The conductive ink used is called AgCite a nanoparticle material that has a conductivity up to 35,700,00 S/m and an antenna performance of 89% efficiency at 2 GHz and the

dielectric ink has a dielectric constant of 2.2 to 3.7 and a dielectric loss of 0.02 to 0.04.

The company is currently taking pre-orders for their printer and should go on sale at the end of Q2 of 2017 for between $50,000 to $100,000 which will classify it as an industrial printer.

Optomec

Another company working on printed electronics is Optomec, which have developed an aerosol jet technology with a Copper and Copper/Nickel inks to successfully print sensors and other electronics in various substrates such as airplane wings for stress analysis. It is one of the machines that are available at CPI (Centre for Process Innovation) which is the UK's national technology and innovation centre for the process and manufacturing industry. CPI collaborates with universities, SME's and large corporates to help overcome fabrication challenges and develop next generation products and processes by providing high-end facilities and expertise.

It is used to produce 3D printed electronics by dispensing a variety of commercially available conductive inks onto a variety of 2D and 3D substrates. This machine is not cheap and not available to the general public.

The advantage of using this technology for printed electronics is that it eliminates the need for hard tool photomasks, stencils and allows for easy and quick changes to be made with no extra time.

As the technique is non-contact with the substrates therefore it allows the printing on both 2D and 3D substrates; multi-level interconnects can be done by creating a dielectric material at the circuit cross over points which is possible because Aerosol Jet process supports multiple ink inputs therefore allowing materials to be switched or blended.

Figure 2-6 The aerosol printer from Optomec [8]

The Optomec machine has two distinct types of depositing ink techniques; through either the ultra-sonic bath Atomizer or the pneumatic Atomizer. These are determined by the type of ink that is required; with thicker, denser and opaque inks the ultrasonic Atomizer is not possible and therefore the pneumatic Atomizer is used.

The printing process begins by creating a mist of ink in the Atomizer container; the mist is guided through a tubing to the depositing head which is then focused into a thin nozzle. The material is jetted on as narrow as 25 microns and a thickness ranging from 60 to 250 nanometres.

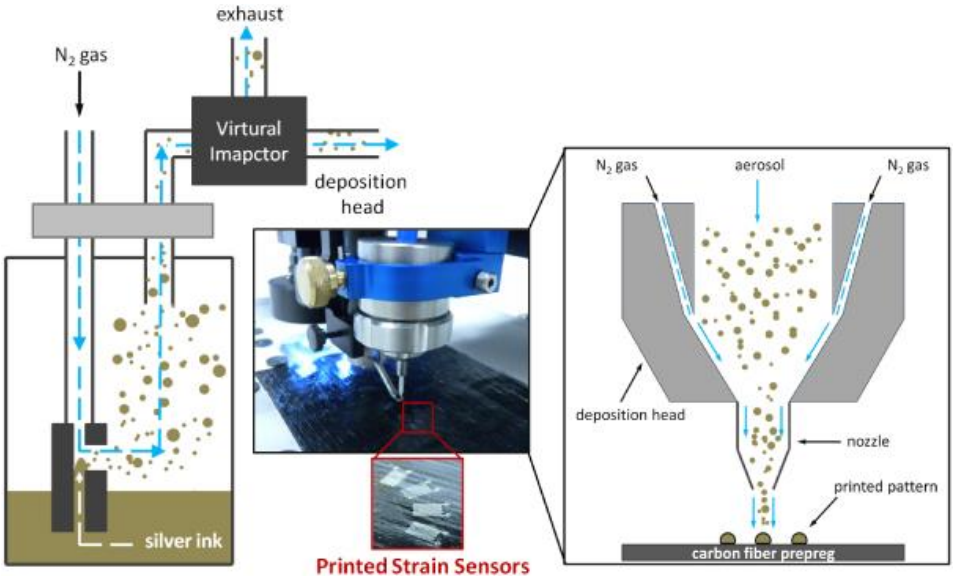

Figure 2-7 The Aerosol printing process overview [9]

Once the print process has started, the ink in the depositing head is constantly flowing without any interruption therefore to make proper designs the ink must be able to stop and start. The machine then has a miniaturised spoon connected to a stepper motor which moves back and forth beneath the deposition head, collecting the ink between travel movements. The spoon is cleaned once it gets full, as the depositing head only jets picolitres of material, this can be done after a few prints.

The Optomec machine is typically used as the first segment of a two-step manufacturing process for printed electronics. To complete the process the printed material needs to be cured to obtain full functionality which is done in an oven, there are variations in the temperature which depend on the type of ink used but typically the material is heated to 170 °C for an hour.

PulseForge Machine

Novacentrix is the company that manufactures the Pulse Forge machine, a machine that is used as a photonic curing technique. The Pulseforge can heat conductive inks and thin films in split seconds without over heating the underlying or adjacent substrates. This is useful when using heat sensitive substrates and inks that require heat to be cured, it is a critical process in the manufacture of printed electronics as very little energy is needed to cure the inks to an elevated temperature.

Figure 2-8 PulseForge machine from Novacentrix [10]

The Pulseforge tool uses a specialist computer which controls a high-intensity pulsed light technology which heat up the ink in a matter of milliseconds. The light pulses can vary in lengths from 25 to 100000 microseconds depending on the substrate and thickness of ink, it also has the ability to sinter features in excess of 20 microns thick.

The Pulseforge is usually the best curing technique used with materials that are printed using the screen printing process. Screen printing is a process that consists of a woven mesh screen with a pattern that is imprinted onto a substrate. The specific pattern is aligned and then placed onto the substrate which is secured by a vacuum. The ink or paste is placed onto the mesh and by using a certain squeegee, it is squeezed through onto the substrate. The thickness, specific feature sizes and other parameters are all determined beforehand when placing the mesh template. Factors such as the squeegee material, speed, the angle and the pressure can influence the type of pattern deposited onto the substrate. The manufacturing process require great expertise to achieve good quality repeatable results.

Botfactory

Botfactory is a company with another approach, where it will offer interchangeable heads that have various purposes depending on the application. A New York City start-up has developed a printer that has a head for printing out a non-conductive material, a head for printing the conductive material and one that can grab and place various electronic components. This technique shows that a 3D printer can become much more than depositing plastic onto a platform.

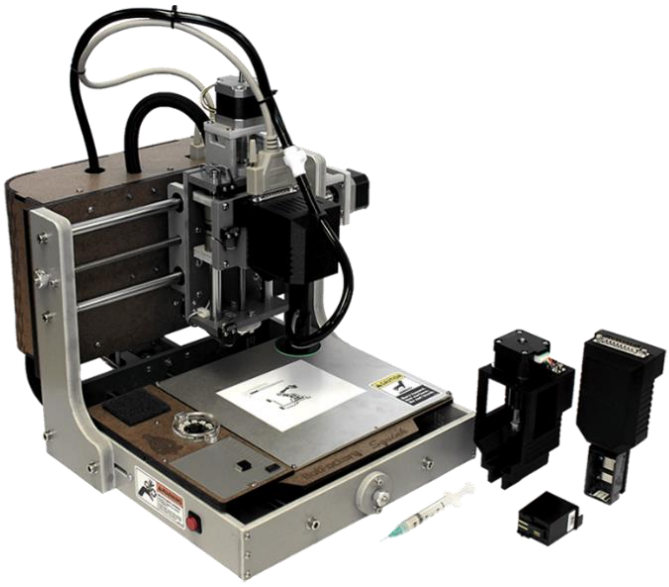

Figure 2-9 BotFactory printer [11]

The printer is equipped with a camera that can register the orientation of the electronic component so that it can adjust accordingly when placing it onto the circuit.

Voxel8

The closest machine to a consumer grade low-cost 3D electronics printer is the work done by a company called Voxel8. Voxel8 started in 2013 which arose from the Lewis Lab at Harvard, where they have researched and developed the first multi-material 3D electronics printer based on the FDM technology. The developed printer is a closed source dual extruder machine; one extruder for the plastic filament and the other for the silver ink.

The printer has a build volume of 150 x 150 x 100 mm, with a maximum layer resolution of 200 microns. The major innovative aspect of the printer is the silver ink that is being used, they have developed a conductive silver ink that can be dispensed in room temperature and cures within 30 minutes without any post process. The printer also includes a pneumatic direct write dispenser which is connected to their conductive silver ink. The silver ink is dispensed through a thin nozzle, the diameter of this nozzle can be changed depending on the application and the print process. The ink has a resistivity rating of less than 5.00 × 10-7 Ω-m which makes it highly conductive.

The printer was available for pre-order with a price tag of $9000 but then got cancelled for unknown reasons. The silver ink that was developed for the printer is still available for purchase along with its accessories.

Figure 2-10 Printer from Voxel8 [12]

2.3 3D Printed Antennas

This thesis is the focus of taking additive manufacturing and showing its integration into the fabrication of electronic devices; especially the focus on the various antenna elements. Over the past few years, the interest for the expanding the capabilities of 3D printing has been growing which has the fabrication of various 3D elements gaining better functionality and new integration. When thinking about the current electronic hand-held devices and how they have evolved into smaller, compact and light weight devices, we tend to think about their manufacturing technique. Within a typical electronic system, the fabrication of the internal components is done individually and separately from the housing of the overall internal system. Although, with the current strides in the 3D printing industry, distinct processes that were once done separately can now be integrated together allowing for the design of complex and high-density systems.

For more than 30 years, researchers have worked on the development to fabricate smaller circuitry for greater efficiency. Currently the most common technique employed is the microfabrication technique, which is a combination of several processes in a specific order. Processes include lithography, the deposition of materials, layering a pattern and finally the etching process. Within each of the processes, there are developments that have been made to suit specific devices. For example, the microfluidic, microsensors and micromechanical systems (MEMS) for integrated circuits have been developed for the focus to fabricate smaller devices within microfabrication [13-16]. As this has given the ability to create smaller devices, it has although developed a need for extra precision ability by the person and technology in place for the fabrication, this has therefore increased the time in the fabrication process [17].

Over the years, there has been some success with the ability to 3D print components and electronics, with the vast number of different additive manufacturing techniques and materials, the method has become very sophisticated. It can be seen in the primal stages of 3D printing and when the idea to integrate 3D printing and electronics emerged, such as a ‘Wire Embedding 3D Printer’ [18]. With the idea to attempt to

make a ‘new approach to manufacturing hybrid wire and plastic parts’ [18], the author develops and tests a FDM 3D printer with a wire printing mechanism in order to create conductive models. While the project did not work, it was an innovative way to integrate electronics with 3D printing. Wireless communication technology plays a significant role in modern electronics and any new fabrication of electronics such as 3D printing will have to handle microwave electronics. The building blocks of any microwave electronics is the transmission lines [19-30] The advantages to use 3D printing can include the time saving aspect and the ability to produce complex designs that were not able using standard fabrication techniques. There have been researchers that have demonstrated the feasibility by combining 3D printing techniques with printed electronics [31]. While this does focus on the 3D fabrication of electronic structures in the dc and low frequencies, there are some other research conducted in microwave devices such as with a copper electroless plated device [32 - 33]. In which, demonstrated the performance of using a new 3D printing technique, stereolithography model to a traditional method such as electroplating. Variations of stereolithography 3D printing have been researched with the intent of microwave antennas with ceramic SL [34 – 41]. The research expands as the demand increases for the wider capabilities ranging from various antennas in mobile phones to keyless entry for automotive [42] and RFID [43].

Through the increased interest in 3D printing for microwave circuits and antennas, the microwave frequency characterisation of various 3D printing materials is vital for the design and fabrication of antennas. Cadman, Zhang and Vardaxoglou [44] conducted a study on the performance in RF with 3D printable FDM materials. The testing of dielectric constants and loss tangent of various FDM materials over the frequency range of 0.1 -11 GHz. The two main materials in FDM are PLA and ABS, and [44] concluded that PLA had a dielectric constant of 2.72 and a tan δ of 0.008 at 2.4GHz while ABS had a dielectric constant of around 4.4 and tan δ of 0.007. but another study by [45] stated that the dielectric constant of PLA was around 3.5. Whereas another study by Nakatsuka [46] states that the dielectric constant of PLA is 3.1, therefore it is clear that the true value of the dielectric constant is not fully determined (Mohd in [47] mentioned that the dielectric constant is between 2.4 –

2.6). Clearly more research has to be done in the characterisation but within this thesis, the dielectric constant of PLA is assumed to be 2.4

A variety of antennas have been fabricated using various techniques and materials, [48] has fabricated a fully 3D printed 2.4 GHz Bluetooth/WiFi antenna, through the technique of using a FDM printer from Stratasys to fabricate the substrate and then printed the antenna using a separate nScript Smart Pump with CB028 conductive paste. The model had to be cured in the oven for full functionality, but the technique yielded good results compared to the simulations. The selected method is expensive and due to the sensitivity of the conductive ink dispensed with the Smart Pump it is affected by the surface roughness of the FDM printed model. Another example of printed antennas using an FDM technique is [47] which also used a Stratasys FDM printer to print various patch and Vivaldi antennas. The antenna in this method was printed using a Deton Vacuum sputtering system which coated it with Titanium and Copper. Mohd proved that high gain wide band Vivialdi antennas can be fabricated using 3D printing, although it had a high resistance. It was also mentioned that if the printed model had better surface roughness and metal adhesion to the printed material, it would have helped improve the results.

The fabrication of 3D antennas using 3D printing equipment are comparable in performance to similar transmission lines fabricated using traditional methods but using less expensive materials. The two main 3D printing technologies that are seen to be most accessible and aim to be inexpensive for the printing of dielectrics, which are; fused deposition modelling (FDM) and stereolithography apparatus (SLA). There have been a couple of examples where both of these technologies are used to fabricate antennas and RF devices. John has described in [49] in using a FDM machine with a mounted airbrush system, to produce printable electronics through one platform. The Iwata airbrush is mounted vertically parallel to the extruder heads and is operated through a servo motor.

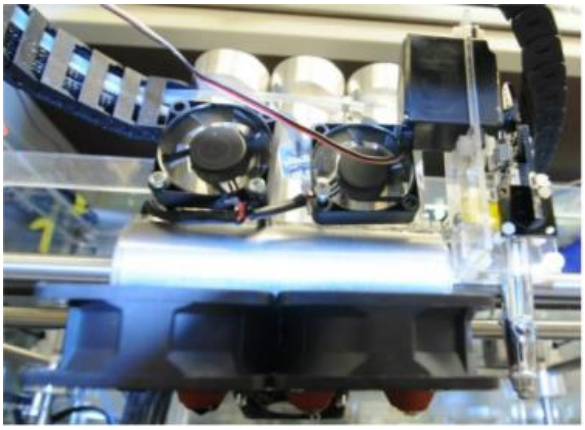

Figure 2-11 An FDM carriage with two heads and an airbrush

The issue with this setup is the available inks that is compatible with the airbrush and their conductivity levels. While the results were not very impressive, it showed the possibility of printable complex structures with embedded three-dimensional conductive traces.

Another example is the fabrication of horn antennas, traditional fabrication of horn antennas is done by a cut out a copper template or other conductive material and then building them in a specific orientation and dimension for a required application. The horn antenna is formed when the waveguide is joined to the front end of the antenna. This process could also be fabricated using a 3D printing technology, [50] investigates the performance and the functionality of a horn antenna fabricated using a FDM printer to be very similar to the traditional fabrication method, the materials used is an electrically conductive ABS filament and a PLA filament containing 35% copper.

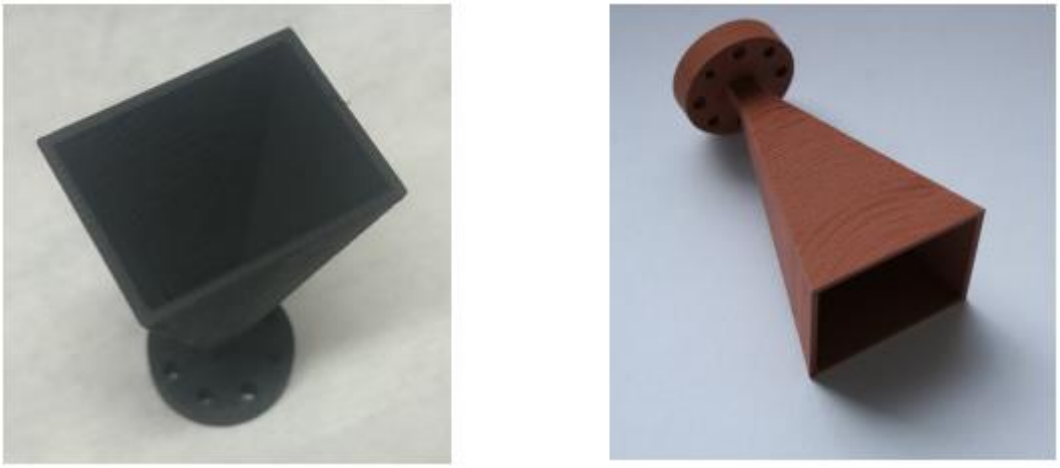

(a) (b)

Figure 2-12 A 3D printed horn antenna using (a) electrically conductive ABS and (b) copper PLA

The issues with this technique is the quality of the surface finish and the difficulty of printing such materials. The quality limitations are linked to the thermal creep that occurs during the printing process and the minimum required filament feed rate. These materials have a limited number of applications due to their low conductivity and layer adhesion characteristics.

A different approach, is to use a separate two-step process, where the 3D printer prints out the dielectric and then a conductive component is applied to it. In [51], a non-planar EBG substrate was fabricated using PLA filament and then silver-loaded conductive ink was evenly spread on the substrate by hand. The results showed that this particular setup yielded good antenna matching and gain improvements. The silver ink that was used had to be put in an oven for about 15 minutes to be fully cured which was an extra process in the fabrication; the model was not damaged because it was left at 90°, which is about the thermal limit of PLA plastic.

Figure 2-13 3D printed EBG configuration and stencil [51]

FSS structures were also investigated using 3D printing, where [52] used an FDM printer to print a 3D model of both a triple cross element and a tetrahedral caltrop with dissimilar materials and then two coats of silver ink were applied to the models by hand. These elements were then mounted onto a fibreboard support approximately 2 mm thick to give support strength. The first element was printed using a plaster material which is typically used in building and operated at about 5.5 GHz and had low angular stability. Whereas the second was printed using an inexpensive PLA filament which operated at 2.5 GHz and offered good stability to various angles. The minor differences seen in the results can be blamed on the resolution of the 3D printed models and errors from the non-uniform coating of the silver ink.

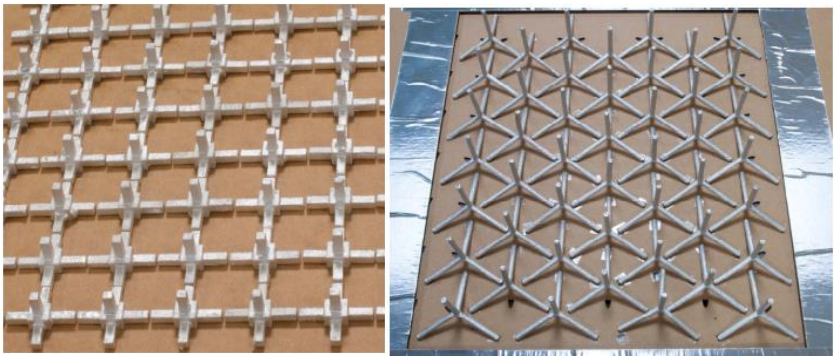

Figure 2-14 FSS printed structures, (a) triple cross, (b) Caltrop [52]

One of the problems with FDM substrates is the surface roughness of the printed models which therefore limits the metallic layers to thicker metallic materials. On the other hand, another type of low cost printing is SLA, which provide smoother surfaces which can be seen as an advantage when printing with other metallic deposition techniques. In [53], which uses an SLA printer to print out the substrate of a patch antenna. The metallic patch is not printed out by layering down silver ink by hand but printed out using an inkjet printer that prints out silver nitrate. A Form 1+ SLA printer is used to print out the substrate that has a surface roughness of 206 nm, and then the substrate is put into an Argentum Cartesian Co. printer to print the patch antenna, the antenna is shown in figure 2-15. The patch required 25 layers of silver nitrate to give a resistivity of $3 \times 10^{-7} \Omega m$ then was grounded using a square brass plate on the backside. The antenna yielded satisfactory results with good circular polarization but this fabrication process required two separate machines to finish the

antenna. When two machines are required, more errors that are susceptible are caused, along with the calibration in the alignment of the machines and not to mention that it requires 25 layers of material to yield acceptable conductivity.

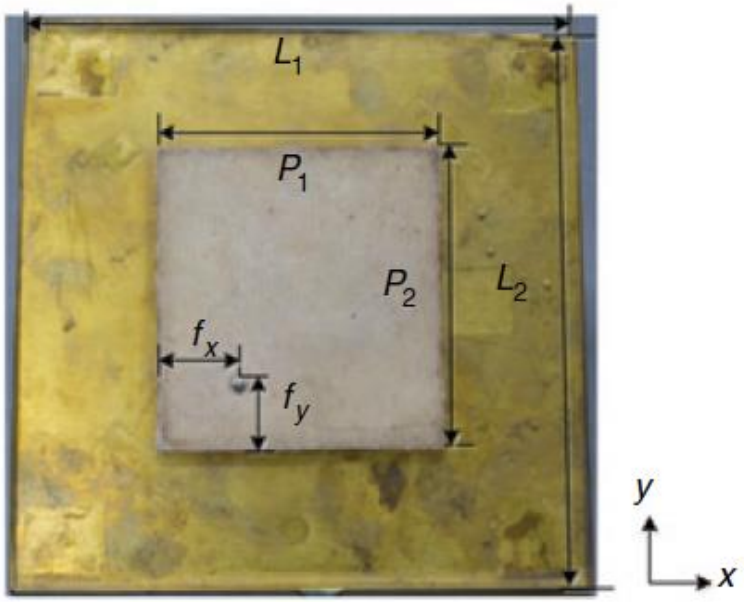

Figure 2-15 Patch antenna printed using SLA and an inkjet printer [53]

Although it can be seen in these early results of the benefit of 3D printing in the replacement of the traditional fabrication processes, there is a significant potential in the use of various technologies in the 3D printing industry to design novel antenna structures. This possibility of innovative designs could eventually improve the antenna performance and possibly create new deigns that were once thought to be too difficult to fabricate through conventional approaches. To truly fabricate a low cost fully 3D printable RF component a combination of low cost techniques must be integrated into one machine.

2.4 Conclusion of literature review

Recently there has been an increase in attention and development of 3D printing technologies within the research and manufacturing industries. With the ability to create complex structures easily and a decrease in manufacturing costs, it becomes a valuable tool for the development of new products and services. 3D printing has been around since the late 1980s, with the development of stereolithographic apparatus, and since then 3D printing has been mainly used for the development of artistic and non-functional models. This has put a limit on the capabilities of the materials used and the overall usability, and it is only recently possible to find materials to stretch these capabilities into different fields. However, until now there is little-to-none conductive materials commercially available.

References

[1] [online] Available at: https://redshift.autodesk.com/history-of-3d-printing/ [Accessed 30 Jul. 2017].

[2] [online] Available at: https://en.wikipedia.org/wiki/Fusedfilamentfabrication [Accessed 30 Jul. 2017].

[3] Church, K., Tsang, H., Rodriguez, R., Defembaugh, P. and Rumpf, R. (2013). Printed Circuit Structures: The Evolution of Printed Circuit Boards. The PCB Magazine, pp.12-26, 2013

[4] [online] Available at: https://i.materialise.com/blog/an-intro-to-our-3d-printing-technologies-stereolithography/ [Accessed 30 Apr. 2017].

[5] [online] Available at: https://en.wikipedia.org/wiki/Selective_laser_sintering [Accessed 30 Jul. 2017].

[6] [online] Available at: http://nextgenlog.blogspot.co.uk/2008/07/materials-nano-inks-could-advance.html [Accessed 30 Jul. 2017].

[7] [online] Available at: http://www.nano-di.com/) [Accessed 30 Jul. 2017].

[8] [online] Available at: https://www.novacentrix.com/index.php [Accessed 30 Jul. 2017].

[9] Zhao, D., Liu, T., Zhang, M., Liang, R. and Wang, B. (2012). Fabrication and characterization of aerosol-jet printed strain sensors for multifunctional composite structures. Smart Materials and Structures, [online] 21(11), p.115008. Available at: http://iopscience.iop.org/article/10.1088/0964-1726/21/11/115008/pdf.

[10] [online] Available at: https://www.optomec.com/printed-electronics/aerosol-jet-printers/aerosol-jet-5x-system [Accessed 30 Jul. 2017].

[11] Grunewald, S. (2017). BotFactory COO Explains How Shapeways Helped Them Suck Better. [online] 3DPrint.com | The Voice of 3D Printing / Additive Manufacturing. Available at: https://3dprint.com/113004/botfactory-shapeways-squink [Accessed 30 Jul. 2017].

[12] [online] Available at: https://techcrunch.com/2015/07/24/voxel8-raises-12m-to-bring-its-3d-electronics-printers-to-market/ [Accessed 30 Jul. 2017].

[13] Brown, E.R., "RF-MEMS switches for reconfigurable integrated circuits," Microwave Theory and Techniques, *IEEE Transactions* on, vol.46, no.11, pp.1868,1880, Nov 1998

[14] Becker, Holger, and Claudia Gärtner. "Polymer microfabrication methods for microfluidic analytical applications." Electrophoresis 21, no. 1, pp 12-26. 2000

[15] Guiseppi - Elie, Anthony, Norman F. Sheppard, Sean Brahim, and Dyer Narinesingh. "Enzyme microgels in packed- bed bioreactors with downstream amperometric detection using microfabricated interdigitated microsensor electrode arrays." Biotechnology and bioengineering 75, no. 4, pp 475-484, 2001

[16] Waits, C. M., Brian Morgan, M. Kastantin, and R. Ghodssi. "Microfabrication of 3D silicon MEMS structures using gray-scale lithography and deep reactive ion etching." Sensors and Actuators A: Physical 119, no. 1 pp 245-253, 2005

[17] Voldman, Joel, Martha L. Gray, and Martin A. Schmidt. "Microfabrication in biology and medicine." Annual review of biomedical engineering 1, no. 1 pp 401-425, 1999

[18] Bayless, J., Chen, M., Dai, B., "Wire Embedding 3D printer", University of British Columbia, 2010

[19] Agilent Technologies, "Applying the 8510 TRL Calibration for Non-Coaxial Measurements," Product Note 8510-8A, May 4, 2001.

[20] Inder J. Bahl, D.K. Trivedi, "A Designer's Guide to Microstrip Line," Microwaves, 1977.

[21] P. Barnwell, M.P. O'Neill and C. Free, "Integrated microwave structures using an advanced thick-film technology," 1999 IEEE Radio and Wireless Conference (RAWCON), pp.259-262, 1999

[22] M.C. Bailey, and M.D. Despande, "Characteristic Impedance of Microstrip Lines,", Nov. 1989.

[23] T. Bjorninen, "Performance Comparison of Silver paste and Copper Conductors for Microwave Applications," Microwaves, Antennas & Propagation (IET), vol.4, no.9, pp.1224-1231, Sep. 2010.

[24] S. Canaragiu, “Analysis of shielded microstrip lines by finite-difference method,” Proceedings of the 6th *IEEE International Conference on Electronics*, Circuits and Systems (ICECS), vol.1, pp.565-567, 1999.

[25] E. J. Denlinger, “Losses of Microstrip Lines,” *IEEE Transactions*. on MTT, vol. 28, no 6, Jun. 1980.

[26] M.J. Degerstrom, B.K. Gilbert, E.S. Daniel, “Accurate Resistance, Inductance, Capacitance, and Conductance (RLCG) from Uniform Transmission Line Measurements,” Electrical Performance of Electronic Packaging, pp.77,80, Oct. 27 29, 2008.

[27] W.J. Getsinger, “Measurement and Modeling of the Apparent Characteristic Impedance of Microstrip,” Microwave Theory and Techniques, *IEEE Transactions* on, vol.31, no.8, pp.624-632, Aug. 1983.

[28] E.O. Hammerstad, “Equations for Microstrip Circuit Design,” 5th European Microwave Conference, pp.268-272, Sep. 1-4, 1975.

[29] M.V. Schneider, "Microstrip lines for microwave integrated circuits," The Bell System Technical Journal, vol.48, no.5, pp.1421-1444, May-Jun. 1969.

[30] Dave Kirkby, “Finding the Characteristics of Arbitrary Transmission Lines,” Dec. 1996.

[31] Gutierrez, C. Denise, "Three-dimensional structural electronic integration for small satellite fabrication", *ETD Collection for University of Texas, El Paso*. AAI1512575, 2012

[32] Bosui Liu, Xun Gong and W. J. Chappell, "Layer-by-layer polymer stereolithography fabrication for three-dimensional RF components," *2004 IEEE MTT-S International Microwave Symposium Digest (IEEE Cat. No.04CH37535)*, 2004, pp. 481-484 Vol.2

[33] Yilei Huang, Xun Gong, S. Hajela and W. J. Chappell, "Layer-by-layer stereolithography of three-dimensional antennas," *2005 IEEE Antennas and Propagation Society International Symposium*, 2005, pp. 276-279 Vol. 1A.

[34] N. Delhote, D. Baillargeat, S. Verdeyme, C. Delage, and C. Chaput, “Ceramic layer-by-layer stereolithography for the manufacturing of 3-D millimeter-wave filters,” *IEEE Trans. Microw. Theory Tech.*, vol. 55, no. 3, pp. 548–554, Mar. 2007.

[35] N. T. Nguyen, N. Delhote, M. Ettorre, D. Baillargeat, L. Le Coq, and R. Sauleau, "Design and characterization of 60-GHz integrated lens antennas fabricated through ceramic stereolithography," *IEEE Trans. Antennas Propag*., vol. 58, no. 8, pp. 2757–2762, Aug. 2010.

[36] K. F. Brakora, J. Halloran, and K. Sarabandi, "Design of 3-D monolithic MMW antennas using ceramic stereolithography," *IEEE Trans. Antennas Propag*., vol. 55, no. 3, pp. 790–797, Mar. 2007.

[37] N. Delhote, D. Baillargeat, S. Verdeyme, C. Delage, C. Chaput, C. Duterte, Y. Abouliatim, and T. Chartier, "Electromagnetic band gap millimeter and sub-millimeter 3D resonators manufactured by ceramic stereolithography," in Proc. Asia-Pacific Microw. Conf. Dec, pp. 1–4, 2007

[38] M. L. Griffith and J. W. Halloran, "Freeform fabrication of ceramics via stereolithography," J. Amer. Ceram. Soc., vol. 79, no. 10, pp. 2601–2608, 1996.

[39] N. Delhote, D. Baillargeat, S. Verdeyme, C. Delage, and C. Chaput, "Innovative shielded high dielectric resonator made of alumina by layer-by-layer stereolithography," *IEEE Microw*. Wireless Compon. Lett., vol. 17, no. 6, pp. 433–435, Jun. 2007.

[40] N. Delhote, D. Baillargeat, S. Verdeyme, C. Delage, and C. Chaput, "Large experimental bandpass waveguide in 3D EBG woodpile manufactured by layer-by-layer ceramic stereolithography," in Proc. *IEEE/MTT-S Int. Microw*. Symp., Jun. 2007, pp. 1431–1434.

[41] N. Delhote, D. Baillargeat, S. Verdeyme, C. Delage, and C. Chaput, "Narrow Ka bandpass filters made of high permittivity ceramic by layerby-layer polymer stereolithography," in Proc. 36th Eur. Microw. Conf., Sep. 2006, pp. 510–513

[42] [Online]. Available: http://www.makerbot.com/blog/tag/key-fob/ [Accessed 30 Jul. 2017]

[43] A. Dziedzic and P. Slobodzian. (2011, Apr.). "Modern microelectronic technologies in fabrication of RFID tags," Radioeng. Proc. Czech Slovak Tech. Univ. [Online]. Available:

http://www.radioeng.cz/fulltexts/2011/11_01_187 _193.pdf [Accessed 30 Jul. 2017]

[44] D. Cadman, S. Zhang and Y. Vardaxoglou, "Fused deposition modelling for microwave circuits & antennas," *2016 International Symposium on Antennas and Propagation (ISAP)*, Okinawa, 2016, pp. 418-419.

[45] E. Huber, M. Mirzaee, J. Bjorgaard, M. Hoyack, S. Noghanian and I. Chang, "Dielectric property measurement of PLA," 2016 IEEE International Conference on Electro Information Technology (EIT), Grand Forks, ND, 2016, pp. 0788-0792.

[46] T. Nakatsuka, “Polylactic Acid Coated Cable”, 2011 Fujikura Technical Review, 2011

[47] M. I. M. Ghazali, E. Gutierrez, J. C. Myers, A. Kaur, B. Wright and P. Chahal, "Affordable 3D printed microwave antennas," 2015 IEEE 65th Electronic Components and Technology Conference (ECTC), San Diego, CA, 2015, pp. 240-246.

[48] P. Deffenbaugh, “3D printed electromagnetic transmission and electronic structures fabricated on a single platform using advanced process integration techniques”, 2014 Thesis (Ph.D.), The University of Texas at El Paso, Vol. 76-01(E), 2014

[49] Sarik, John, et al., “Combining 3D printing and printable electronics”, Proceedings of TEI, 2012

[50] E. Köhler at al., “Evaluation of 3D printed materials used to print WR10 horn antennas”, Journal of Physics: Conference Series 757 (2016) 012026

[51] S. Jun, B. Sanz-Izquierdo and E. A. Parker, "3D printing technique for the development of non-planar electromagnetic bandgap structures for antenna applications," in Electronics Letters, vol. 52, no. 3, pp. 175-176, 2 4 2016.

[52] B. Sanz-Izquierdo and E. A. Parker, "3D printed FSS arrays for long wavelength applications," The 8th European Conference on Antennas and Propagation (EuCAP 2014), The Hague, 2014, pp. 2382-2386.

[53] S. Jun et al., "Circular polarised antenna fabricated with low-cost 3D and inkjet printing equipment," in Electronics Letters, vol. 53, no. 6, pp. 370-371, 3 16 2017

Chapter 3 – Antenna Theory

3.1 Theory

Antennas and its electromagnetic propagation have been around for a very long time; back in 1873, one James Clerk Maxwell published a book that is now the cornerstone of antennas called ‘A Treatise on Electricity and Magnetism’ [1]. He was able to talk about antennas by expanding on work from previous scientist such as Ampere, Gauss, Faraday and others. In his book, he has defined a few equations that have been proven to be important in the theory of electricity and magnetism. These equations define the fundaments for the calculations of the radiated fields from a charge [3].

$$\nabla \times \acute{E} = \frac{-\partial B}{\partial t} - M \quad (1.1)$$

$$\nabla \times H = \frac{\partial D}{\partial t} + J \quad (1.2)$$

$$\nabla . D = \rho \quad (1.3)$$

$$\nabla . B = 0 \quad (1.4)$$

Where, É is the electric field intensity (V/m)

H is the magnetic field intensity (A/m)

D is the electric flux density (C/m^2)

B is the magnetic flux density (Wb/m^2)

M is the magnetic current density (V/m^2)

J is the electric current density (A/m^2)

P is the electric charge density (C/m^3)

An antenna is defined as 'a means for radiating or receiving radio waves' [2] the radio waves could refer to electromagnetic waves and these waves travel at a certain speed, the speed of light and in a vacuum, is noted as $3 \times 10^8\ m/s$. The wavelength (λ) is known as the amount of distance travelled of a wave in one cycle

$$\lambda = \frac{c}{f} \qquad (2.1)$$

Where f is the frequency and c is the speed of light

An antenna can be represented as an energy converter because it is a device that sends and receives electromagnetic waves, which are converted from free space radiation to a transmission line and in the other direction. The entire process can be seen in figure 3-1.

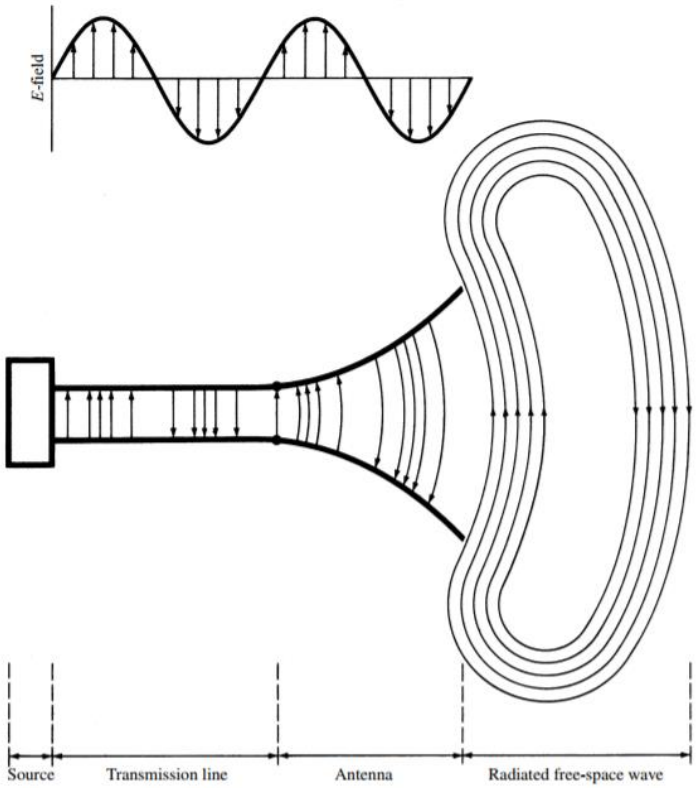

Figure 3-1 Process of antennas on a transmission line [3]

A common area of antennas, is the antenna losses, this can be explained by first looking at a Thevenin equivalent circuit based antenna. The model shown in figure 3-2 is a combination of a voltage regulator (V_s) with an impedance in series (Z_g), the section of the transmission line with characteristic impedance Z_c and the antenna with a load of Z_a connected to the transmission line. The losses come from the load resistance (R_L) which is a combination of conduction and dielectric losses within the antenna structure.

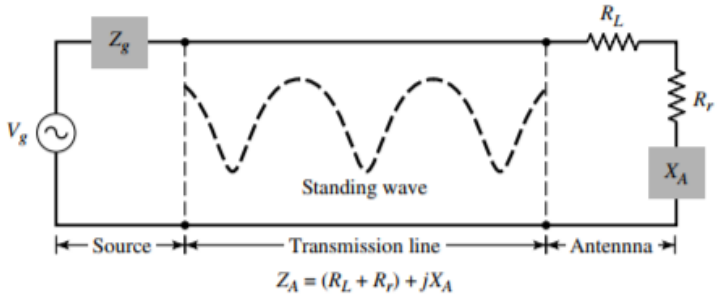

Figure 3-2 Thevenin equivalent of an antenna [3]

3.1.1 Antenna types overview

The abundance of antennas developed in the modern technological industry can be arranged into four discrete groups.

Wire antennas

The wire antenna is the most abundant and exploited antenna. They can be seen in a wide variety of areas such as on vehicles, Televisions, aircrafts, radio stereos and so on. They come in various shapes including loop, dipoles, helix, Yagi-Uda. These antennas are known to run at lower frequencies and have a low gain. Advantages being that they are simple to design and inexpensive.

Aperture antennas

A type of antenna with increasing popularity is the complex designs of the aperture antenna due to its use in higher frequencies. Aperture antennas differ in types; the horn antenna contains an opening to allow electromagnetic waves to flow through, directing the waves into the waveguide. The antenna tends to be useful for applications such as on an aircraft or spacecraft as it can be easily flush-mounted.

Microstrip antennas

Microstrip antennas comprises of a metallic patch on a grounded substrate. The specific shape of the patch varies as it can produce different radiation characteristics and polarization. These antennas low profile, and can be conformed onto different surfaces.

Array antennas

Array antennas are simply an arrangement of radiating elements in an electrical and geometrical structure. They are used when a single cell cannot achieve a certain radiation characteristic. Arrays are usually made up of dipoles, monopoles, slots.

3.1.2 Antenna analysis

Even though there are so many different types of antennas used, there are several discrete parameters that can describe them all. A bit of background information on the different types of parameters are described.

The parameters that are used when describing the range of antennas are:

1. S-Parameters
2. Impedance Bandwidth
3. Radiation Patterns
4. Directivity
5. Efficiency
6. Gain

3.1.2.1 S-parameters

It is advantageous when designing antennas as part of a network to create a model to show the detailed performance of the antenna/system. To collect the useful information a Vector Network Analyser (VNA) is used. The data is normally illustrated through the form of Scattering parameters or commonly known S-Parameters. Especially at higher frequencies a distributed model is needed to show the electrical behaviour of linear electrical systems when signal is applied the parameter values are measured in the various units of power [5].

The S parameters are defined by measuring the voltage travelling waves between the N-ports. This can be illustrated in figure 3-3.

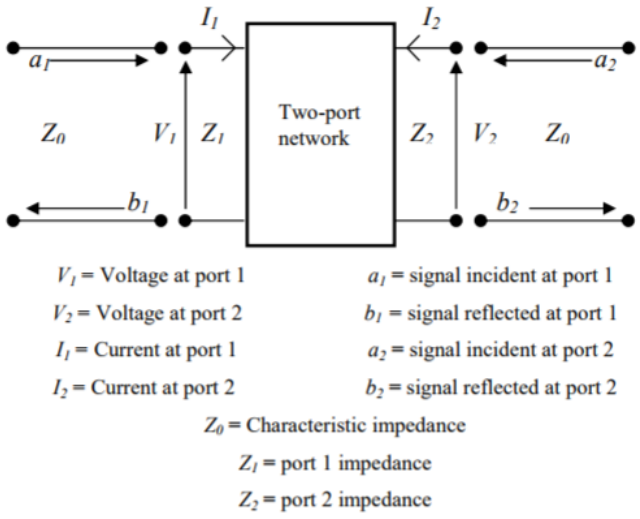

Figure 3-3 A two-port network

The definition of the incident and reflected signals are vital which are shown below:

$$a_x = \frac{|V_x^+|}{\sqrt{Z_0}} \ (\sqrt{watts} \qquad (3.1)$$

$$b_x = \frac{|V_x^-|}{\sqrt{Z_0}} \ (\sqrt{watts} \qquad (3.2)$$

The scattering matrix (14) relates the voltage wave's incident on the ports to those reflected from the ports. The scattering matrix is defined as:

$$\begin{bmatrix} V_1^- \\ V_1^- \\ . \\ . \\ V_N^- \end{bmatrix} = \begin{bmatrix} S_{11} & S_{12} & \dots & S_{1N} \\ S_{21} & & & . \\ . & & & . \\ . & & & . \\ S_{N1} & & & S_{NN} \end{bmatrix} = \begin{bmatrix} V_1^+ \\ V_2^+ \\ . \\ . \\ V_N^+ \end{bmatrix} \qquad (3.3)$$

Where the amplitude of the voltage incident wave on the port is denoted as V_n^+ and the amplitude of the voltage wave that is reflected off the port n is V_n^-. A random element of the S matrix can be explained as:

$$S_{ij} = \left.\frac{V_i^-}{V_j^+}\right|_{V_k^+ = 0 \ for \ k \neq j} \qquad (3.4)$$

When there are 2 different ports; a port 1 and port 2. To describe the power that is transferred from port 2 towards port 1, the parameter S_{12} is used and to describe the power from port 1 towards port 2, the parameter S_{21} is used. Therefore, S_{ij} is the value of the reflected wave amplitude V_i^- coming out of port i, when an incident wave of voltage V_i^+ is driven into port j.

The S_{11} in the practical and experimental stage is the most commonly used parameter for them all, also commonly known as the reflection coefficient of the antenna, which gives a representation of the amount of power reflected off the antennas' aperture. For example, if the S_{11} was equal to 0 dB then it would mean that the entire power is reflected off the antenna and none of it is radiated, whereas if S_{11} was -10 dB would imply a reflection of -7 dB if the received power was at 3 dB. All of the results when testing an antenna for the S-parameters are collected using a Vector Network Analyser (VNA) which gives a graphical representation of the frequency the antenna radiates best at. An example is seen in figure 3-4.

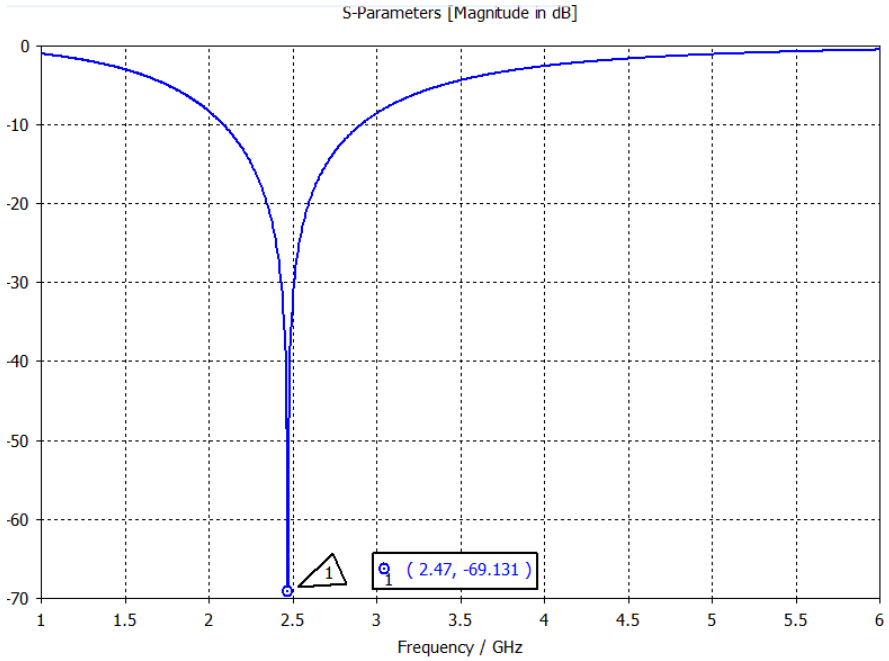

Figure 3-4 Reflection coefficient graph or S11 parameter for an antenna

It can be seen from the graph in Figure 3-4 that at the frequency of 2.47GHz the magnitude in dB has attained the maximum of around -70 dB. Through the use of a simulation modelling tool such as CST Studio [6], it indicates that the antenna is well

matched at the frequency of 2.47GHz, while any changes in the antennas' aperture dimensions or characteristics will result in changes in the matching frequency.

3.1.2.2 Impedance Bandwidth

This term is used to show how much bandwidth of the antenna has to its acceptable losses from mismatch, it is measured using two fundamental equations being the Voltage Standing Wave Ratio (VSWR) and the Return Loss (RL) at a certain frequency band. The VSWR is a ratio between the maximum and minimum voltage of the standing wave and the equation is:

$$VSWR = \frac{|Z_L|}{|Z_0|} = \frac{1+|\Gamma|}{1-|\Gamma|} \qquad (4.1)$$

Where Γ is the reflection coefficient and its formula is given as with V0 + is the amplitude of the incident wave and the V0- is the amplitude of the reflected wave:

$$\Gamma = \frac{V_0^+}{V_0^-} \qquad (4.2)$$

The RL is known as the ratio of the reeflected wave to that of the incident wave which is calculated through this equation and is in dB:

$$RL = -20Log|\Gamma| \quad (4.3)$$

3.1.2.3 Radiation Patterns

Radiation patterns are used to give a graphical representation of the radiation properties from a specific antenna as a function of space co-ordinates. An example is shown in the figure 3-5.

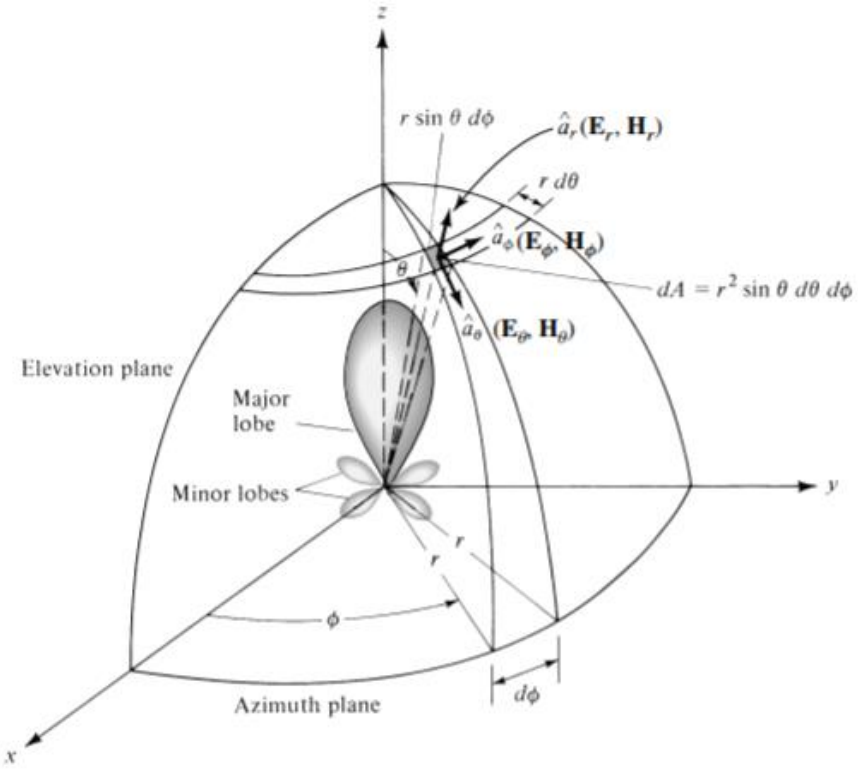

Figure 3-5 Representation of the radiation patterns from an antenna [7]

The antenna is placed in the centre and the power in the far-field is measured as it is rotated. The radiational patterns are represented in a 3D model, indicating the variational magnitude of the radiation as a function of the spherical coordinates theta (ϑ) and pi (ϕ) as seen in figure 18. There are three main plan cuts in the full three-dimensional pattern, which are in the XY for ϑ = 90, the XZ plane for ϑ = 0 and the YZ plane for ϕ = 90. [8]

3.1.2.4 Directivity

The directivity is essentially the amount of radiation from a given antenna in a specific direction over that of an isotropic source. The directivity can be calculated by this equation:

$$D = \frac{U}{U_0} = \frac{4\pi U}{P_{rad}} \qquad (5.1)$$

Where, U is the radiation intensity

U_0 is the radiation intensity of an isotropic source

P_{rad} is the total radiated power (W)

The directivity is written as an ordinary number through the ratio or in dB. With an antenna that can radiate equally well in all directions has a directivity of 1 (0 dB). The directivity of a short dipole is 1.5, antennas with higher directivity means that the radiation is directed at a specific direction.

3.1.2.5 Efficiency

Antennas are susceptible to losses; therefore, it is a good thing to measure the efficiency of an antenna. The overall efficiency can be written as:

$$e_0 = e_r e_c e_d \qquad (6.1)$$

Where e_0 = total efficiency

e_r = reflection(mismatch) efficiency = $(1 - |\Gamma|^2)$

e_c = conduction efficiency

e_d = dielectric efficiency

Γ = voltage reflection coefficient at the input terminals of the antenna

3.1.2.6 Gain

Gain is another important parameter, although gain is closely related to the directivity of an antenna. It considers the efficiency along with the directivity. It is expressed using this equation:

$$G = \frac{4\pi U(\theta,\phi)}{P_{in}} \qquad (7.1)$$

3.2 Types of antennas

3.2.1 Dipole

The dipole antenna is the simplest and the most frequently used antenna of its kind. It consists of a conductive wire rod or metal tube that is half the length of the maximum wavelength the antenna is to generate. Where a Monopole is known to have a single pole, the dipole has the characteristic properties to function with two poles. The wire is split in the middle and an insulator separates the two sections, each rod is connected to a coaxial cable at the end closest to the middle of the antenna. Therefore, the antenna consists of the feeder connected to two quarter wavelength elements extending in opposite directions.

The antenna is typically fed in the centre where the impedance is the lowest, the voltage and current levels vary along the length of the radiating section of the antenna. This is illustrated in figure 3-6.

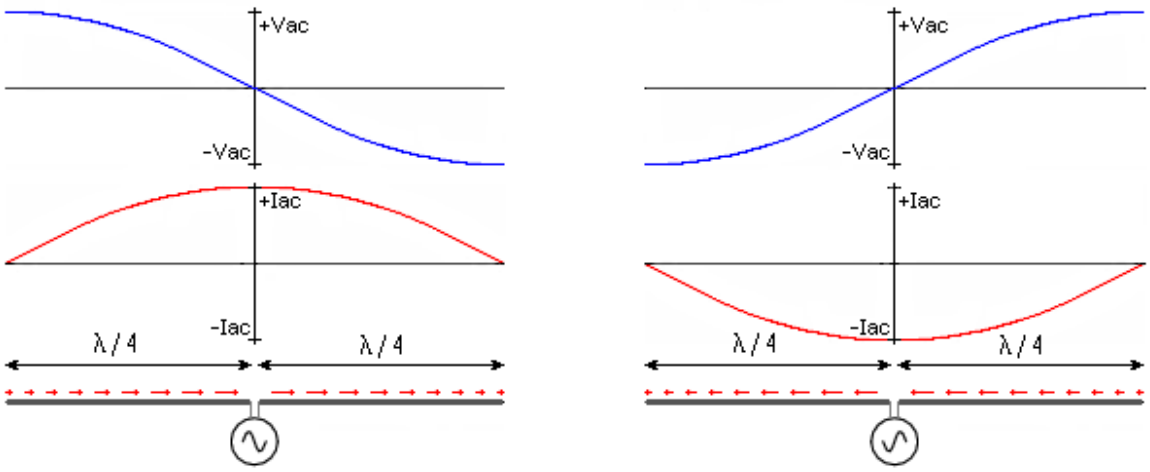

Figure 3-6 Voltage and current changes along a dipole antenna [18]

The figure shows the two charges of equal magnitude and opposite polarity oscillating in a harmonic motion. At t=0 the charges are at their maximum magnitude and separation and then as they reverse direction, they will have maximum acceleration. The antenna does not radiate uniformly along the length of the wire; the current at the ends are zero and therefore the electromagnetic radiation at the ends will be zero.

As for the radiation, it is at its maximum in the plane that is perpendicular to the dipole and zero in the direction the wires are pointing. This results in an emission diagram that is a torus shape with a zero-inner diameter. This is illustrated in figure 3-7.

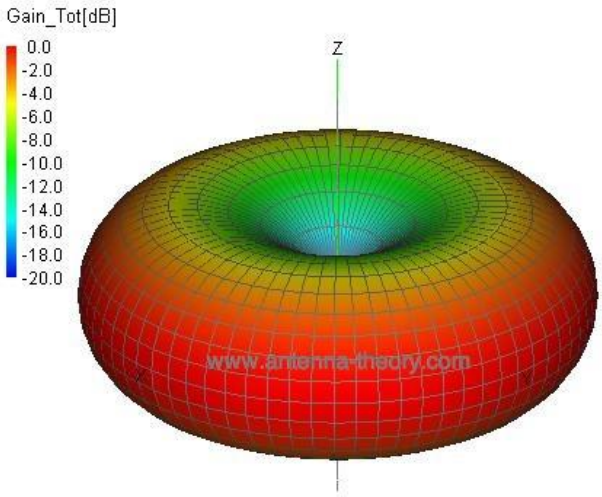

Figure 3-7 Illustration of the radiation from a dipole [19]

The formula for the electric field is given by;

$$E_\theta = \frac{j\eta I_0 e^{-jkr}\cos\left(\frac{\pi\cos\theta}{2}\right)}{2\pi r\sin\theta}$$

$$H_\phi = \frac{E_\theta}{\eta} \qquad (9.1)$$

3.2.2 Patch

The patch antenna is based on a voltage element of which the patch represents an aperture which collects or transmits the electromagnetic energy. The patch antenna can come in many shapes as shown in figure 3-8.

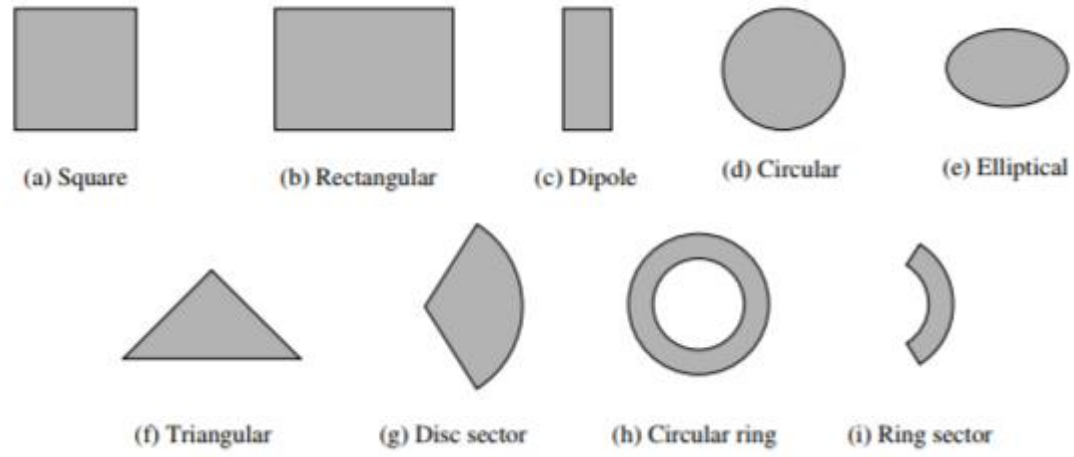

Figure 3-8 Various shapes of patch antennas [20]

For this application, the focus is on the rectangular element. The patch is typically made out of metallic strip, which is mounted on a dielectric substrate of thickness (h) much smaller than the free space wave length (h<<λ0) with a ground plane underneath it. This is illustrated in figure 3-9.

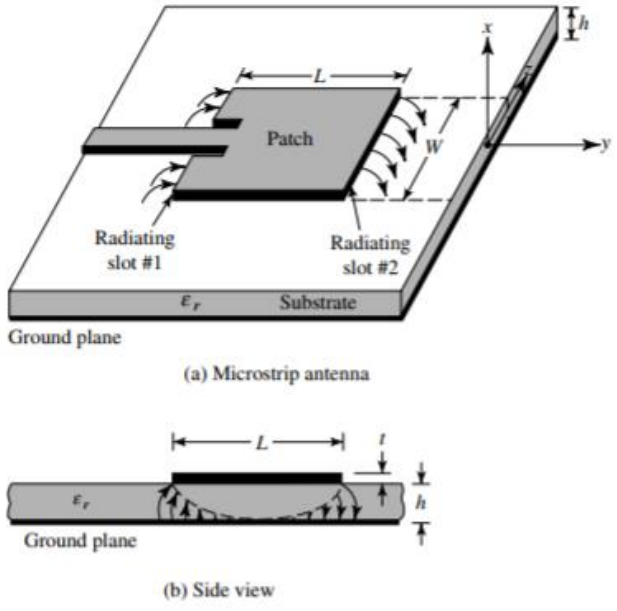

Figure 3-9 Diagram of a patch and its fields [21]

With λg being the wavelength in the dielectric, the patch acts as a λg/2 parallel-plate microstrip transmission line. The fringing fields between the patch and the ground plane create radiation, which is seen in the radiating slot #1 and #2 in figure 3-9(a).

Maximising the radiation is a trade-off between having good antenna performance and the needed element size. The size of the element can be lowered by increasing the dielectric constant (ε_r) along with reducing the height (h) of the substrate although this does affect the overall performance of the antenna by having the gap too close and therefore binds the fields closely which in turn increases losses and decreases the bandwidth. In other words, the antenna can achieve exceptional performance by increasing the substrate height and have a lower dielectric constant. This way, by having more room for the fields, it makes the antenna have a better efficiency and bandwidth, but this means the radiating element becomes much larger in size.

One of the ways to analyse the characterisations of patch antennas is the use of the transmission line model. Patches are viewed as transmission line resonators with no transverse field variations i.e. the field only varies along the length, and the radiation occurs from the fringing of fields, which are viewed as open circuits at the ends of the transmission line.

The fundamental mode of a patch antenna is the TM_{01} mode, in order to excite the TM_{01} mode, the length L should be slightly less than λg/2, where λg is:

$$\lambda_g = \frac{\lambda_0}{\sqrt{\varepsilon_f}} \quad (10.1)$$

Where ϵ_f is the effective dielectric constant in the medium and this shows that not all the fringing fields are bound inside the substrate. The dielectric constant is greater than the effective dielectric constant and is shown as:

$$\varepsilon_f = \frac{\varepsilon_r+1}{2} + \frac{\varepsilon_r-1}{2}\left[1 + \frac{12h}{W}\right]^{-\frac{1}{2}} \quad (10.2)$$

Where W is the width of the patch.

The equation 10.2 shows that the effective dielectric constant relies on the frequency, therefore as frequency decreases, the fields within the substrate reduce and the value of the effective dielectric constant moves away from the value of the dielectric constant of the substrate.

The fringing fields from the patch require the electrical length to be greater than the physical length of the patch, which is shown in figure 3-10.

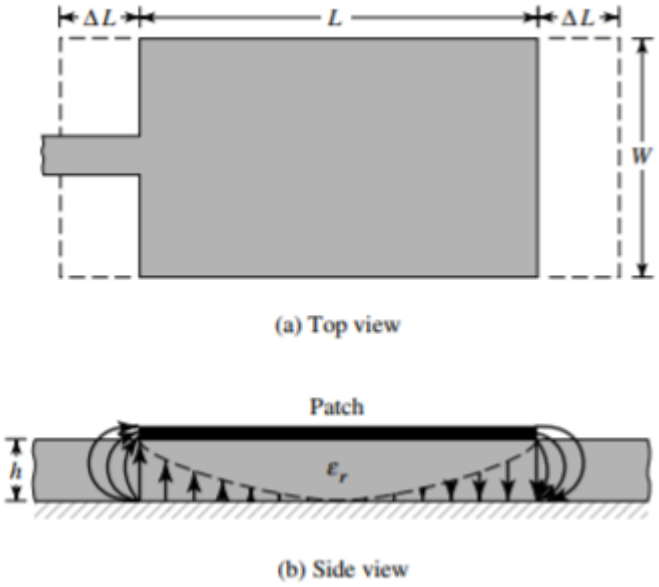

Figure 3-10 The length of the patch compared to the fringing fields [21]

As seen in the figure, the fringing fields are covered in the distance of DL, which are linked to the effective dielectric constant. Therefore, the total length of the patch is calculated by:

$$L_{eff} = L + 2\Delta L \quad (10.3)$$

Whereas the extra length in the substrate is given by:

$$\Delta L = \frac{h}{\sqrt{\varepsilon_f}} \quad (10.4)$$

As mentioned before the effective length of the patch for a certain frequency (f_0) is λg/2, therefore, the effective length is shown to be:

$$L_{eff} = L + 2\Delta L = \frac{\lambda_0}{\sqrt{\varepsilon_f}} = \frac{c}{2f_0\sqrt{\varepsilon_f}} \quad (10.5)$$

Where, c equals the velocity of light in free space ($3 \times 10^8\ m/s$)

To calculate the resonant frequency for any TM_n mode and in the above equation the equation below is used:

$$f_0 = \frac{c}{2\sqrt{\varepsilon_r}}\left[\left(\frac{m}{L}\right)^2 + \left(\frac{n}{W}\right)^2\right]^{\frac{1}{2}} \qquad (10.6)$$

In order to use the formula above the W has to be known, and this is known to be half wavelength, which is the average of the two dielectric mediums.

$$W = \frac{c}{2f_0\sqrt{\frac{\varepsilon_r+1}{2}}} \qquad (10.7)$$

The W value can be altered depending on the application, and it has a direct link to the bandwidth value and the directivity of the antenna. Increasing the value of W then increases the other two variables and vice-versa. Decreasing W can also be beneficial when the aim is to have circular polarisation.

To sum up in the design of the patch antenna is:

- Know the substrate dielectric constant (ε_r) and the operating frequency (f_0)
- Calculate the width size (W)
- Calculate the effective permittivity (ε_f)
- Calculate the total physical length (L)

3.2.3 Circularly polarized patch

The polarization of an antenna is defined as the direction of the electromagnetic wave is transmitted by the antenna. Polarization of the antenna can be classified as linear and circular.

Linear polarization is described when the electrical field at a point in space as a function of time is always directed along one line.

As for circular polarization, the electromagnetic waves radiate in both the horizontal and the vertical planes and the planes in between. The conditions to accomplish the circular polarization is if the electric field has all of the following:

1. the field must have two orthogonal linear components

2. the two components must have the same magnitude
3. the two components must be shifted by odd multiples of 90° in the time-phase

3.2.4 Frequency Selective Surfaces

A frequency selective surface is a surface that exhibits different reflection and/or transmission properties as a function of frequency. A basic surface type could have an array of wires or an array of slots with a dielectric slab on them. FSS have the ability to act as a band-pass or a band-stop filter, with a band-pass filter, passing waves at the resonant frequency but blocking the ones at higher and lower frequency. The band-stop filter passes waves above and below the resonant frequency but not the resonant frequency.

FSS have several important applications in today's society, the most common and interesting is the use for making radomes. Radomes can be thought as a protective cover placed over an antenna, protecting or blocking certain frequencies [9].

An FSS is an organised and calculated array of periodic elements, known as cells. There are passive arrays and there are capacitive arrays. The passive consists of slots on a conducting sheet, each cell resonates and disbands the energy when an electromagnetic wave is incident on the surface. Part of the wave is transmitted through the slots but most is reflected off. As for the capacitive structures, which are a series of metallic patches on a substrate, this type is considered to act like a low pass filter.

There are many variables that can cause a certain structure to act as a frequency selective surface. The array of elements must be symmetrical and are repeated equally (P). An example of this is shown in figure 3-11 of an array of square loops with a conductor width (W) and length (l) organised in a square lattice geometry with a periodicity (P) and a gap between elements (g).

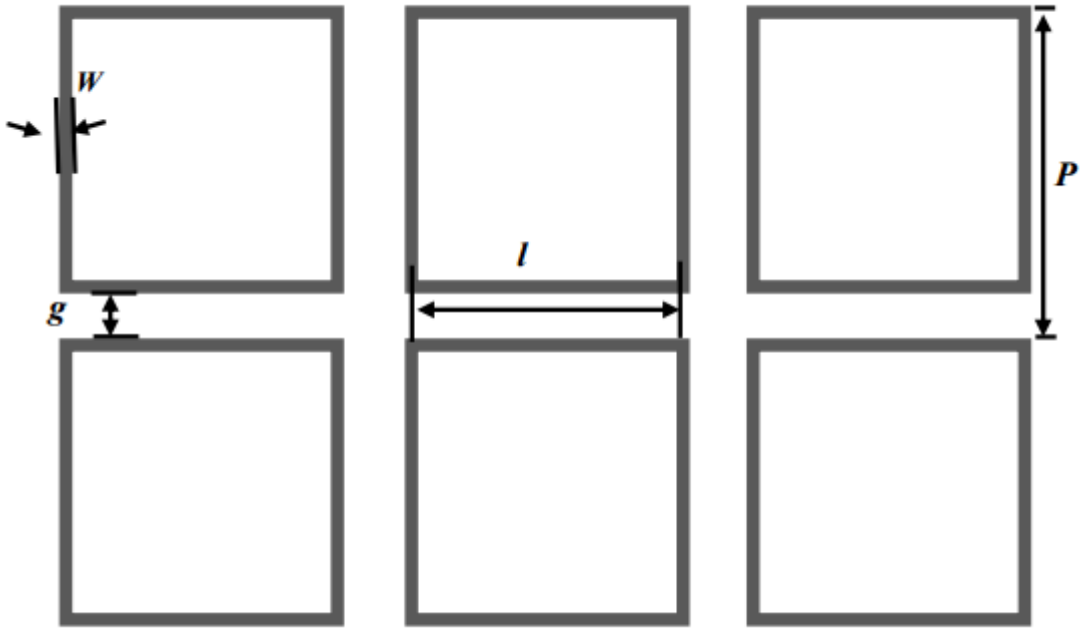

Figure 3-11 An array of square looped elements

The representation of FSS is as lumped elements with an inductance (L) and a capacitance (C). The value of the inductance is given by the length of the element (l) and the capacitance is given from the length of the gap between the elements (g) [10 – 12]. By increasing both C and L, the resonance frequency decreases by using the equation 8.1 to achieve a loss-less surface.

$$f_r = \frac{1}{2\pi\sqrt{LC}} \qquad (8.1)$$

There could be multiple resonant frequencies as seen in figure 3-12 with a double square loop [13 – 15].

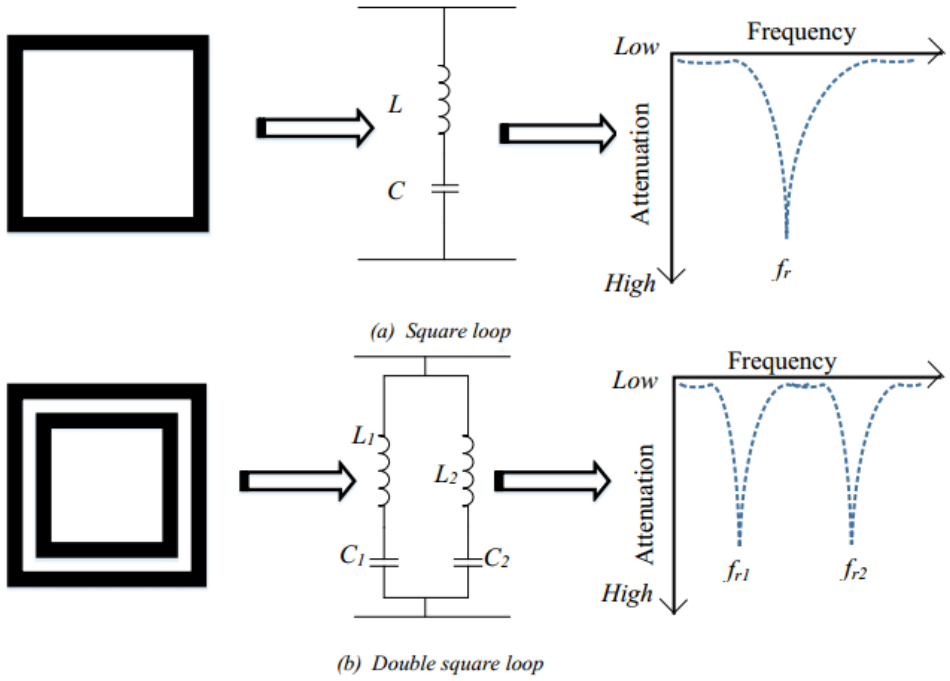

Figure 3-12 Circuit equivalent FSS and transmission graph (a) single loop, (b) double loop

The bandwidth of the FSS is measured as the values between the -10 dB of the lower and upper frequency points of the transmitted/reflected band, this can increase when there is an increase in the inductance in respect to the capacitance [12, 16]. Therefore, in terms of the designing, the bandwidth increases if the periodicity (P) increases or the width (W) decreases.

$$BW \propto \sqrt{\frac{L}{C}} \qquad (8.2)$$

There are distinct types of element designs, ranging from simple dipoles to complex fractal and convoluted structures. Calculating the correct type of cell requires the understanding of the applications propagation characteristics, which could determine the different angles of incidence or polarization, which results from diffraction, reflection, and scattering [17]. According to [10] FSS arrays are divided into four separate groups:

a. Centre connected or n-poles

This includes a simple straight element, which can be seen in figure 3-13(a) which could include dipoles, tripoles, anchor elements, and Jerusalem cross.

b. Loop Elements

This could be the most popular type of element used which are square and circular loops or rings along with loaded cross dipoles and hexagons as seen in figure 3-13 (b)

c. Solid interior or plate

Various shapes of solids such as squares, circular patches are in this group. Seen in figure 3-13 (c) and (d)

d. Combining elements

As different elements have specific characteristics, a combination of various elements designed together in order to improve a certain parameter.

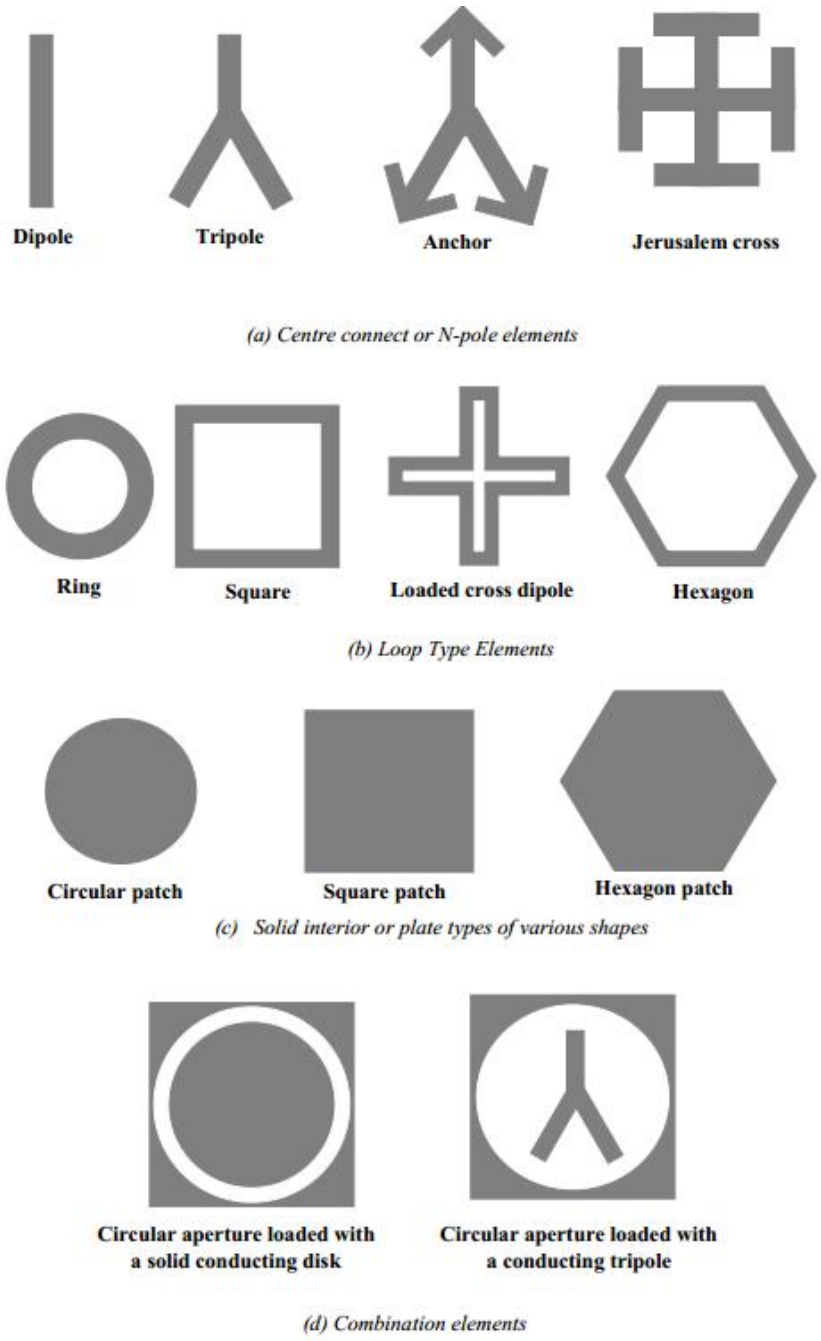

Figure 3-13 The major FSS element shapes [10]

References

[1] Maxwell, J. (1873). A Treatise on Electricity and Magnetism. Nature, 1,2.

[2] C. A. BaIanis, Antenna theory: AnaIysis and design, 3rd ed. Chichester, United Kingdom: WiIeyBIackweII (an imprint of John WiIey & Sons Itd), pp. 1, 2005.

[3] C. A. BaIanis, Antenna theory: AnaIysis and design, 3rd ed. Chichester, United Kingdom: WiIeyBIackweII (an imprint of John WiIey & Sons Itd), pp 2, 2005

[4] [online] http://www.maxwells-equations.com/ [Accessed 30 Jul. 2017]

[5] [online]http://www.antenna-theory.com/definitions/sparameters.php [Accessed 30 Jul. 2017]

[6] CST Microwave Studio 2010

[7] C. A. BaIanis, Antenna theory: AnaIysis and design, 3rd ed. Chichester, United Kingdom: WiIeyBIackweII (an imprint of John WiIey & Sons Itd), pp 28, 2005

[8] [online] http://data.eefocus.com/myspace/0/942/bbs/1174163529/29c6d0e7.pdf [Accessed 30 Aug. 2017]

[9] J. D. Kraus and R. J. Marhefka, Antennas for All Applications: McGraw-Hill, 2002

[10] B. A. Munk, Frequency Selective Surfaces: Theory and Design. John Wiley & Sons, 2000

[11] E. A. Parker, “The Gentleman’s Guide to Frequency Selective Surfaces,” 17th Q.M.W Antenna Symposium, April, pp. 1–18, 1991

[12] N. Marcuvitz, Waveguide Handbook. IET, 1951

[13] C. K. Lee and R. J. Langley, "Equivalent-circuit models for frequency-selective surfaces at oblique angles of incidence," in *IEE Proceedings H - Microwaves, Antennas and Propagation*, vol. 132, no. 6, pp. 395-399, October 1985

[14] R. J. Langley and E. A. Parker, "Equivalent circuit model for arrays of square loops," in Electronics Letters, vol. 18, no. 7, pp. 294-296, April 1 1982

[15] A. E. Yilmaz and M. Kuzuoglu, “Design of the square loop frequency selective surfaces with particle swarm optimization via the equivalent circuit model,” Radioengineering, vol. 18, no. 2, pp. 95–102, 2009

[16] M. Hosseinipanah, Q. Wu, and C. Zhang, “Design of Square-Loop Frequency Selective Surfaces Utilize C-band Radar Stations,” in International Conference on Microwave and Millimetre Wave Technology (ICMMT),pp. 2–4, 2008.

[17] [online]https://kar.kent.ac.uk/28365/1/Dual_State_Rings_IEEE_Kar_version.pdf [Accessed 30 Aug. 2017]

[18] [online] http://www.siranah.de/html/sail018h.htm [Accessed 30 Aug. 2017]

[19] [online] http://www.antenna-theory.com/antennas/dipole.php [Accessed 30 Aug. 2017]

[20] [online] http://www.unimasr.net/ums/upload/files/2011/Apr/UniMasr.com_1165919310b71469c1b283601611c79c.pdf- p771 [Accessed 30 Aug. 2017]

[21] [online] http://www.unimasr.net/ums/upload/files/2011/Apr/UniMasr.com_1165919310b71469c1b283601611c79c.pdf- p771 [Accessed 30 Aug. 2017]

Chapter 4 - Printer Assembly and Calibration

4.1 Materials and Method

The project requires a printer that can print plastic and metal at the same time to allow for the eventual printing of antennas. As there was no available printer with these capabilities on the market, the printer had to be built for this purpose.

The printer that was chosen for this project was the Mbot Cube 3D [1], this printer is a clone of the open sourced Makerbot Replicator [2], which is allowed by their copyright terms. It comes as a kit version which includes all the frame components and the electronics that is required to print. Although this printer had to be modified to allow for two extruders to work simultaneously, this included changes in the structure, mechanics and electronics.

The printer uses a Cartesian frame structure; this is one of the most widely used type of coordinate system to determine and control motors along the X, Y and Z-axis plane. Usually printers will have a square or rectangle platform bed and will be attached to the z-axis which will move up and down, the x-axis carries the extruder mount, while the y-axis moves the whole of the x-axis carriage. There are some

variations of this design which still fall under the Cartesian frame where the extruder and hot end are not moving and the platform moves in all directions.

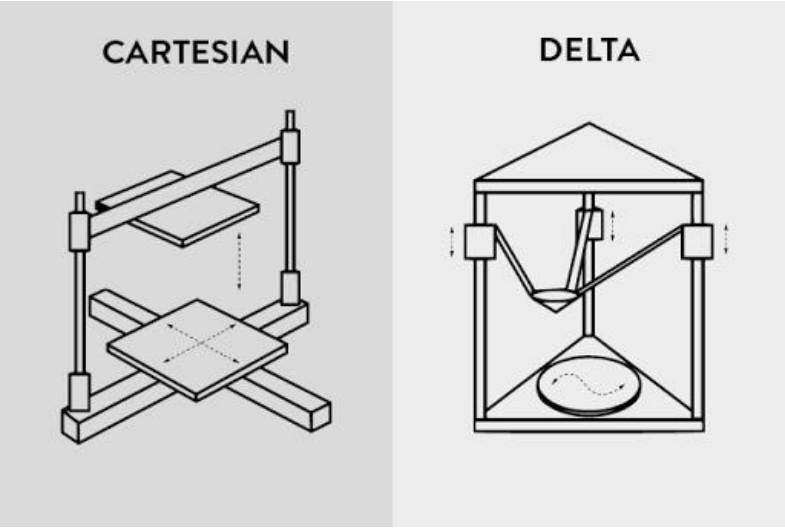

Figure 4-1 Distinct types of FDM frame; Cartesian (left) and Delta (right) [3]

The Mbot Cube printer features a chassis made out of wood and PVC with an overall dimension of 405 x 405 x 410 mm and the printing build volume of 200 x 200 x 170 mm for a dual extrusion mount which is average for a top 3D printer [1]. The printer has a layer resolution range of 0.1 - 0.3 mm for smooth quality prints with the stock 0.4mm extruder hot end. The motors have a travel speed of 50 – 120 mm/s and printing speeds up to 80 mm/s [1]. The hot end accepts a filament diameter of 1.75mm in PLA and ABS although ABS filament can be used if a heated bed is equipped. The printer is also equipped with a LCD screen to display key information on the status of the printer and also allow the user to control the printer without the need of a computer, it is a basic 20 x 4 character display which is connected to the microcontroller. The LCD display also features an SD card input to allow offline printing, however the printer does not offer connection through Wi-Fi or a flash drive.

FDM printers come in two different extruder setups, either with Bowden, or Direct drive systems and each of them has their advantages and disadvantages discussed below.

Bowden – style Extruder

In this setup of extruder, the hot end is physically separated from the extruder, the extruder is usually mounted on the back or side of the printer while a flexible tube guides the filament from the extruding motor to the hot end, the tubing is usually mad of Teflon. The advantage of this method is that when the motor and mount of the extruder is removed off the carriage assembly, it reduces a significant amount of weight of the moving parts. This should in theory result in more accurate prints when printing at higher speeds and less vibrations due to inertia, as there is less weight to move. Overall, the Bowden extruders can be able to print faster than the other methods. Another advantage is that the build area of the printer can be larger as there is more space on the hot end carriage, the extruder carriage does not have a bulky motor that takes up space. There are disadvantages to the Bowden setup, the length of the tubing can introduce a certain 'play' to the filament especially on larger machines and the Bowden tubes are much longer, this therefore requires finer tuning of the extruder engagement. One factor that plays a big issue on is the retraction, when during the printing process the filament needs to be pulled the other way to remove the stringing effect, with Bowden the retraction needs to be much higher than to direct drive as there is a larger distance between the extruder and the hot end. Another disadvantage of the Bowden extruder is the difficulty to print flexible filaments; this is because the extruder can have difficulty pushing some flexible filaments for a long distance with enough pressure to enter the hot end. Therefore, flexible filaments such as NinjaFlex [4] are not recommended for printers that have Bowden extruders.

Direct Drive Extruder

In the Direct approach, the extruder is mounted directly on top of the hot end. This is the more common type of extruder system. A gear that is tightly gripping the filament rotates and drives the filament a short distance to the hot end, the gear can

rotate backwards or forwards to extract the filament from the hot end. The advantages to this method is that flexible filaments are easier to print because there is a shorter distance between the motor and hot end, therefore the filament will not bend too much. Another advantage is that it has better retraction and resume control, when the extruder motor rotates to retract 1 mm the resulted retraction is very close, therefore making it very precise and easier to control. The disadvantage to this setup is that there is more weight on the carriage therefore cannot move as fast while printing. The MBot Cube printer uses the Direct Drive extruder system.

The dispenser that will be used is the Techcon TS250, it is a digital fluid dispenser that dispenses low, medium and high-viscosity fluids accurately and consistently [5]. It is a highly responsive air pressure and vacuum management system, along with a digital timing circuit, which provides a consistent and repeatable fluid dispensing. The dispenser features an adjustable vacuum-driven 'suck back' option to control material waste, which is vital for the application on the printer, a maximum input pressure of 100 psi and a wide 1-100 psi output pressure. There is also a digital timer from 0.02-60.00 seconds for automating dispensing with a repeatable tolerance of +/- 0.001%. The dispenser also has precise scaled air pressure gauges along with a 16 x 2 LCD display for essential information. The ports that are available on the dispenser is a serial input/output connection and a foot switch receptacle. Within the system of the dispenser, there is a function that controls the flow of air through the pedal switch; the pedal switch is a physical switch that closes the circuit.

The microcontroller that will control the operation of the printer is the Arduino Mega 2560 which is a well-known and popular open source board. Featuring the ATMEL ATMEGA 2560 core chip running on a 16 MHz crystal oscillator, 54 digital input/output pins, 16 analogue inputs, 4 UARTs and a USB connection. Most FDM printers run off the ATMEGA 2560 chip, which make it a reliable option.

RAMPS 1.4 Shield

The RAMPS 1.4 board is a shield for the Arduino Mega 2560, it contains ports and headers which allow for connections to up to 6 stepper motors and their drivers, auxiliary header outputs to peripherals such as a Liquid Crystal Display (LCD) and an SD card reader which allow the controller to print without the requirement of a computer. The RAMPS also have connections for end-stops which tell the system that it has reached the boundary of an axis, there are also three thermistor connections for temperature readings of extruders and heat beds, servo ports and power connections for heaters and fans for extruders.

Motor Drivers

The motor drivers that is used on the RAMPS 1.4 board is the Pololu A4988 motor drivers, which uses the micro-stepping integrated circuit with built-in translator to control of the axis motors and extruders accurately, efficiently and safely. To set the amount of Microstep needed, three signals were set to a specific logic, the Table 1 show the different types of Microstep resolution with their logic signals needed.

Table 1 Micro stepping definition [6]

MS1	MS2	MS3	Microstep Resolution
Low	Low	Low	Full Step
High	Low	Low	Half Step
Low	High	Low	Quarter Step
High	High	Low	Eighth Step
High	High	High	Sixteenth Step

Stepper Motors

The motors that are used are the NEMA 17 motors, there are a total of four motors that are used in the movement of the print nozzle; one for each axis of direction X, Y and Z and one for the extruder to push the filament through to the hot end. These motors are most commonly used in FDM printers; they are driven by the stepper motor driver in pulses which is referred as steps. Each step is a known distance which makes them have repeatable positioning, there is 1.8 degrees per full step and for a full 360 degrees is equivalent to 200 steps per revolution.

Power supply

The system is powered using a 12V 20.8A power supply, which is capable of three separate outputs, it has a built-in cooling fan, which is controlled by an internal temperature sensor and is mounted on the bottom of the printer frame next to the microcontroller. It is able to constantly power the printer for long prints, which is necessary as prints can take a considerable amount of time. The power supply offers enough power for the powering of the microcontroller and the RAMPS shield along with other add-ons and upgrades such as an addition of fans for the stepper drivers as they can get really hot and the addition of a heated bed which requires at least 10A.

LCD Screen

The LCD screen and controller that is used on the printer is the RepRap Discount Full Graphic Smart Controller. The LCD display is used to display vital information about the status of the printer such as; the temperatures of all the extruders and the heated bed, the time elapsed throughout a print cycle and the status of the SD card. The LCD controller can also control the movement of the motors along with enabling and disabling the pre-heating cycles without an external computer. The controller can also tap into the loaded firmware for selective changes in the settings. It is connected through the auxiliary ports, which are available on the RAMPS controller, and is configured through the firmware.

Heated bed

The use of a heated bed is not a requirement for the printing process, although it helps with the print quality and bed adhesion, some materials such as ABS can only be printed if a heated platform is used. The heat bed is 200 x 200 mm and uses an input voltage of 12 or 24. The temperature is measured by a thermistor that is placed in the centre of the bed. Various bed surfaces can be placed on the heated bed to add better adhesion such as the use of a glue stick or painters tape.

Silver ink

To get metallic tracks to be printed using a printer, the metal has to be melted and then deposited in a controlled and repeatable manner. As metal requires very high temperatures to be melted and then cooled immediately as to not damage the printer especially if it is needed to be deposited alongside another material such as plastic, this technique is not feasible. Therefore, research was undertaken to come up with an alternative and the result is to use an already liquefied metal and dispensed through a controlled tube such as a syringe. Previously the metallic material would have been solder paste as it has the conductivity characteristics required for the application and has the right consistency to be dispensed through a syringe, the only drawback is that it required post-process curing to achieve full conductivity. Solder paste is currently used in the manufacture of printed circuit boards (PCB) to connect surface mount components to copper traces of the board.

Although, there is another alternative, an ink coming from a company called Voxel8 [7] that have developed a silver nanoparticle ink optimised for the use in 3D printing applications. The ink has an electrical resistivity of under 3×10^{-7} Ωm when cured and an electrical conductance of 2 million S/m. For comparison, the conductive pastes that could have been used have about 400 S/m and there are conductive filaments used in FDM machines have about 100 S/m, which is much lower and would have been an issue with printing electrical components. The ink is stored in a syringe and is cured at room temperature, the company claims that it takes about 15 minutes to dry ad adhere to the material. Moreover, the advantage to using this silver

ink rather than a solder paste is that it is not affected by heat so when it is mounted next to the plastic heated nozzle it will not be affected.

4.2 Design and Fabrication of parts

As mentioned before the printer had to be modified in a structural manor to accommodate the extra extruder and be able to print two materials at the same time. This process requires new, modified parts within the printer, including an extended extruder carriage on the X-axis, which will have enough space to mount the plastic extruder motor and space for an interchangeable syringe. The other modification is on the motor mount for the X-axis, as extruder carriage will be extended, then the x-axis motor mount must be decreased in size and have the end stop switch mounted in an appropriate location as to have contact with the modified carriage. Another modification is the printers bed platform, to allow for a wider range of printable materials, a heated platform will be installed. Some thermoplastic materials such as flexible filaments require a heated bed for successful bed adhesion. The bed could also be extended to the maximum widths of the printer, to allow for a bigger print volume.

The models for these parts were designed and the plan was to print them using another printer and then assembled onto the Mbot printer. They were designed using the CST Studio modelling software.

The extruder carriage runs along the x-axis by two smooth 8 mm steel rods and is connected to the X-axis motor using a GT2 looped timing belt with a 2-mm pitch. The section in the middle where the hot end nozzle would be mounted was extended by 40 mm to accommodate a 20-mm diameter syringe next to it. The design can be seen in figure 4-2.

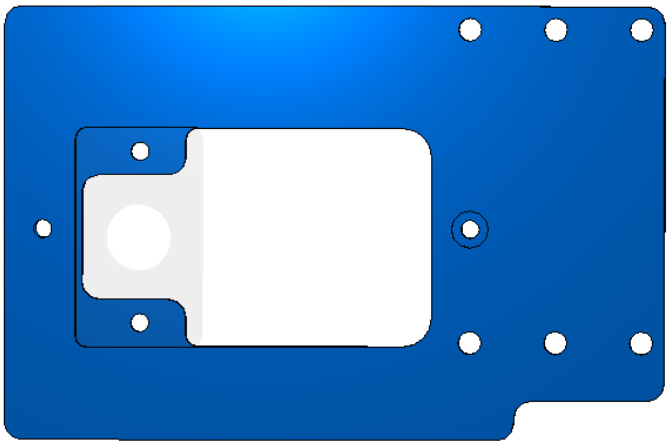

(a)

(b)

Figure 4-2 Design of the modified extruder carriage (a) top view, (b) side view

The parts that need to be printed out must be printed out to a certain degree of accuracy and specification. The printer that will be used to print out the parts that are needed for the MBot printer is the LeapFrog Creatr HS, which is an industrial grade FDM printer, and it is capable of printing large models at high speeds. The LeapFrog Creatr HS has a maximum print volume of 13.6 litres covering 280 x 240 x 180 mm in dimensions; it is capable of dual nozzle printing which allows two different colours or materials to be printed at the same time with nozzle sizes of 0.35mm. The printer has a layer thickness of 0.02 – 0.35 mm, which means that it can print at very high resolutions and a maximum print speed of 300 mm/s. Once all of the designs are finalised and checked they are exported as a stl file where it is imported into the slicing software. To ensure that the printed parts fit correctly and be able to withstand the printer's rapid movement and environment, the following parameters must be met;

- The models to be printed using ABS – one of the types of plastics used in FDM printers, ABS is an easily printed material and has durable material characteristics, whereas Nylon is also a strong material but has strict printing parameters and it prone to failing. ABS also can withstand higher temperatures than other types of plastics such as PLA making it suitable for this task.

- The models should be printed at 100 µm layer resolution – this ensures that the surfaces of the objects will be smooth and allow parts to be fitted together easily. When there is a lower layer resolution, the model is made up of more layers which therefore increase the strength factor which is also vital.

- Printed with an infill of 75 – 85 % - when the models are printed with an infill of around 75 – 85 % makes the object to have the required strength needed to hold the printer together and not break apart without adding much weight. The infill could be increased to a higher percentage though it would not drastically increase the strength factor and would just use extra filament.

- Printed with a perimeter layer of 2 – 3 - the perimeters are the lines of material extruded on the outer side of the model, the common number of perimeters is 2, with a higher number ensures that the layers of the model have a higher adhesion together and don't split over time.

4.3 Firmware and Dispenser Integration

For this project, there are two main parts of software that will be designed; the Marlin firmware and the second extruder trigger script. The Marlin firmware is the set of instructions that most FDM RepRap printers run on, this set of files will be modified to suit the MBot printer mechanical settings and then uploaded onto the RAMPS 1.4 board to run the necessary G-codes.

The RepRap [8] open source community initially developed the Marlin firmware, it acts as a guideline for the configuration of the printer and is unique to every printer. The code is modified to suit the model and the application of the printer.

The firmware is very comprehensive and once completed consists of around 10,000 lines of code. The firmware defines all the characteristics within the printer's mechanism and movement as well as specialised functions for connected devices.

The firmware is split up into several script pages, the main settings page is in the Configuration.h file of the Marlin folder. It is also split up into several sub-sections which define a plethora of functions, of which the main ones include;

- Communication speed

The communication speed sets the printers baud rate when connected to a computer. There are two most popular baud rates 2500000 and 115200.

- Motherboard type

As mentioned before the firmware is used on most RepRap FDM printers therefore there could be a variety of different microcontrollers being used. Each microcontroller has a distinct set of pins, and each one has to be defined in order to allow the printer to work at its fullest potential. Moreover, the number of power outputs are defined, for example in this case there will be three power outputs; two extruders and a heat bed.

- Extruders

This defines the number of extruders that are used in the printer, this is important because when the G-code is sent to the printer, it can understand which command is for which extruder. It also links to the power output settings discussed previously and will link to the thermal settings.

- Thermal settings

This variable defines the type of thermistor that is used to measure the temperature of the heater block or heat bed. There are several types of thermistors that can be used, they are placed in the heater block of the hot end and collects the temperature readings, there are also thermistors used on the underside of the heated bed which needs to be monitored. Typically for a printer that has two extruders, there will be a thermistor on each, but for this project the second extruder is considered to be an

experimental extruder with no heated element therefore will not require a thermistor. During a dual extruder print, both extruder temperatures have to be over a certain limit to allow it to print, therefore the pin is left floating high as to not raise any issues. The temperature is set to a constant 200 °C because within the Marlin firmware there are a few safety regulations in place for temperature extrusions; one being the minimum temperature for the hot end to extruder material which is set to 170 °C because any lower will affect or damage the motor. A maximum temperature limit is also another safety setting which is set to 260 °C which is dependent on the type of hot end that is used. Several hot ends include a PTFE tubing guiding the filament from the extruder shaft to the heater block and if the heater block gets too hot, it could damage the tubbing resulting in blocked extruders. The heated bed also has a maximum temperature of 120 °C to limit the amount of power received.

- Mechanical settings

Mechanical end stops are used along each axis to help define the boundary of the printer, they are switches that are triggered when the extruder carriage has reached them. Within the Marlin firmware, these end stops have to be defined as a min or max position so that the microcontroller knows where the extruder carriage is. There is a total of three end stops; one on each axis and on the projects printer they are paced at the minimum of their axis. The stepper motor direction is also defined, using a series of if statements to control the direction of the motor, the extruder carriage is placed in the centre of each axis and by observing the direction of the movement when a +10 mm command is sent to each axis, the directivity can be adjusted.

Then the maximum print dimensions are defined to stop the extruder carriage from going over the size limit of the platform.

- Movement settings

This section controls a couple of variables linking to the movement of the stepper motor, the major variable in this section is the steps per millimetre value for all of the axis and extruders. The default speed and acceleration of the stepper motors during printing and homing movements are defined. The speed and acceleration values are

set by the manufacturer but are sometimes changed for experimenting with the limits or upgrading certain electrical components.

Second extruder

The second extruder is an experimental system that was modified to fit with the Mbot 3D printer, with the Marlin firmware controlling almost all functions within the printer a second microcontroller had to be implemented to control the second extruder.

The approach for the second extruder integration is to link the RAMPS board and the pneumatic dispenser through an Arduino microcontroller. Using the stepper signals from the RAMPS, the Arduino can translate to control the pneumatic dispenser.

The second extruder system, the Techcon Systems TS250, has a digital input pin that can control when the dispenser is on or off, therefore it makes it easier to control it with a microcontroller. The Arduino will analyse the signal from the RAMPS board and then output a single signal to drive the pneumatic dispenser. The signal from the Arduino will have to first go through a transistor that will open or close the switch connected to the dispenser.

To be able to connect the dispenser to the RAMPS board the stepper motor and signals that drive it were analysed.

A stepper motor is an electrically powered motor that when current pulses are applied to it, it generates a discrete rotation of the motor shaft, unlike a DC motor which has a continuous rotation. Inside a stepper motor, it consists of a stator, a rotor with a shaft and coil windings. When electrical current flows through the coil windings, a magnetic field is generated within the coil. Several coils are placed in specific places around the motor shaft, and the closest permanent magnetic field on

the disk, an attraction or repulsion force will exist. By controlling which coils are active, controls the direction of the motor shaft.

The stepper motor driver is the component that controls which coils are active, they determine that through a few of the input signals. The Reset, Step, Direction and Enable signals are the main contributions that control the movement of the stepper motor.

The Reset input sets the translator to a predefined Home state and turns off all the FET outputs. The translator controls the input to the DAC's and the direction of current flow in each winding. The Reset input must be set to 'high' for any Step signals to be executed.

The Step input controls the movement within the stepper motor, where a low to high transition in the Step input sent to the translator and advances the motor one full increment which usually represents 1.8°. The size of the increment is determined by the combined state of the MSx (Micro stepping) inputs.

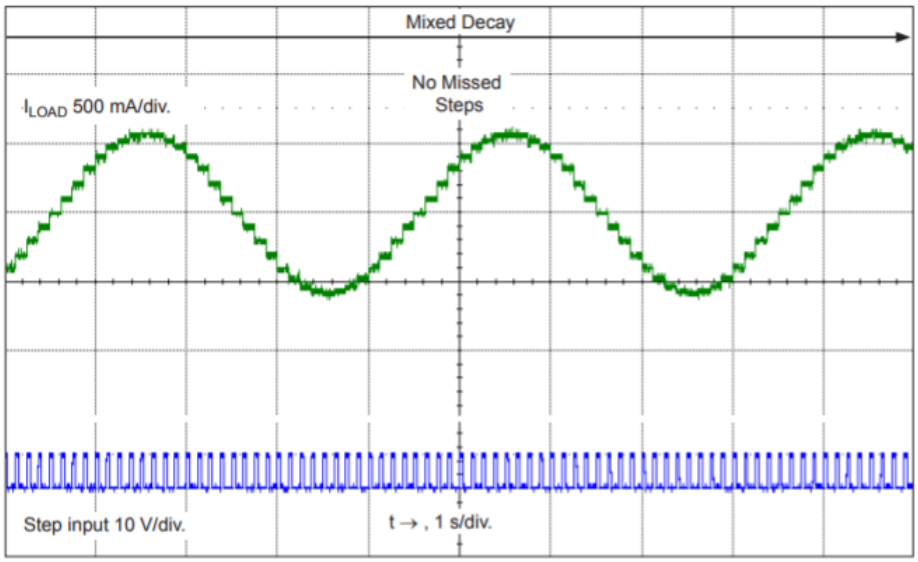

Figure 4-3 The represented steps within a stepper motor [9]

Direction input determines the direction of the rotation of the motor, changes to this input do not take effect until the next Step rising edge.

Enable input simply turns the stepper motor on or off. When the logic is high, the outputs are disabled and when the logic is low, all signals are sent out through the translator.

A combination of these signals is sent to the stepper driver and the output to the motor through four wires; two for each coil.

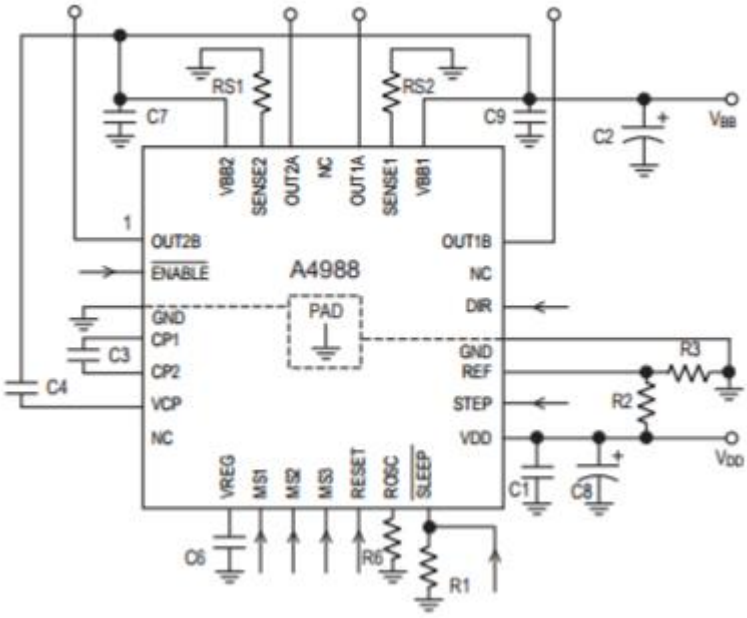

Figure 4-4 Wiring diagram of a stepper motor driver, the A4988 [9]

For the second extruder, the stepper driver is not needed on the RAMPS board because we are not driving a stepper motor. Therefore the 4 main inputs that would normally be connected to the stepper driver will be connected to another Arduino to be translated to a useful signal to drive the pneumatic dispenser.

To fully understand the magnitude of the signals that were generated, an oscilloscope was connected to the Step and Direction pins. As the signals were sent to the motor, the changes were observed on the oscilloscope as seen in figure 4-5.

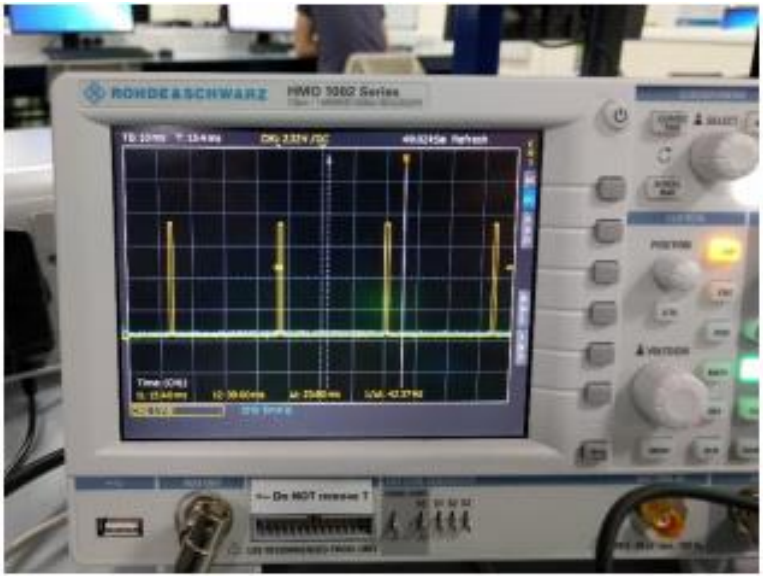

Figure 4-5 Signals observed when connected to the Step signal

The Step signal generated a series of pulses when the microcontroller sent a command to move, the pulses had a peak magnitude of 5V for a period of 10 microseconds, the frequency of the pulses depended on the value for the micro stepping. The direction signal changed to high as soon as the motor started to rotate and then stayed high when the motor was moving in the forward position, the signal only changed when the motor changed to the reverse direction.

A script was written on an Arduino Nano board to collect the signals from the RAMPS board and analyse the data in order to output a single signal to the pneumatic dispenser through the pedal switch input. When the pedal switch is connected to the dispenser, to initiate the air flow the pedal closes an open circuit and as long as the circuit is closed the dispenser will be on.

Using the PulseIn read function in the Arduino library, the Step and Direction signals were read. By using the PulseIn function the exact values of the signals were displayed on the serial monitor of the Arduino. Observing the range of the values, it was concluded that the Step signal ranged between 3 to 14 which depended on the duration the signal was high for. The Direction signal displayed a 1 or high when it was extruding and only changed to low when the motor changed to the other direction (retract).

Within the code which is seen in the appendix A, the work flow included an if-statement that would set the output of pin 3 when the value of the Step signal is between 1 and 15 along with the Direction signal being high, otherwise the output would be kept low. The limit of 15 was used to not interpret noise within the circuit as a valid signal, and the maximum value observed while testing was 14. The if-statement would be triggered only when the Enable signal was low.

In order to control the dispenser from the Arduino through the input of the pedal switch, a transistor should be used. A PNP transistor would be connected to the output of the Arduino and the input of the dispenser, this will allow the transistor to create an open or closed circuit depending on the output of the Arduino.

The final setup of both the extruders can be seen in figure 4-6, with the plastic extruder on the right and the silver ink tube on the right which is controlled by the pneumatic dispenser.

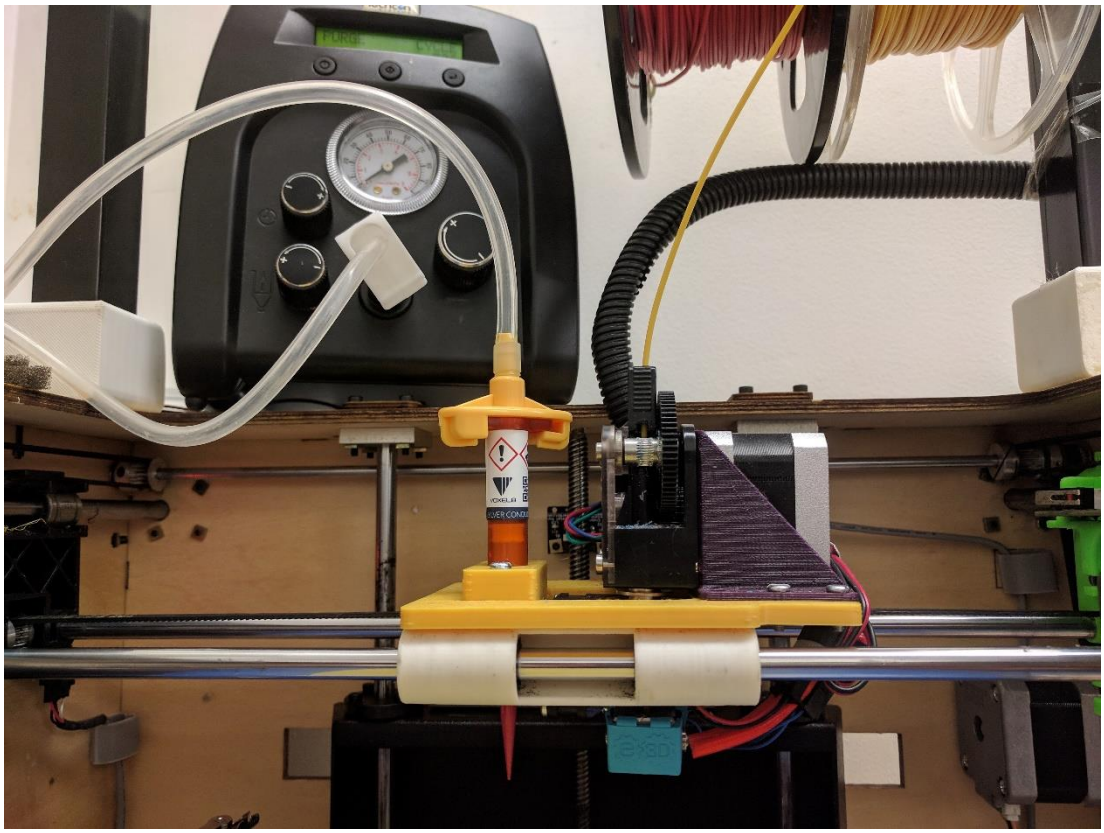

Figure 4-6 Complete dual extruder setup

4.4 Calibration

One of the most vital steps with using a 3D printer or any precise machine is the extent of calibration. Calibration could be the sole cause of failed prints, any two FDM 3D printers will not be the same even though they happen to be the same model, the extent of the calibration and the alignment of the parts in the printer may be off by a fraction of a millimetre and therefore can cause issues with the print.

Especially with a printer that has two extruders, the calibration is a very important process. Within the calibration process, there are some tasks that must be done at the beginning of every print, but the essential ones are when setting up the printer for the first time. These include adjusting the steps per millimetre for all the axis, and calibrating the bed height. For the software side, the print temperature and speed need to be tuned according to the process, along with the extrusion multiplier and the perimeter width.

The first step is to calculate the value of the steps per millimetre, the steps per millimetre is a value that is set in the firmware of the printer that determines the amount of revolutions that the microcontroller should send to the stepper motor to make the timing belt or rotary shaft to move one millimetre. This is one of the most important values set in a printer and tends to not be changed after the initial calculation and calibration. For the X and Y axis the steps per millimetre can vary depending on the type stepper motor and timing belt used on the carriage way, the Z axis values depend on the type of stepper motor and the lead screw threading count. As for the extruder values, it depends on the size of the stepper motor and the hob diameter. Formulas used for each of the axis are shown;

Formula for the X and Y axis is:

$$steps\ per\ mm = \frac{M_t \times d_s}{b \times p_t} \qquad (8.1)$$

Formula for the Z axis:

$$steps\ per\ mm = \frac{M_t \times d_s}{l} \qquad (8.2)$$

Formula for the E motor:

$$steps\ per\ mm = \frac{M_t \times d_s}{\pi h} \qquad (8.3)$$

Where M_t is the motor steps per revolution

d_s is the driver microstep value

b is the belt pitch

p_t is the number of teeth on the pulley

l is the pitch of the lead screw

h is the diameter of the hob of the extruder

The calibration of the steps per millimetre is achieved by using a ruler to measure the exact distance a certain motor moves when sent by the microcontroller. The difference between the two values determines the new steps per millimetre value, the calculation is done through using this formula;

$$New\ steps = old\ steps\ \times (\frac{expected\ length}{actual\ length})$$

Firstly, the microcontroller sends the axis motors to move to their home position [0, 0, 0] then using a ruler that is placed on a specific axis rod, the microcontroller sends a command to move 100 mm along that axis, the movement is measured and noted. Ideally the measured value should be the same as the 100 mm. This process is repeated for each of the X, Y and Z axis, as for the extruder the procedure is slightly different.

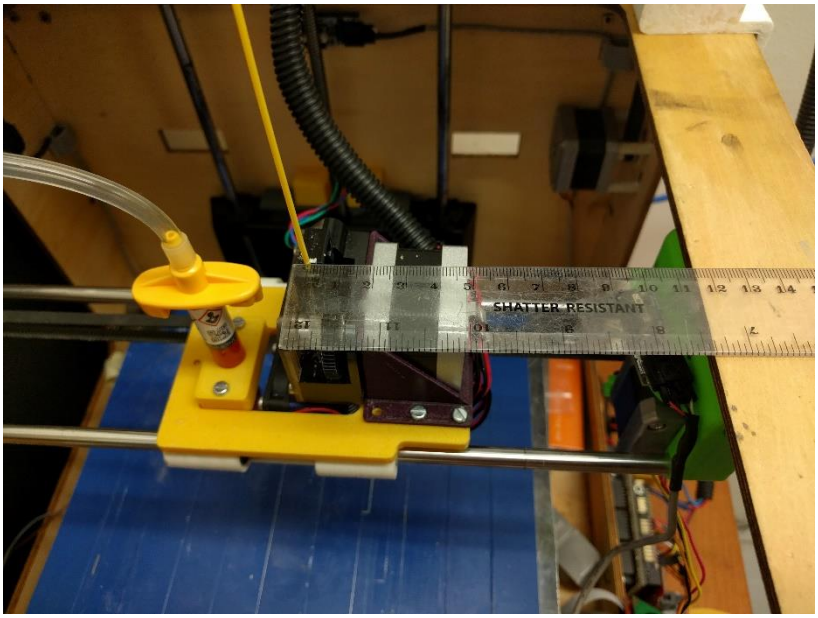

Figure 4-7 Calibration of the motor axis

The extruder motor steps per millimetre controls the amount of filament that is fed through to the hot end, therefore once the hot end has reached the optimum printing temperature, 150 mm of filament is measured and marked from the top edge of the extruder motor. A command is send to the motor to extrude a 100 mm of filament; the distance is measured again, for the correct step there should be 50 mm left between the mark and the edge of the extruder motor.

Pneumatic dispenser calibration

The Techcon TS250 dispenser used in this project for the silver ink has a variable output air pressure control to be able to control the flow of various pastes and inks, a test was conducted to understand the best pressure flow for the silver ink from Voxel8. The dispenser has a range between 0.1 to 7.9 bar of pressure and therefore to calculate the best suitable pressure for the ink, a model was printed with different pressures and then measured to see which matched the modelled version.

The air pressure tested would range from 1 to 7 bar at increments of 1 bar, and the model used is a thin line measuring 20 x 1 x 0.2 mm. The value that is more concerned about is the width of the track, the correct air pressure will result in a specific flow of silver ink and therefore produce the correct width of track. A 1 mm width track can also test the tolerance of the dispenser, to see whether it can deposit

the silver ink reliably and continuously. The value can also be reduced to 0.5 mm to see the limits of the dispenser.

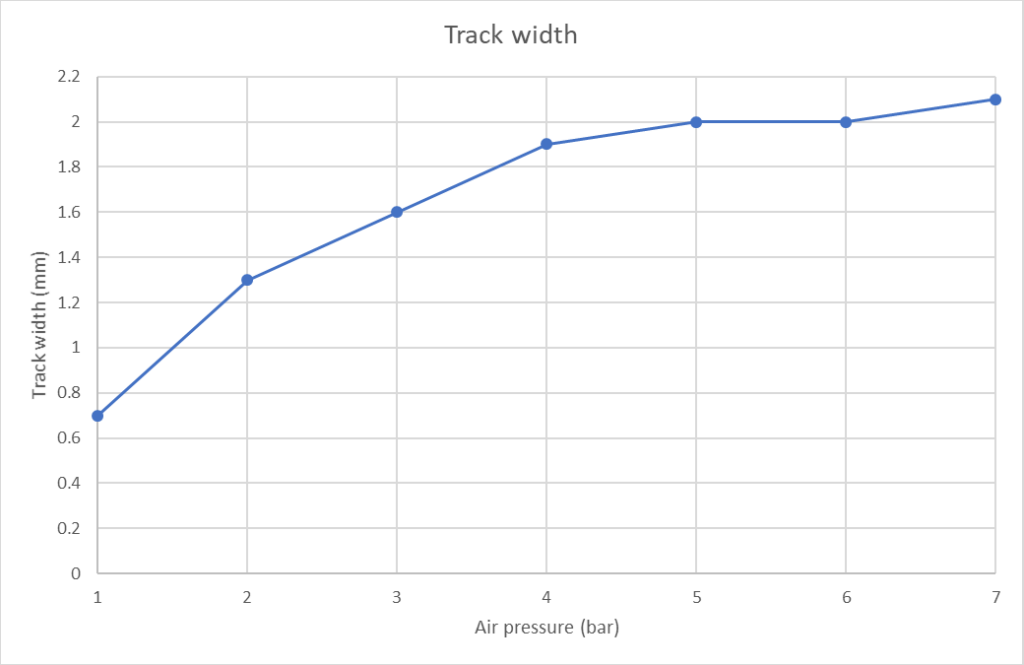

Figure 4-8 Results of track widths against different air pressures

The results in figure 4-8 indicate that the pressure of the dispenser should clearly be between 1 and 2 bars for the correct amount of ink flow. The results also show that above 4 bars the flow of ink does not increase as rapidly as lower than 4 bars which ties into the nozzle size used in the syringe tip.

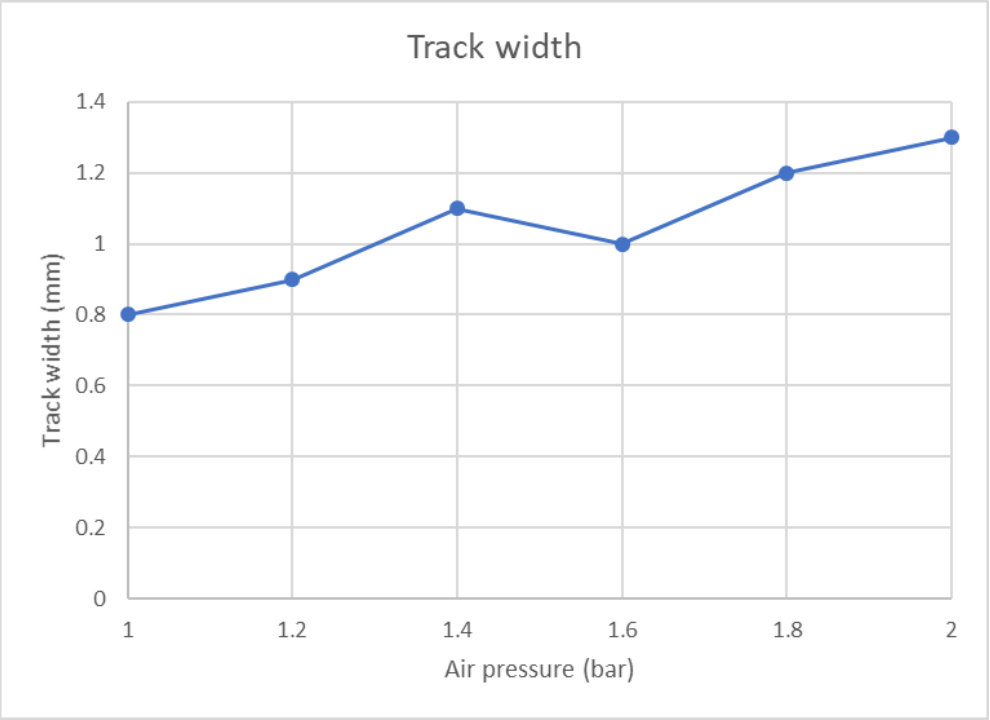

Figure 4-9 Track widths for pressures between 1 - 2 bars

Another test was conducted to focus on pressures between 1 and 2 bars, and the results shown in figure 4-9, show that the best pressure is between 1.2 and 1.8 bars. This experiment could show some human error as the measuring tool for the widths of the tack is a standard ruler; therefore, the pressure can be varied within this range to acquire best results in each print.

4.5 Improvements

Once all the calibration and testing was done, the actual printing of the antennas was done. During the printing process of both extruders an issue was noticed, as the extruders were moving between print commands; i.e. when an extruder finished printing a section of the model and then moves to another section, the tips of the extruders were scrapping on the previously printing section. Especially on the silver ink that has not yet cured, the tracks would be destroyed.

The solution was to lower the platform by a certain amount as to allow the extruders to pass without touching the model. This was achieved by writing a script in the slicing software of the printer, during the retraction section of the printing stage the platform would lower by 5 mm, the tool head would move to the next co-ordinate to

print and then the platform would rise to resume printing. This also helped with oozing on the extruder tips; when the extruder would stop extruding material there would be a small amount of material hanging on the tip of the nozzle and if the platform would not be lowered that small amount of material would get left on the model.

The ink that is used in this project, as mentioned previously cures in room temperature when exposed to air, throughout the printing with the second extruder the tip of the syringe would get blocked and covered with cured ink. To solve this issue Voxel8 who manufacture the ink, also sell a capping solution, which is supposed to be used when the extruder is not in operation. The solution is a combination of chemicals to stop the ink on the tip of the syringe to cure; it is supposed to be applied through a sponge covering the tip of the syringe. Voxel8's printer has a mechanism that clamps two pieces of sponges dipped in the capping solution around the tip of the syringe, as this was not feasible for the current printer, therefore a different solution was proposed.

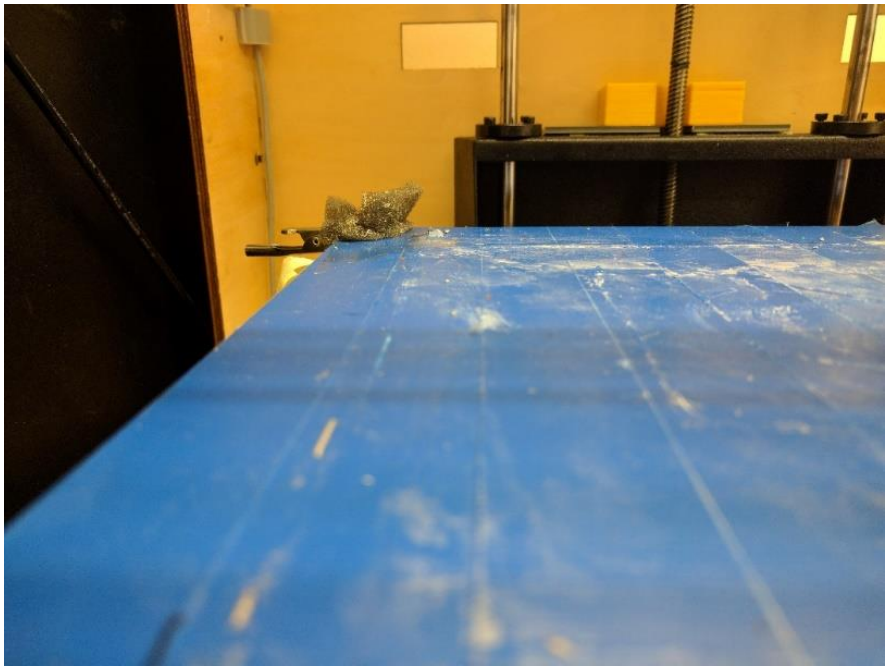

Figure 4-10 Printers' bed platform

One corner of the platform had a small sponge mounted to it and every few prints, two drops of the capping solution was used on the sponge. A short script was written

to command the tool head to move to the corner and wipe the tip of the syringe in the sponge. A combination of G-codes allowed the syringe to be wiped every time the second extruder did a retraction command.

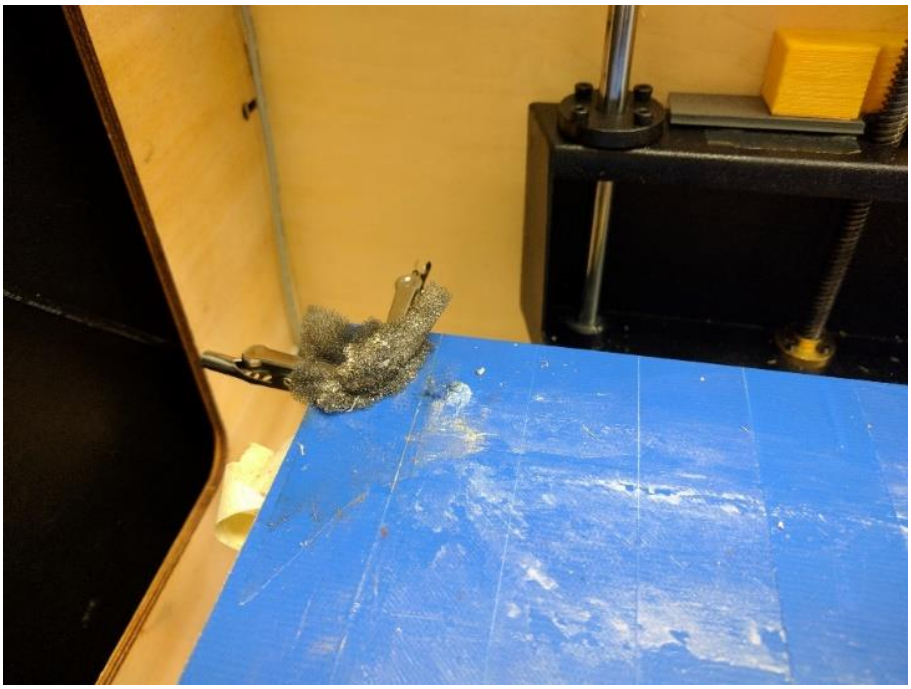

Figure 4-11 Placement of the syringe wiper on the platform

DC resistance measurements

The quality of the silver ink had to be tested; a small model of a microstrip was designed. The testing of the microstrip is shown in figure 4-12, it was printed in order to enable a quick and convenient assessment of the quality of the printed samples, with a low value for the resistance would indicate a good quality print with good conductivity.

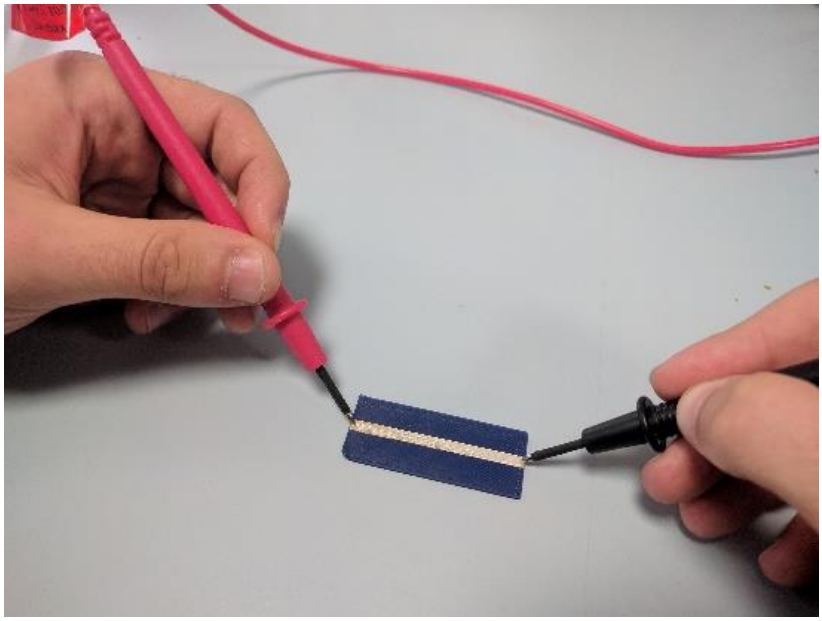

Figure 4-12 Printed microstrip line testing

Several layers were tested; the relationship between the measured DC resistance and the number of ink layers is illustrated in figure 4-1.

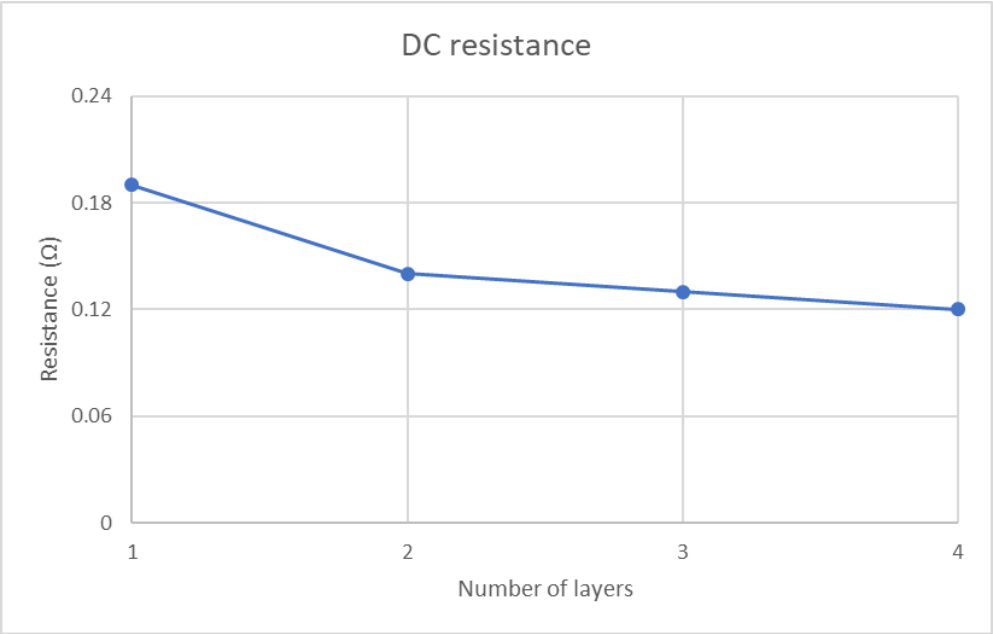

Figure 4-13 Results of the varying layers against the resistance

It was assumed that there was not a significant difference between the measured resistance and the number of ink layers after the second layer of ink.

References

1. [online] http://www.mbot3d.com/ [Accessed 30 Aug. 2017]
2. [online] https://www.makerbot.com/ [Accessed 30 Aug. 2017]
3. [online]

   https://www.matterhackers.com/articles/getting_started_with_3D_printing

   [Accessed 30 Aug. 2017]
4. [online] https://ninjatek.com/ [Accessed 30 Aug. 2017]
5. [online]http://www.techconsystems.com/en/fluid-dispensers/digital-fluid-dispensers/basic-digital-dispensers/ts250-digital-fluid-dispenser/?sef_rewrite=1 [Accessed 30 Aug. 2017]
6. [online] https://www.pololu.com/file/0J450/A4988.pdf [Accessed 30 Aug. 2017]
7. [online] www.voxel8.co [Accessed 30 Aug. 2017]
8. [online] http://reprap.org/ [Accessed 30 Aug. 2017]
9. [online]https://www.pololu.com/file/download/a4988_DMOS_microstepping_driver_with_translator.pdf?file_id=0J450 [Accessed 30 Aug. 2017]

Chapter 5 – Frequency Selective Surfaces

5.1 Element design

The initial design of this FSS was the loaded cross dipole element and was designed for the frequency of 2.45 GHz range. The FSS structures were modelled and simulated using Computer Simulation Technology Microwave Studio® (CST), the total size of one of the elements was 30 x 30 mm. The dimensions of the element is shown in figure 5-1 and table 2, along with the simulated transmission response of the element in figure 5-2.

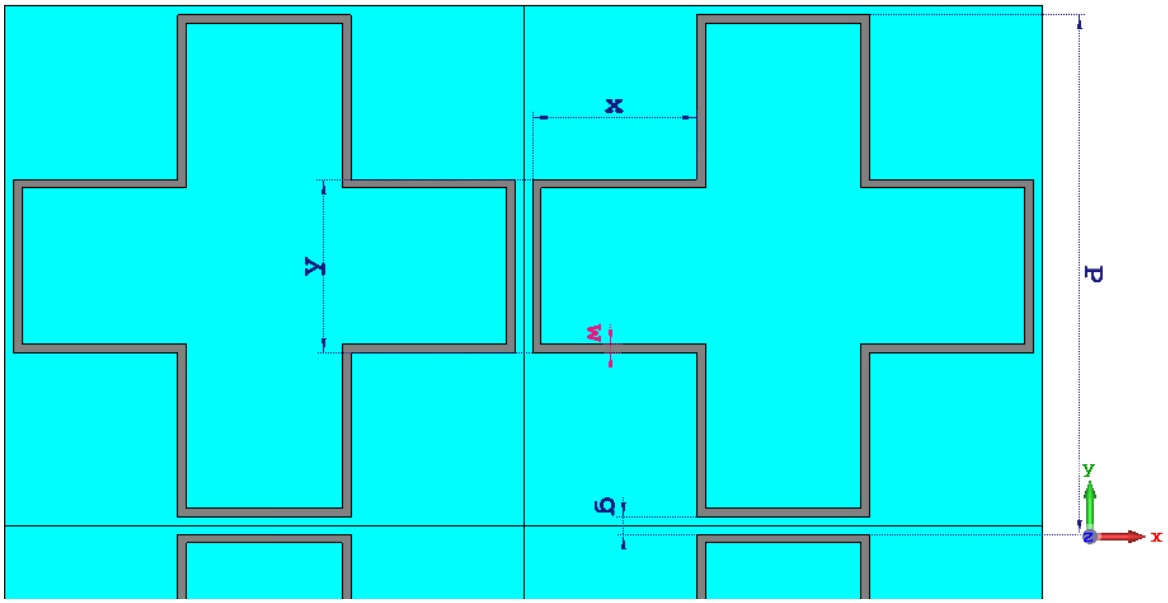

Figure 5-1 Loaded cross dipole design

Table 2 Dimensions of the loaded cross dipole element

	X	Y	G	W	P
DIMENSION (MM)	9.5	10	1	0.5	30

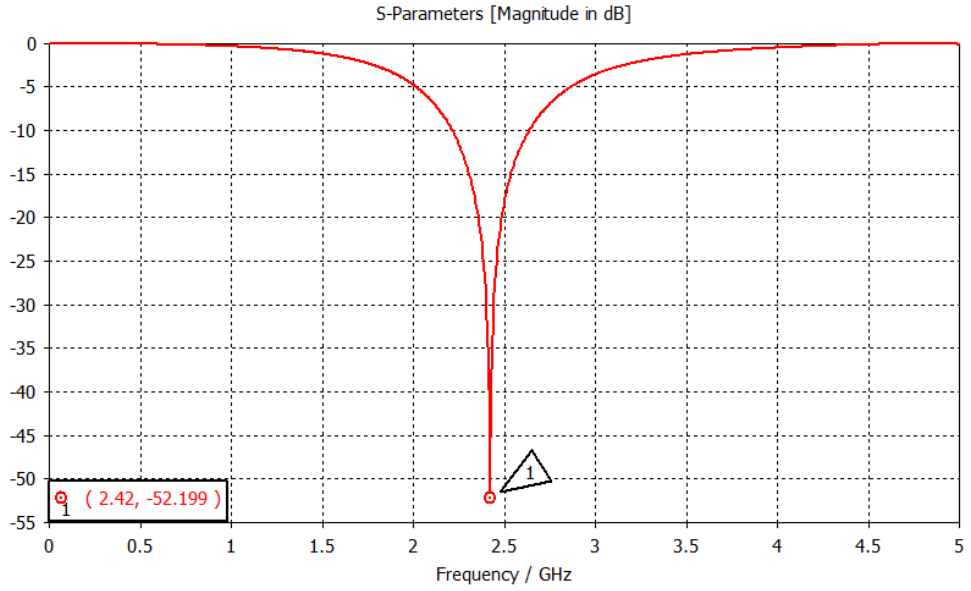

Figure 5-2 Simulated transmission response of the loaded cross dipole FSS

To get reliable results the FSS must include a sufficent number of elements, therefore the elements were duplicated to the maximum number the printers platform can fit in

one print, the platform has a dimension of 200 x 200 mm but with the addition of the second extruder the available print area decreased to 180 x 150 mm. The FSS consisted of an array of 5 x 6 elements to make use of the entire platform.

Due to fabrication issues discussed in the fabrication section, another element shape was designed. The design of the second element was a square based cell which initally had the same frequency as the first element but then increased to the frequency of 2.71 GHz due to the issues in the fabrication. Each cell was reduced, the dimensions of this element is shown in figure 5-3 and table 3.

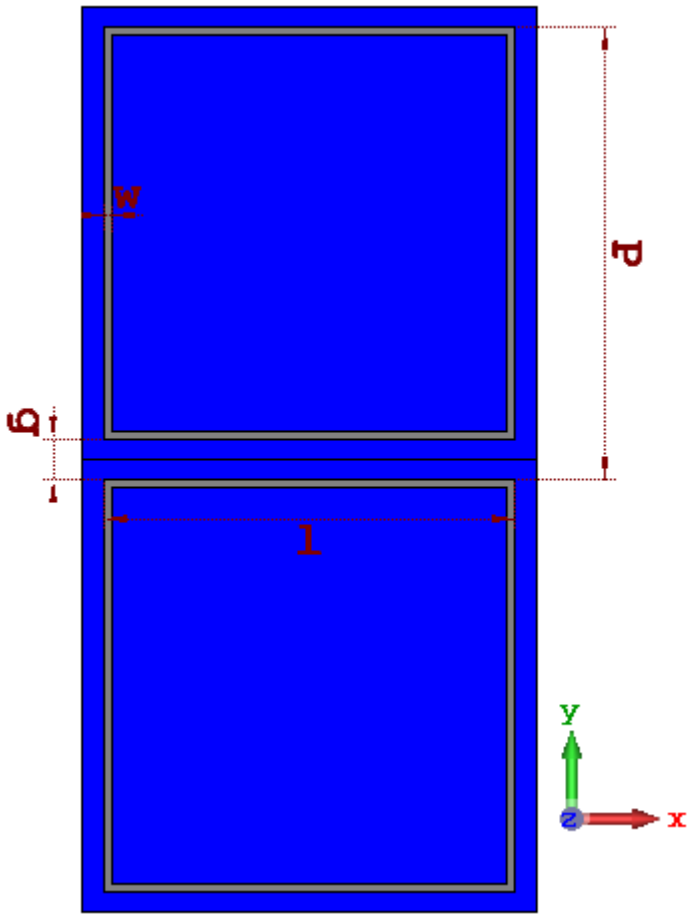

Figure 5-3 Square based element design

Table 3 Dimensions of the square based element

	L	W	G	P
DIMENSION (MM)	26.4	1.2	3.1	29.5

Along with the resonant frequency and the bandwidth of the structure, another characteristic of the FSS is as important which is the stability of the resonant frequency with respect to the incident angle of the plane wave. It can be seen in figure 5-4 the variation of the resonant frequency due to the incident angles for transverse electric (TE) 45 and transverse magnetic (TM) 45 polarizations, the resonant frequency of both TE and TM are slightly increased. The TE polarization is slightly more stable than the TM mode.

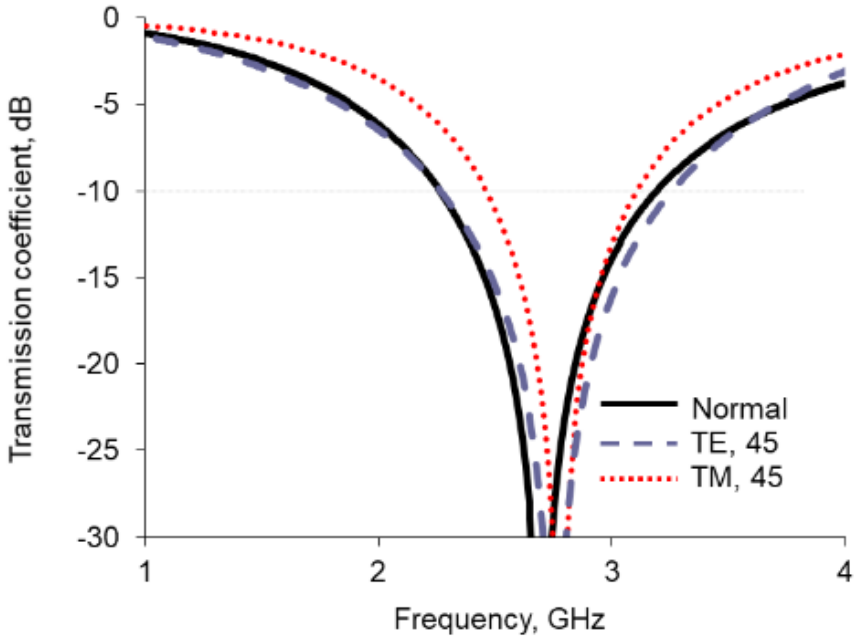

Figure 5-4 Simulated transmission coefficient of normal and different angles of incidence

Parameter study

The dimensions were calculated by conducting a parameter sweep within the CST Studio software. A parameter sweep can show how slight changes within the dimensions can change the resonant frequency. As the fabrication process can cause some of the parameters to slightly change because the printer is calibrated to +- 0.5 mm.

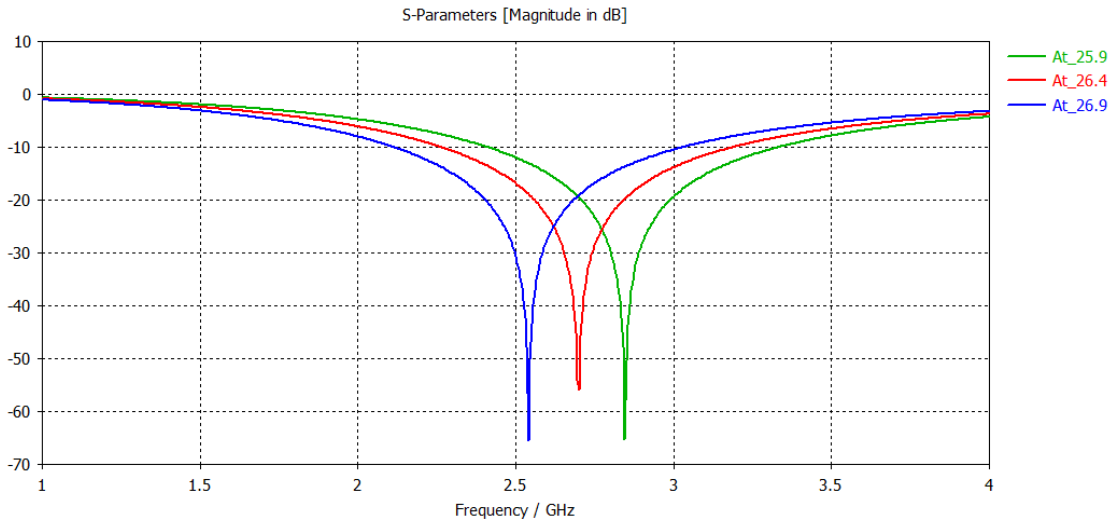

Figure 5-5 Frequency change from element length change

When increasing the length of the element it represents an increase of both the inductance and capacitance. When looking at equation 8.1, it clear that as the capacitance and the inductance increase it results to a lower resonant frequency. Figure 46 shows the variation of the resonant frequency when there are changes to the element length. The changes to the length are from 25.9 mm to 26.9 mm with the desired length of 26.4 mm, at 25.9 mm resulted in the increase of the resonant frequency by 4.8% and at 26.9 mm a decrease by 6.3%.

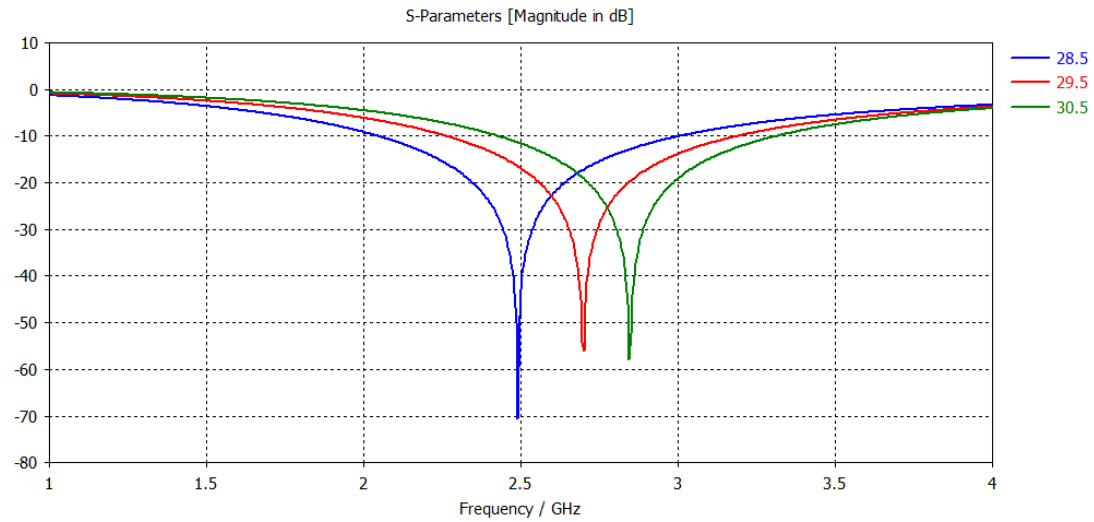

Figure 5-6 Transmission response for changes in the gap between the elements

Figure 5-6 represents the effect of the resonant frequency when there is a change in the gap between the elements. The dimensions of the square loop stays the same size

as in table 3, the increased gap is achieved by increasing the substrate size. Therefore, the periodicy of the array increases and the equivalent capacitance is reduced. As the gap increases, it causes the resonant frequency to increase and the bandwidth to decease. With an increase of 0.5 mm gap, the resonant frequency increases by 4.8% and a decrease of 0.5 mm gives a 8.2% decrease in frequency.

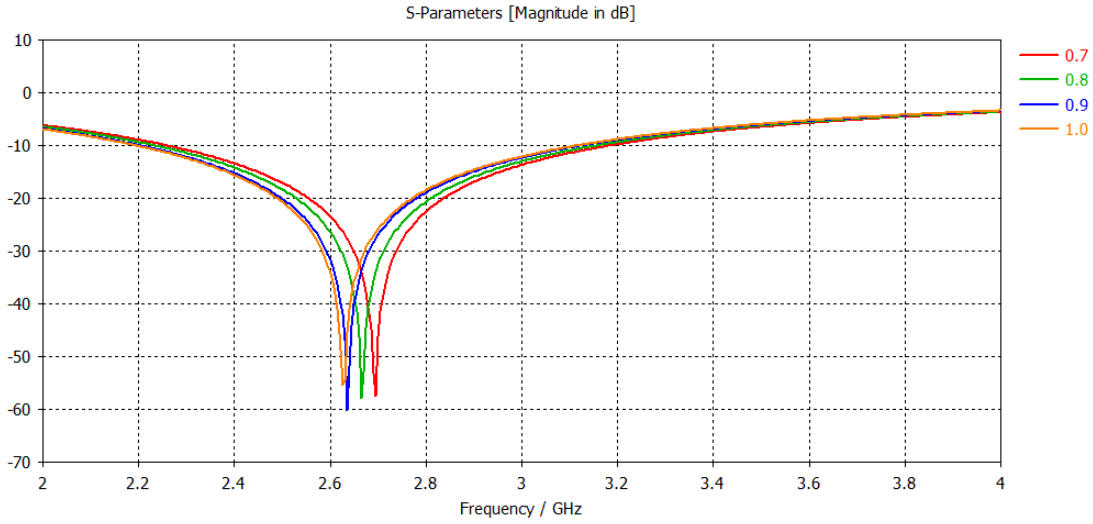

Figure 5-7 Transmission response due to changes in thickness of the substrate

Figure 5-7 shows the variation in the resonant frequency due to the change in the thickness of the substrate. The resonant frequency does not have a major change when the thickness of the substrate increases.

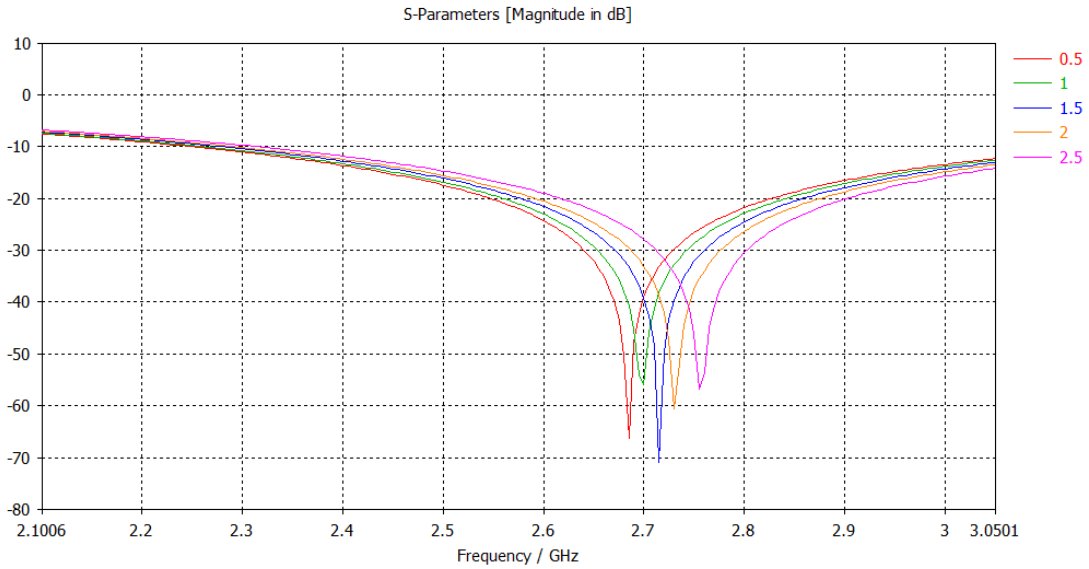

Figure 5-8 Transmission response due to changes in the curvature of the corners

Figure 5-8 shows the variation of the resonant frequency due to the change in the curvature in the corners of the square element. The changes in the frequency increase by 1.8% for bents of 2.5 radients and decrease by 1.1%. Due to the fabrication process not being micron perfect, when the silver ink is printed onto the substrate some imperfections can occur, for example, the corners of the square element are not as sharp as expected. Therefore, these errors must be investigated in the model of the simulation as seen in figure 5-9.

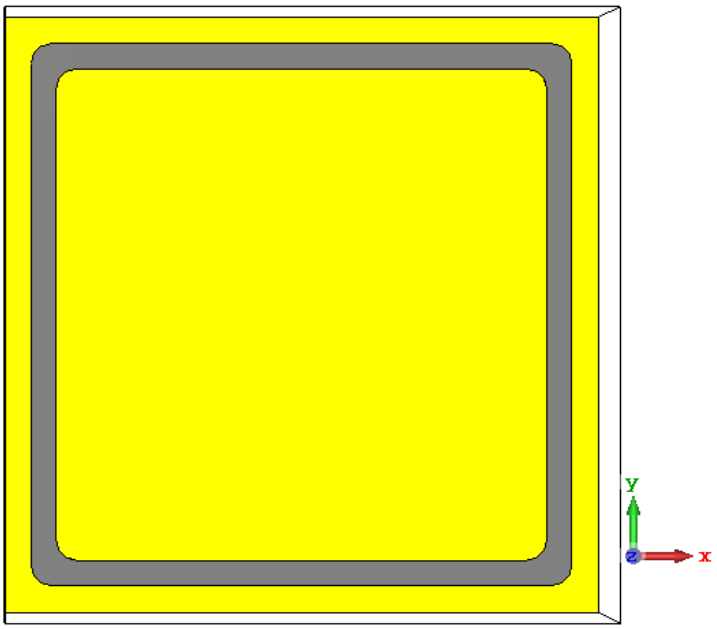

Figure 5-9 Illustrated model of the curvature of the square element

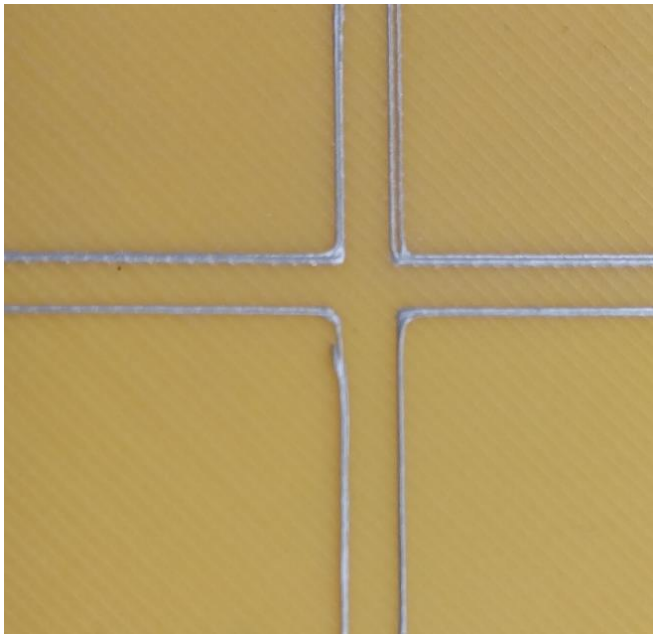

Figure 5-10 Printed corners of the element

With the new element design, the total size of the array was reduced to 177 x 147 mm, which helped in the fabrication process. The thickness of the FSS substrate was set to 0.8 mm, this was modelled to get the substrate as thin as possible without breaking. The substrate had a 100% infill to achieve full strength, and give the calculated permittivty constant. The full array can be seen in figure 5-11.

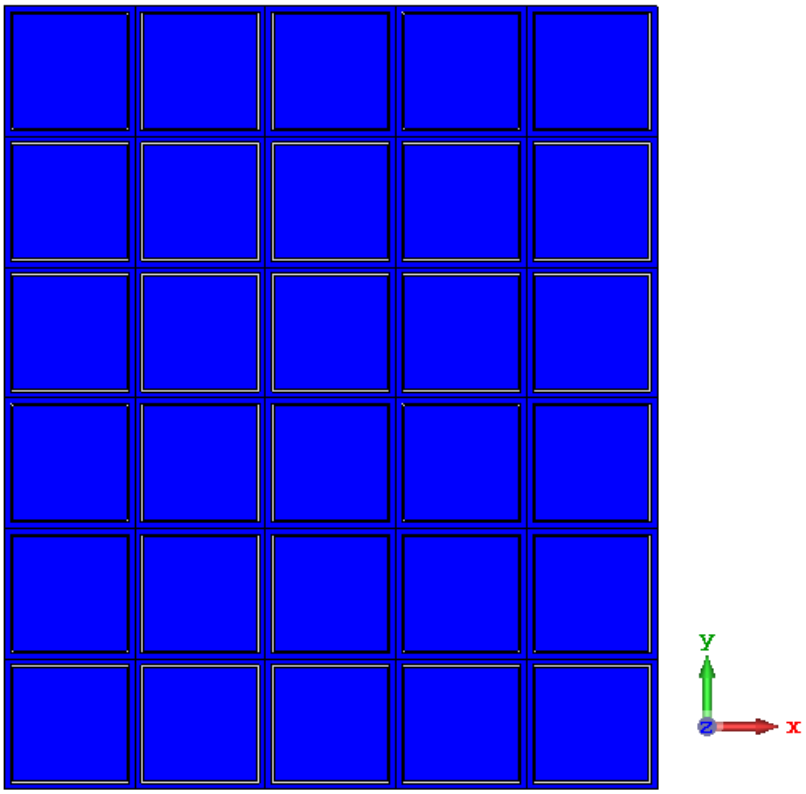

Figure 5-11 Full array of the elements that can fit on the print bed

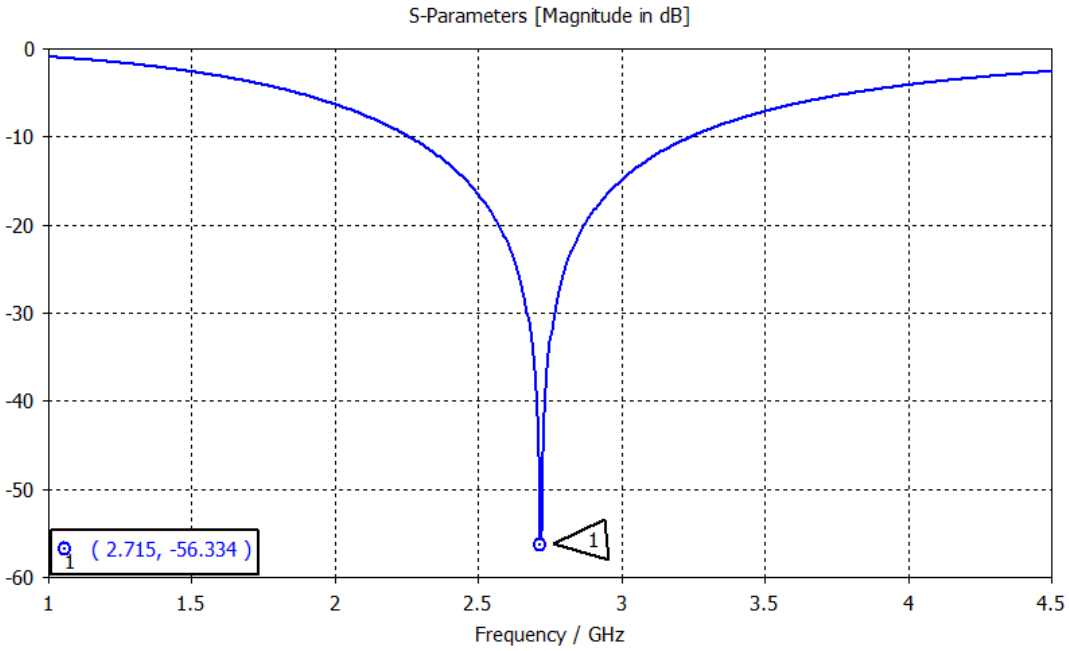

Figure 5-12 Simulated transmission response of the square based FSS design

The simulated reflection coefficient is shown in figure 5-12 with a target frequency set at 2.715 GHz and a bandwidth of 30% at the -10dB.

5.2 Fabrication

The entire FSS was printed on the modified FDM printer, this was the largest print done. The substrate was printed using yellow plastic PLA filament from 3D FilaPrint, with a substrate thickness set at 0.8 mm and 100% infill.

The printing of loaded cross dipole design created issues in the print quality and the depositing of the silver ink. Due to the selected design, the printer showed issues when printing the multiple corners of the element along with the substrate corners. The term ‘warping’ in 3D printing describes the lifting of the printed plastic off the platform in the middle of the print process. This tends to be seen at the corners of the printed model, this issue occurs when the plastic material drastically lowers in temperature and therefore peels off the platform. The solution to this issue is to use a heated platform to therefore lower the speed of temperature change between the molten printed plastic and the platform. The corners of the heated platform are usually the first area to reduce in heat efficiency and therefore will be cooler than the rest of the platform, as this model has the substrate extended to the absolute corners of the platform; it was subject to warping which can be seen in figure 5-13. To fix this issue the total size of the substrate in the second element was reduced.

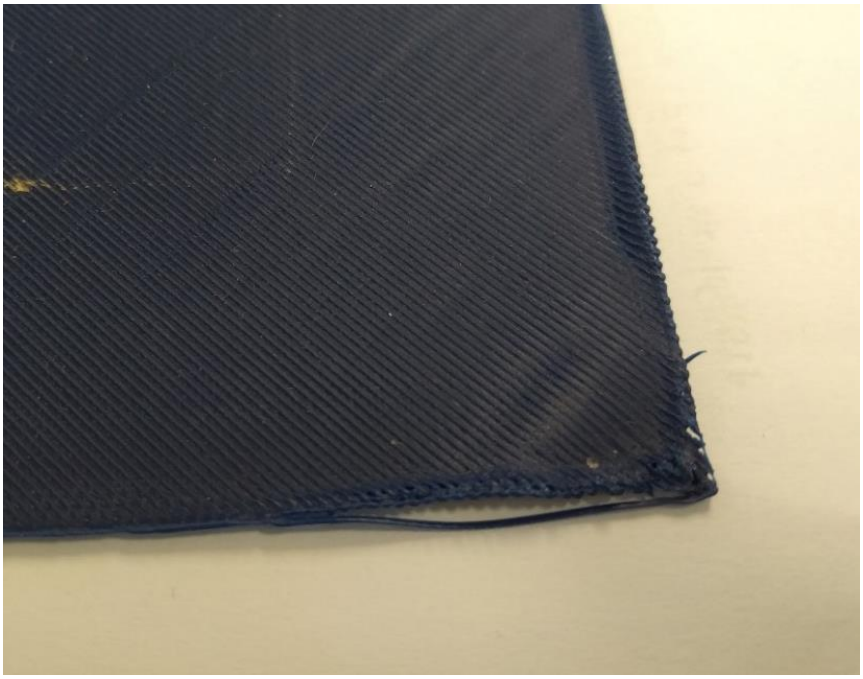

Figure 5-13 Warping in the fabrication of the substrate

The other issue was with the silver ink printed definition, where some of the corners of the loaded cross dipole were not fully filled with silver ink as seen in figure 5-14. This is an issue with the tolerance of the printers' silver ink and its nozzle. This was randomly seen along the FSS structure, but was always seen at the corners of the element and therefore was hard to control. The structure was then modified to a simpler design to address these issues.

Figure 5-14 Silver ink depositing issue on the corners of the element

The second design substrate measured 177 x 147 mm, which used 89% of the build platform. The layer height of 200 microns was used which gave a total of four layers of plastic which was placed in the centre of the build platform. The layer height of the silver ink was set to 200 microns which was one layer, this was enough to ensure that there was continuity and the resistance levels were reliable enough without adding more ink. The pressure of the pneumatic dispenser can be tweaked accordingly, the pressure was set to 1 bar when testing the first design of the FSS (loaded cross dipole) and was observed that the ink deposited was partially patchy with miniscule breaks along the edge. The pressure was increased to 1.65 bar to address this issue and yielded better results. The plastic substrate printed with no issues, although the silver ink had some minor imperfections on a few of the corners of the elements. Some of the corners of the elements had small holes from missing silver ink when it was being printed, this was amended by adding a small amount of silver ink after it finished printing.

5.4 Testing

The FSS was tested in a plane wave chamber, the FSS was placed in an aperture in a large absorbing screen with the size of 2.5 x 2.3 m, the screen was supported by wheels to allow for easy screen rotation. Two probe antennas were placed about 1 m on either side of the FSS, which swept over a frequency range 1 – 4 GHz. The FSS screen size measured 280 x 168 mm, which consisted of two prints of the structure, placed together side by side and then glued. The transmitting and receiving antennas were positioned at the height of the centre of the aperture as seen in figure 5-15.

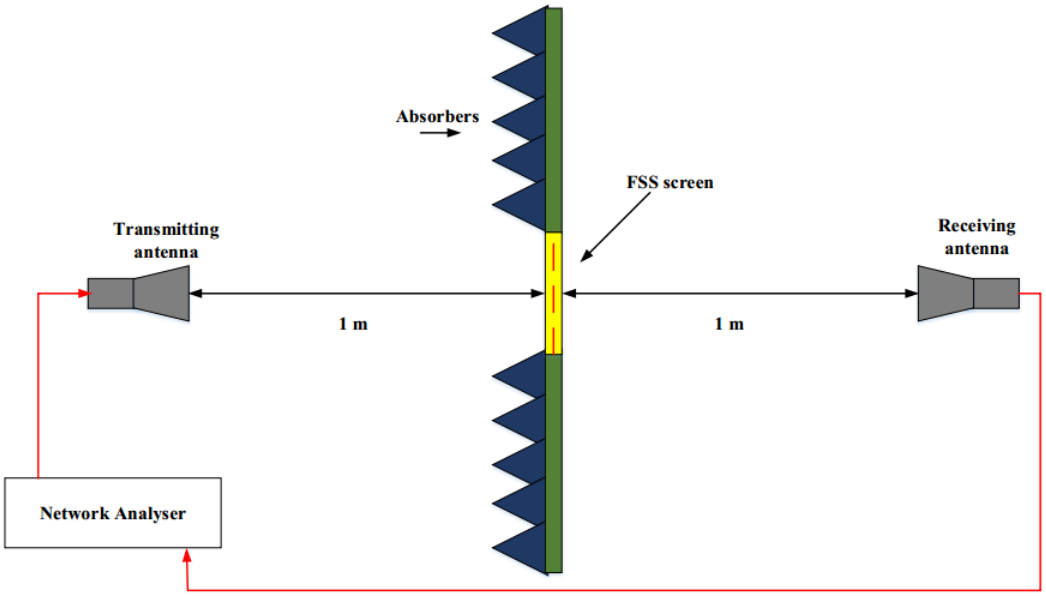

Figure 5-15 Testing rig for the FSS

A Rohde & Schwarz ZVA50 VNA which operates in the frequency range of 10 MHz – 50 GHz was used and the transmitting power was set at 10 dBm. Before the FSS was mounted an initial open space, calibration was taken to ensure the amount of any equipment losses such as within the cables or the antenna probes. This is also conducted when the screen is rotated for different angles. The mounted FSS on the absorbing screen is shown in figure 5-16.

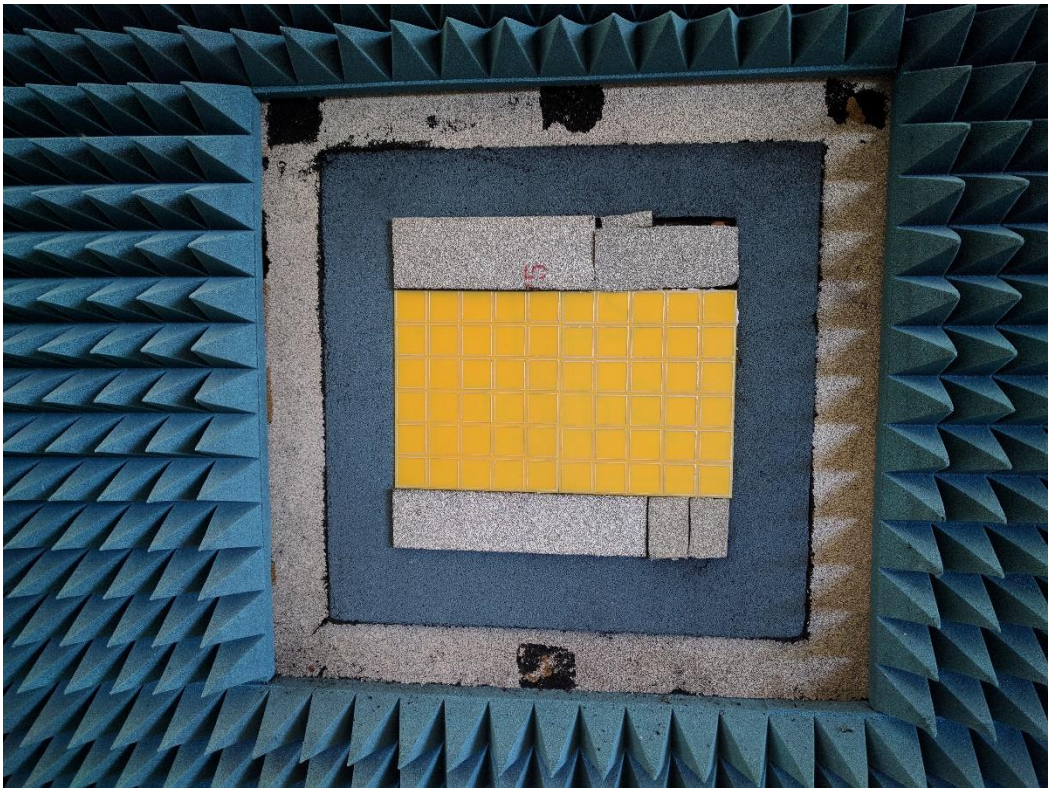

Figure 5-16 FSS mounted onto the aperture

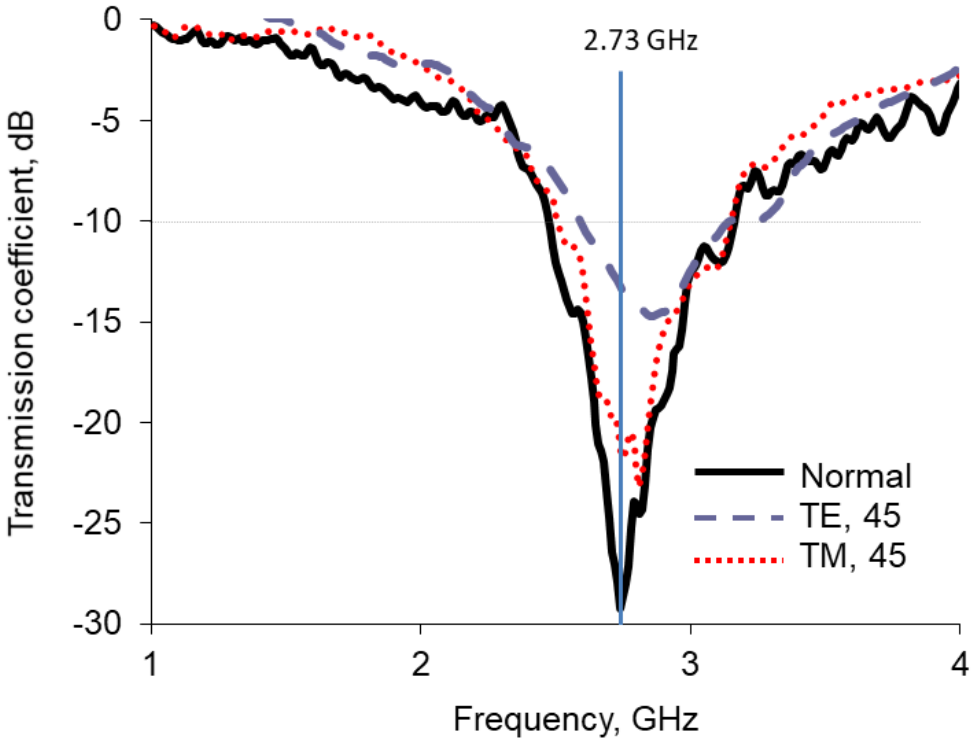

Figure 5-17 Measured transmission coefficient of the printed FSS

The measured transmission response of the square looped FSS can be seen in figure 5-17; the response shows that it is close to the simulated results. At the normal mode, the response measured at 2.73 GHz with about -27 dB in depth and a bandwidth of 17.5% at the -10 dB level, there is a slight shift in the TE 45 degrees and the TM 45 degrees but well within the acceptable results.

5.3 Conclusion

The use of a low-cost open-source FDM 3D printer with a pneumatic dispenser has been possible and proven through the results collected from the VNA, that it is suitable option to fabricate FSS structures. Being a low-cost and relatively fast process, this configuration can be advantageous compared to traditional methods. The substrate was fabricated using inexpensive polylactic acid filament (PLA) and the elements were printed with a silver ink dispensed by a pneumatic dispenser, and only required one layer of ink for sufficient continuity. The final FSS structure operated at about 2.73 GHz and offered reasonable angular stability to angle of illumination.

Some issues were encountered in the beginning but then were addressed, this expressed the limitations of the proposed technique through the size at which the FSS can be printed on and the minimum size features of the elements.

The fabrication method yielded satisfactory results compared to the simulated ones with good angular stability, there was a shift in the frequency and this could be due to a combination of small errors in the fabrication and measurement. As seen in the parameter study, a slight change of less than 1 mm in the element length can alter the frequency by about 300 MHz. Not to mention in the testing of the FSS, there are some losses, such as in the coaxial cables.

Overall, there are advantages in using 3D printing for the fabrication of FSS and further study into different shapes of elements can discover more possibilities in 3D printing FSS structures.

Chapter 6 – GPS Antenna

6.1 Theory

The next fabricated antenna is used as a Geo Positioning Service (GPS) receiver. GPS signals are very weak and therefore require specific demands on the antenna. Antennas used for GPS need to cover a few requirements such as:

- A low level of directivity
- High gain
- Good matching between cable and antenna impedance
- Filter

The GPS signals are known to be using right hand circular polarization (RHCP). The most common antenna type used in GPS signals is the well-known patch antenna. As mentioned in the previous chapter, patch antennas are flat with a metallic patch on top of a grounded substrate. The patch antenna acts as an ideal antenna because GPS receivers are normally mounted on flat surfaces such as, on top of a car and patch antennas can have a very high gain, especially if they are mounted on top of a large ground plane.

Another type of antenna that could be used for GPS signals is a helix antenna, which are typically used in applications where the antenna can be mounted in multiple orientations. The size of the antenna depends on the value of the dielectric constant

that fills the space in between the active parts of the antenna, if there is a high dielectric constant, the antenna has a much smaller form factor. The gain of the antenna will decrease as the antenna gets smaller in size.

The type of antenna will depend on the application, if it is supposed to be used in a hand-held device, the antenna must be designed in a way that the optimum antenna orientation collects signals its natural operation. It is also noted that the antenna gain is directly related to the size of the antenna aperture, therefore the helix antenna will need to be much greater than the patch antenna. The advantages and disadvantages are highlighted in the table 4.

Table 4 Differences between the use of a patch and a helix antenna for GPS applications

Patch antenna	Helix antenna
+ High gain	+ Omnidirectional
+ lower cost	+ robust
- lower isolation in the feed and antenna	- requires more space
	- Cost

A patch antenna is selected with a main target frequency of 1.575GHz.

6.2 Element design and simulations

The design of the antenna included a rectangular patch element on a square substrate, the substrate measured to 100.35 mm x 100.35 mm and a thickness of 3 mm. The antenna was designed to match 1.575 GHz band using CST. The dimensions of the whole design are given in figure 6-1 and table 5.

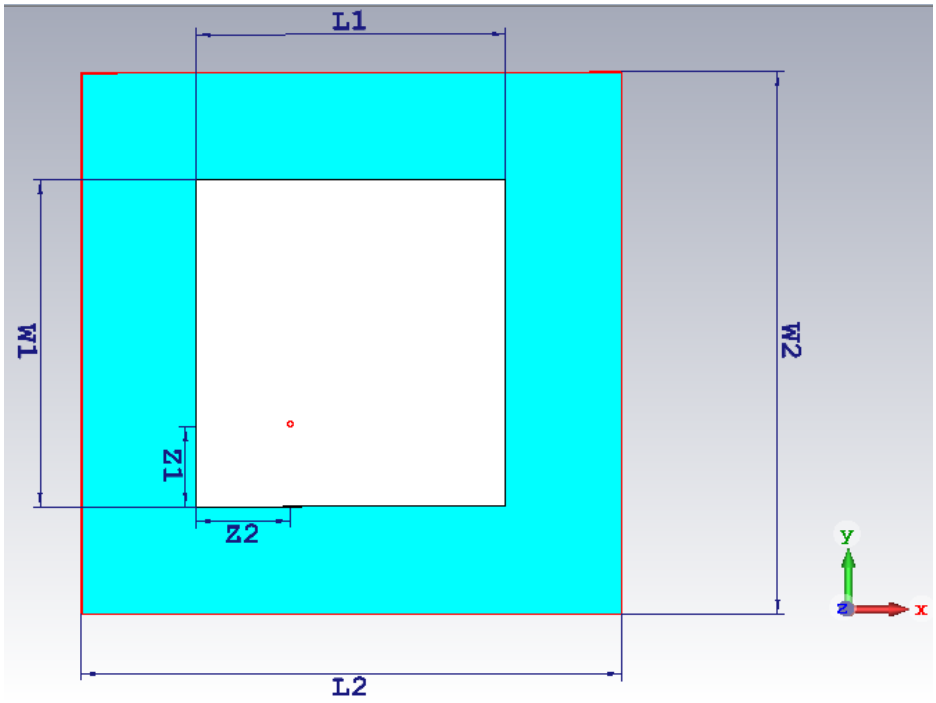

Figure 6-1 Design of the patch antenna

Table 5 Dimensions of the patch antenna

	W1	*L1*	*W2*	*L2*	*Z1*	*Z2*
Dimensions (mm)	60.6	57.42	100.35	100.35	17.32	15.29

The dimensions of the patch and substrate were calculated to fit the frequency of 1.575 GHz. The circular polarization is created by having the patch element in a rectangular shape therefore allowing the currents to flow in a circular pattern. The probe is placed at the bottom left corner of the patch to obtain the required right hand circular polarization (RHCP).

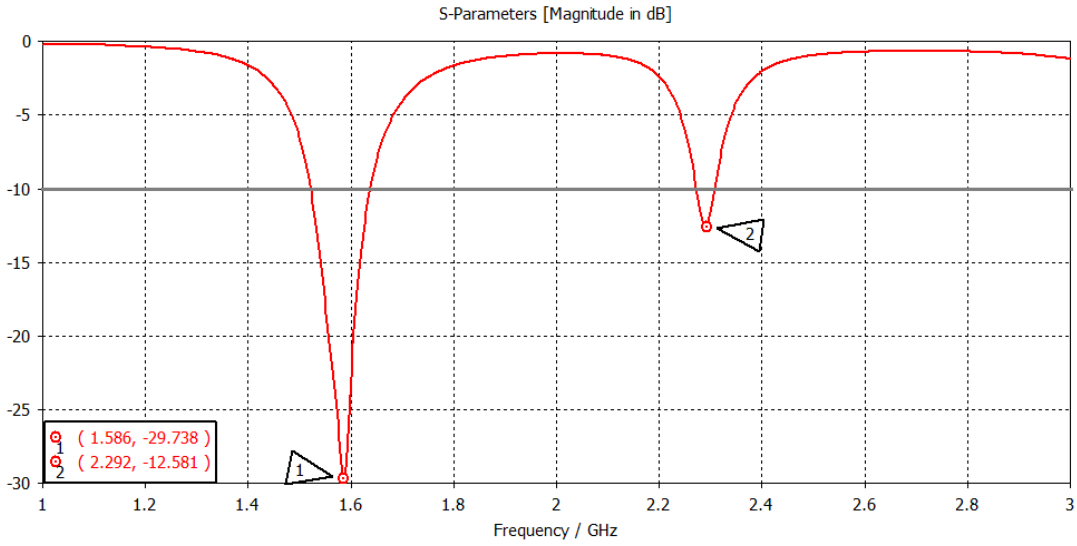

Figure 6-2 Simulated reflection coefficient of the patch antenna

The simulated reflection coefficient is represented in figure 6-2; the antenna was designed to resonate at two frequencies. The first main resonance is at 1.575 GHz with – 10 dB bandwidth from 1.522 GHz to 1.637 GHz giving 115 MHz and a second resonance is found at 2.29 GHz. The simulated axial ratio and the radiation patterns are also shown in figure 6-3 and 6-4 respectively.

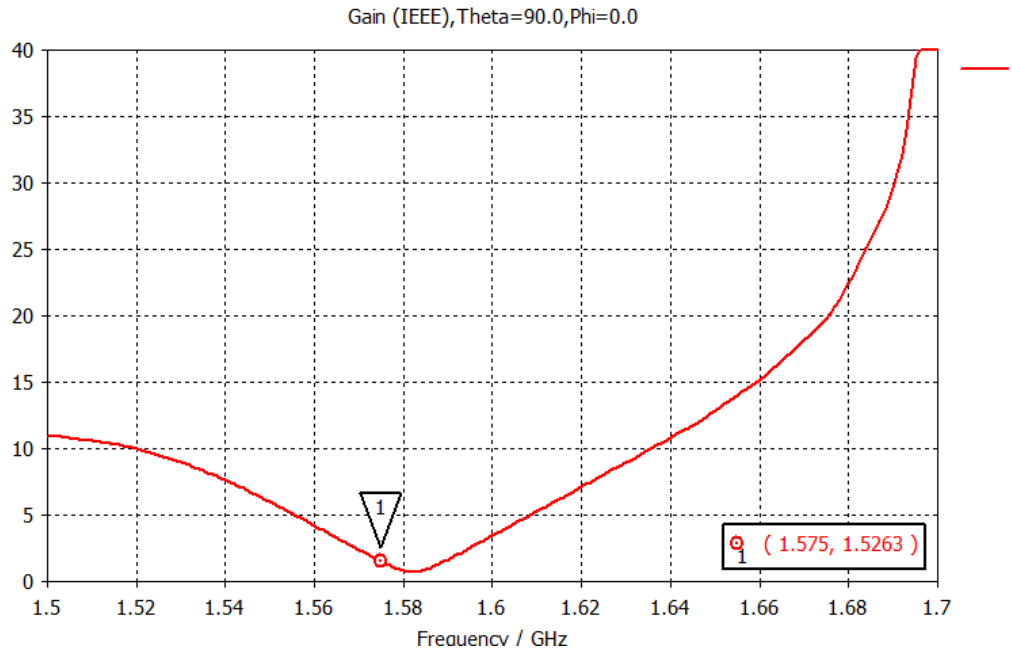

Figure 6-3 Simulated axial ratio of the patch antenna

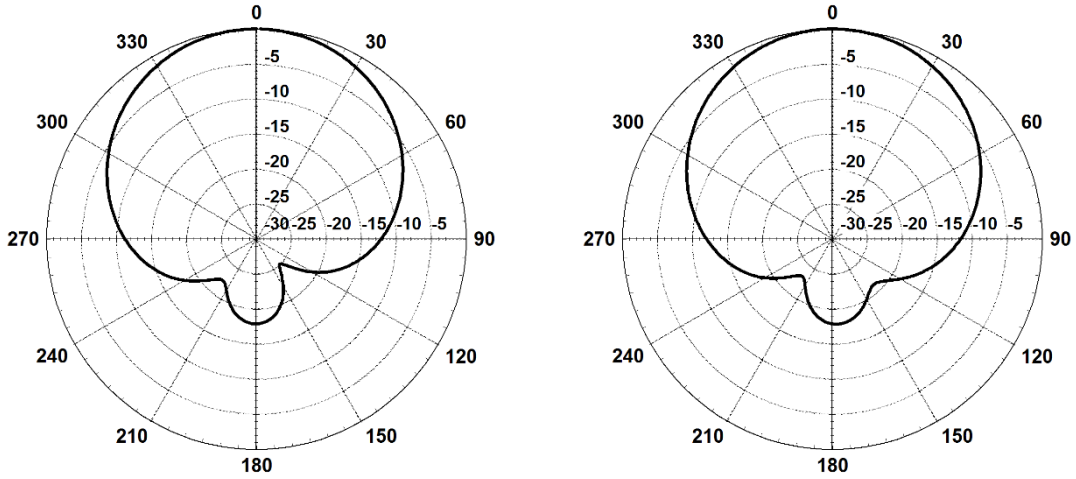

(a) (b)

Figure 6-4 Simulated radiation patterns (a) *xz* plane, (b) *yz* plane

6.3 Fabrication

The GPS antenna including the substrate and the patch was fabricated on the modified FDM printer in a single process. The substrate of the antenna was fabricated using blue plastic PLA filament from 3D FilaPrint, the model was printed with a layer height of 100 microns and an infill at 100%. The substrate had a thickness of 3 mm at a layer height of 100 microns gave a total of 30 layers, the 100% infill was selected as to give an air tight substrate with the relative permittivity of PLA being 2.4. The substrate was printed at 50 mm/s, which is considered high, it was chosen due to the design of the model, being a simple rectangular shape, the increased speed, should not affect the resolution of the print. In addition, the speed can help the infill create a perfect air tight seal as the molten plastic can seam together faster.

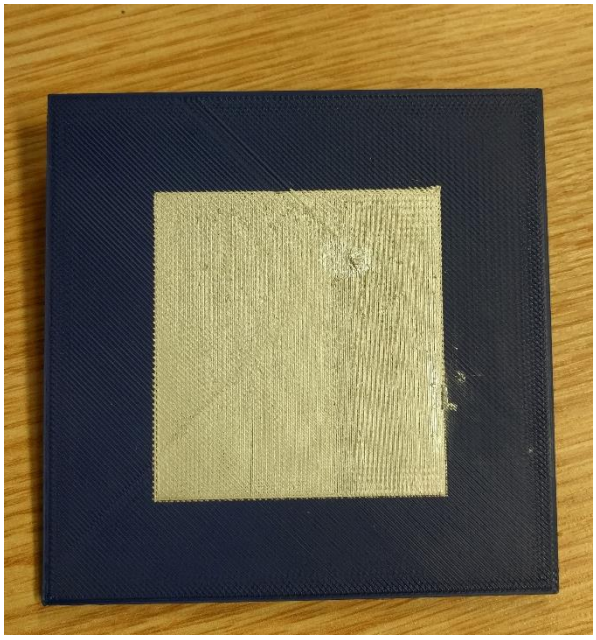

Figure 6-5 Printed patch antenna

After the substrate and the antenna are printed, a ground plate is placed on the underside of the substrate with its exact dimensions. The ground plane is secured to the substrate by using a thin 100-micron layer of double sided tape. A hole was drilled into the ground plane at the location of the 1.5 mm pin hole of the substrate to mount the connector. A SMA connector was placed in the hole and soldered onto the ground plane, on the topside a small amount of silver epoxy glue was used to connect the patch antenna to the pin connector.

6.4 Testing

The patch antenna was tested for the resonant frequency using the VNA and the axial ratio and radiation patterns were measured in an anechoic chamber. The result is shown in figure 6-6 with the simulated values.

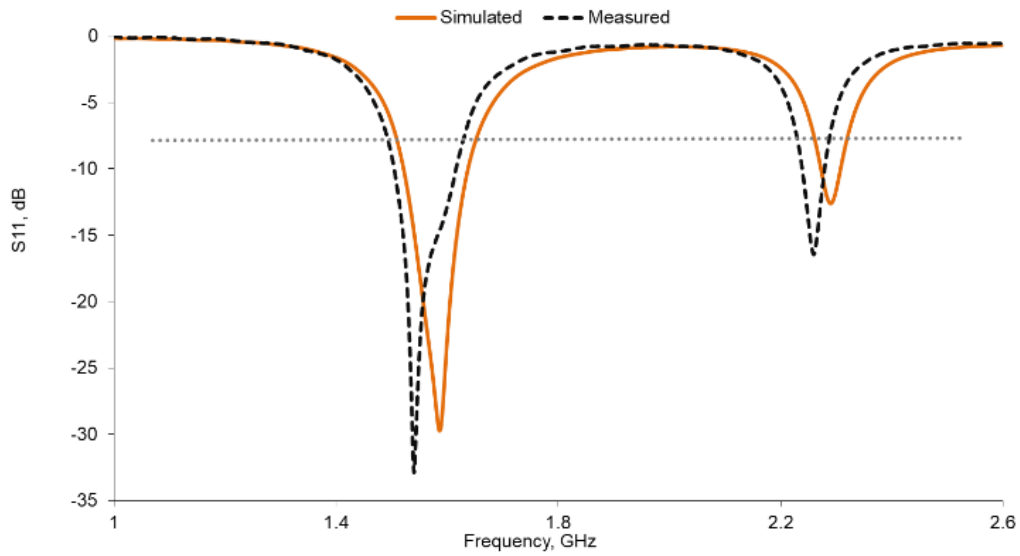

Figure 6-6 Simulated and the measured S11 results

The figure 6-6 shows that the simulated and measured results compared very well, the results turned out to be slightly shifted to the left with the first resonance at 1.54 GHz with – 10 dB bandwidth from 1.505 to 1.615 GHz that gives 110 MHz. The second resonance can also be found at 2.25 GHz, which is only slightly lower than the simulated 2.29 GHz. The axial ratio of the circularly polarised GPS antenna at 1.575 GHz is shown in figure 6-6. The radiation patterns were also collected and are shown in figure 6-9.

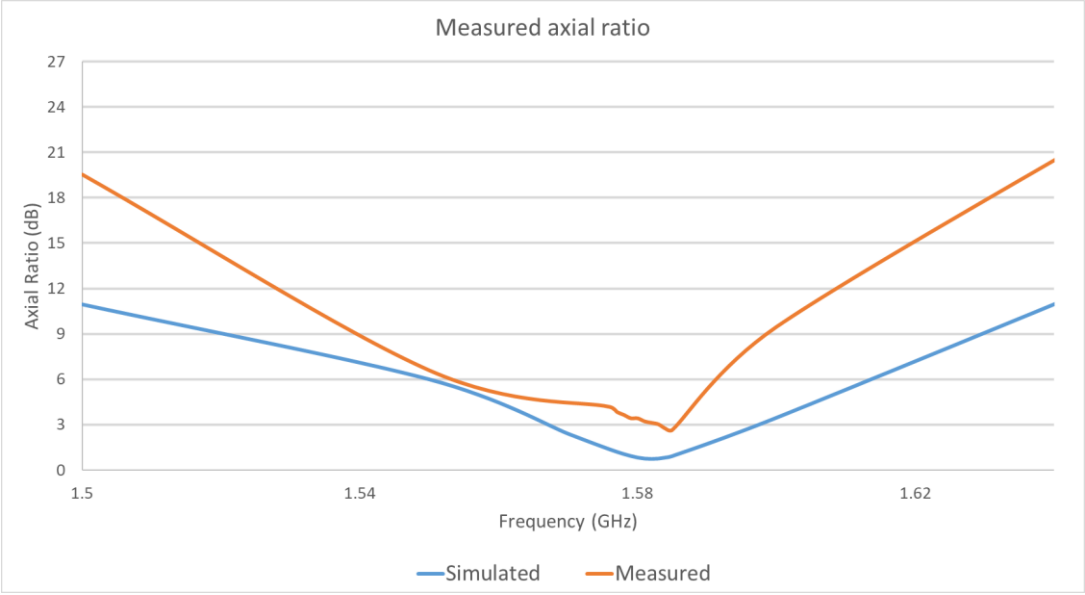

Figure 6-7 Simulated and measured axial ratio results

The results from the axial ratio show that there is a slight shift to the right, the axial ratio standard for an acceptable circular polarized antenna is at 3dB. The measured results showed that it crossed 3dB at 1.582 GHz which is slightly higher. This could be due to the tolerances in the measuring device.

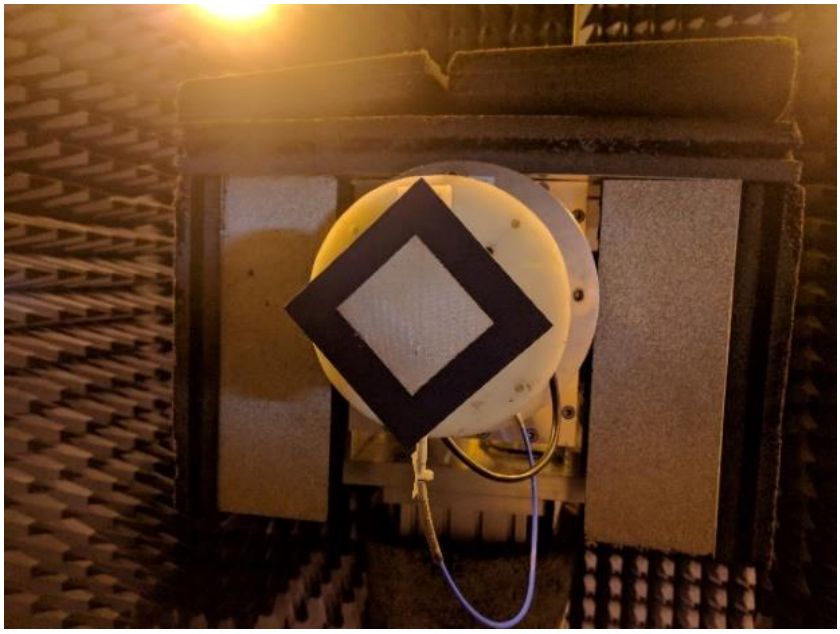

(a)

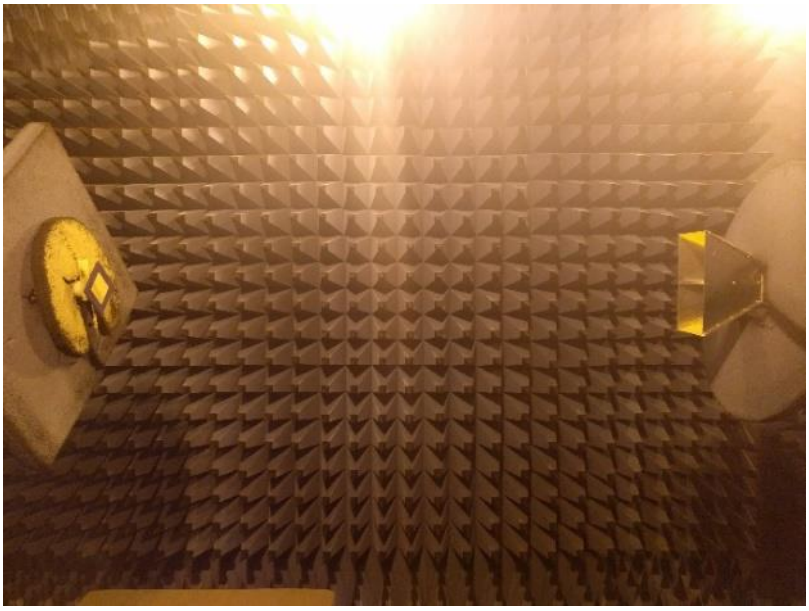

(b)

Figure 6-8 Testing the antenna in the anechoic chamber, (a) patch mounted, (b) test distance

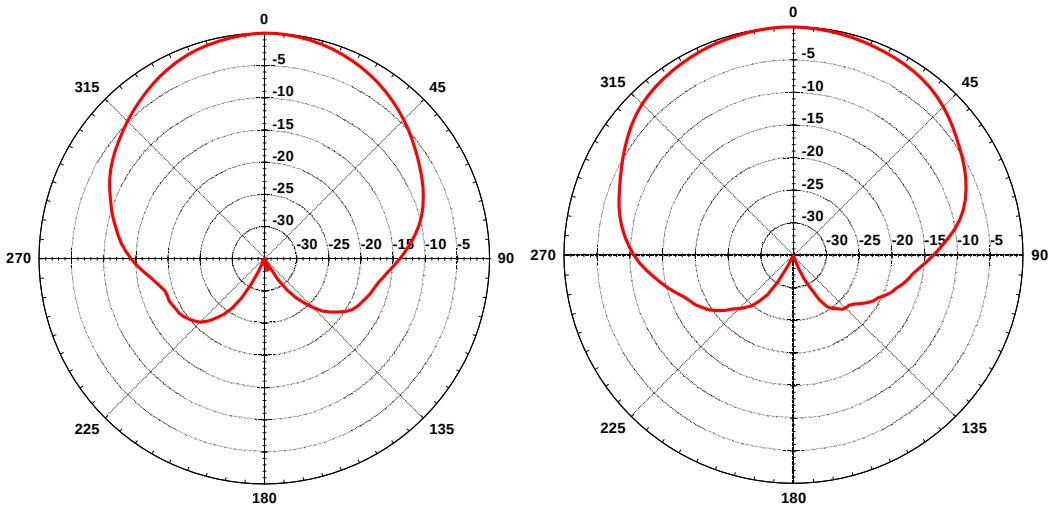

(a) (b)

Figure 6-9 Radiation patterns results at (a) xz plane and (b) yz plane

6.5 Conclusion

The use of a FDM 3D printer with a pneumatic dispenser has again proven suitable to fabricate this patch antenna. Only a layer of silver ink was necessary to produce a sufficient continuity and low resistance. This is a significant advantage when compared with other technologies and techniques that require a large number of layers of ink to be printed.

Although FDM does not produce as smooth surfaces as other previous techniques, it allows for the modification of the software and hardware of the open source version of the machines. The connection of the inexpensive pneumatic dispenser and syringe enables the deposition of layers of materials, and therefore the development of the new devices with enhances features. The newly developed ink from Voxel8 has been proven to be able to deposit metallic layers and therefore create fully electric circuits. The ink has a density that compensates the surface roughness of the substrate, adheres well to the surface, and produces continuous lines. Only one layer of silver ink was necessary to produce a sufficient continuity and low resistance.

A circularly polarized patch antenna was used for this demonstration. The machine is able print such type of antennas with sufficient resolution and accuracy. Only a small shift was observed in the resonant frequencies of the antennas. The measured results compared well with the simulation, with the target GPS L1 bandwidth of 1.55 GHz – 1.61 GHz, the results fit within this band. The shift could be due to fabrication errors and tolerances.

Chapter 7 - 3D printed bracelet antenna

7.1 Wearable antennas

In recent years, the demand for wearable devices has increased, with applications being expanded into several industries, they require the electronic equipment to be light, small and could transfer lots of data. Currently the society has been dependant on a large number of small communication devices like mobiles to different types of sensors, whether it is used for fitness tracking or medical sensors.

The wireless transmission of data takes place through an antenna which is known as wearable antennas.

Wearable antennas mainly have difficulty because of reasons;

- When the antenna is placed near the body, the human body tissue absorbs electromagnetic waves radiated therefore the efficiency of the antenna is drastically reduced.
- The surfaces on the human body are not uniform therefore any changes to the curvature of the antenna must be analysed thoroughly.
- The size and weight has to be small.

There have been several papers published on wearable antennas [1-5] with several applications, the communication between multiple wearable antennas has also been investigated. When discussing wearable connected devices, the antennas tend to be very close to the human body and therefore the specific absorption rate must be taken into consideration.

Various manufacturing techniques have been considered for wearable antennas including conducting paint, conductive metal coated nylon and screen printing.

Wearable antennas can also be fabricated using 3D printing, depositing a conductive layer on top of a printed substrate. The conducting lines are created using silver nanoparticles in a solution, as this is an additive process, it does not require or involve environmentally harmful etching chemicals.

Wearables require complex designs and contours to fit onto the body, 3D printing allows the manufacturer to design and produce an item with the exact dimension and size for the subject.

7.2 Antenna design and simulations

The antenna designed and simulated was a dipole antenna, the antenna was to radiate at two distinct frequencies for the WLAN band. At 2.4 and at 5.5 GHz, this was used to increase the bandwidth and allow for more data to be transferred.

The design of the bracelet antenna is a dipole antenna with two resonant arms on each end. The length of each arm is 24.2 and 9 mm, the long arms control the lower frequency and in order to have the antenna as compact as possible the long arm was folded, whereas the short arms control the higher frequencies. The design and the full dimensions are shown in figure 7-1 and table 6.

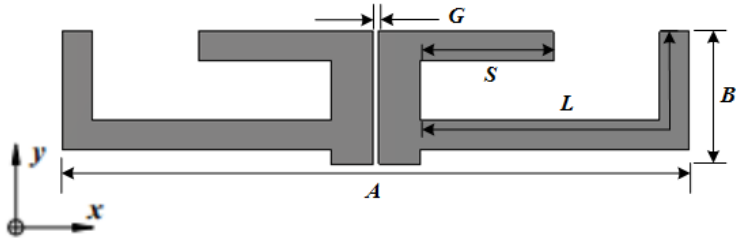

Figure 7-1 Design overview of the dipole bracelet antenna

Table 6 Dimensions of the bracelet antenna

	A	**B**	**G**	**L**	**S**
Dimension (mm)	42.4	9	0.4	24.2	9

In order to be able to get full radiation around the bracelet, two more antennas were replicated along the surface of the bracelet, the left and right antennas were phased 120° apart from the centre antenna.

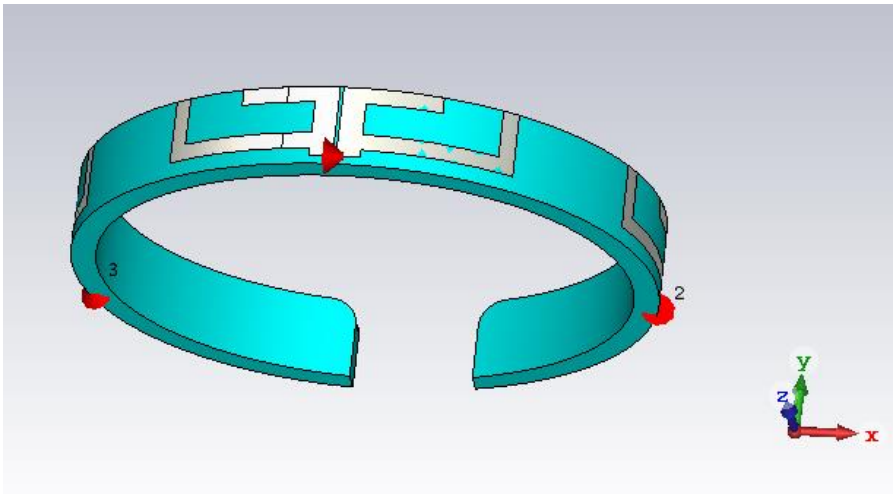

Figure 7-2 View of the bracelet and the top antenna

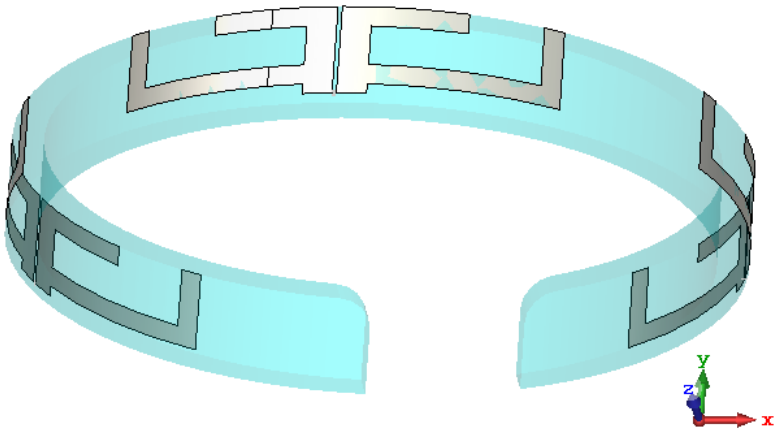

Figure 7-3 View of the bracelet and the three separate antennas

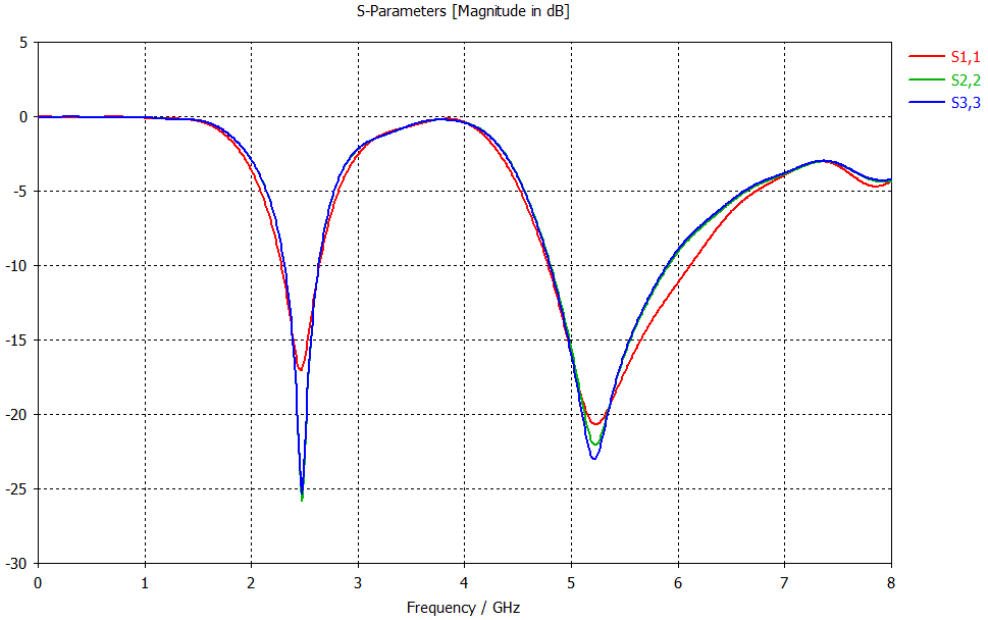

Figure 7-4 Simulated reflection coefficients for the bracelet three antennas (S_{11}, S_{22}, S_{33})

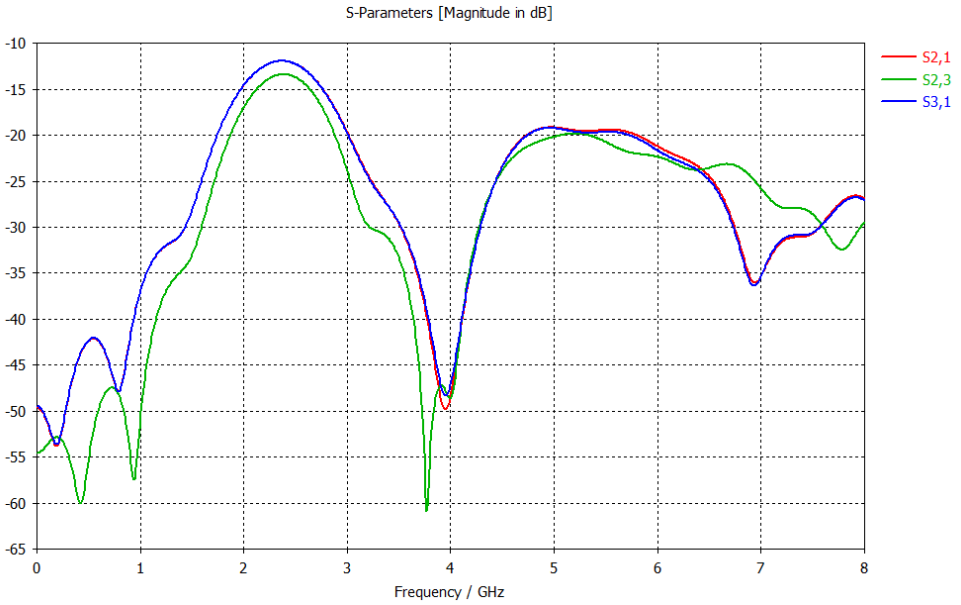

Figure 7-5 Simulated correlation coefficients of the bracelet antennas (S_{21}, S_{23}, S_{31})

The figures show the simulated results of the S-parameters, the reflection coefficients S_{11}, S_{22}, S_{33} in figure 7-4 is seen with a less than -10 dB in free space. For the lower frequency, ranging from 2.35 to 2.80 GHz giving a 0.45 GHz bandwidth to cover the 2.4 GHz, whereas for the higher frequency ranging from 4.85 to 6.10 GHz to cover the 5.5 GHz band. Figure 7-5 shows the correlation coefficients (S_{21}, S_{23}, S_{31}) indicating the isolation between the antennas being satisfactory as it is less than -10 and -20 dB in the relative frequency bands. As the high relative permittivity of the human body, an antenna presented on the human body shifts the resonance frequency and reduces antenna performance compared the results in free space and according to the distance between an antenna and human body [6].

7.3 Fabrication and assembly

The whole bracelet along with the antenna was printed using the FDM 3D printer. The nature of the curvature in the bracelet along with the curvature of the antenna requires the fabrication to be done in a specific way. The bracelet must be light and not bulky as to not disturb the user, the bracelet must also be able to withstand a great deal of strain without breaking. Several issues arose with the initial design and the fabrication process.

The first attempt is to print the whole design with the orientation of the bracelet upright as seen in figure 7-6. This orientation yielded issues in the fabrication process, especially with the strength of the model. In order for the bracelet to stay upright and have a high resolution, the model has to be printed with support material. While this is normal in a FDM print process, it tends to leave material residue and markings on the model adds drastically to the print time.

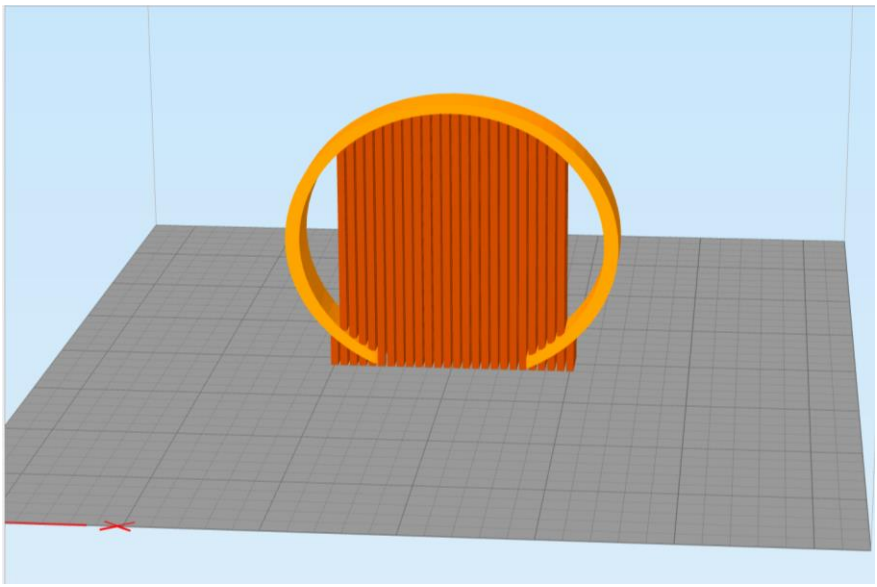

Figure 7-6 The orientation of the bracelet antenna in the slicing software

Another issue with this attempt is the strength of the bracelet itself, the area of the printed model between individual layers is very minimum. The nature of a bracelet is that it is taken off and put on several times this therefore requires the model to be reasonably strong. With this orientation the bracelet will be very weak as all the stress will focused on the adhesion between the printed layers.

The next attempt is to rotate the model 90° so that it can lay flat on the print bed. This alteration fixed both issues with the first attempt, as there was no need for any support material therefore the model had a smooth finish.

This also added to the model's strength, the area printed between the layers was much greater and the nature of the printing process allowed the bracelet to attain a bit of flexibility without breaking.

As this might seem as the best print process, a different issue arose from this attempt; the antenna part could not be printed with the orientation of the bracelet being flat. The antenna part sits 200 microns on top of the bracelet, and when the bracelet is lying flat, the antenna section is floating with nothing supporting it. Normally, this would be fixed using support material although the antenna is being printed using a silver ink with the second extruder and only adheres to the material that is below it. Therefore, if support material was used, the antenna would stick to the support material and not the bracelet itself which would deem it useless.

The strategy of the print process had to be re-thought, and the solution that came up was to print the bracelet in two parts. One for the frame of the bracelet and another to house the antennas. This process still meant that we had a fully 3D printed bracelet antenna but was printed over two print orders.

This printing solution allows all the previous issues to be tacked and allows for the printed materials to be changed. The idea was that for the frame of the bracelet, a rigid and durable plastic was to be used and then all the dipole antennas would be printed on a flexible plastic, which would then be wrapped around the previously printed frame of the bracelet. This would then add a new feature; conformable antennas. The designs were altered with this innovative approach in mind, the final print out is shown in figure 7-8.

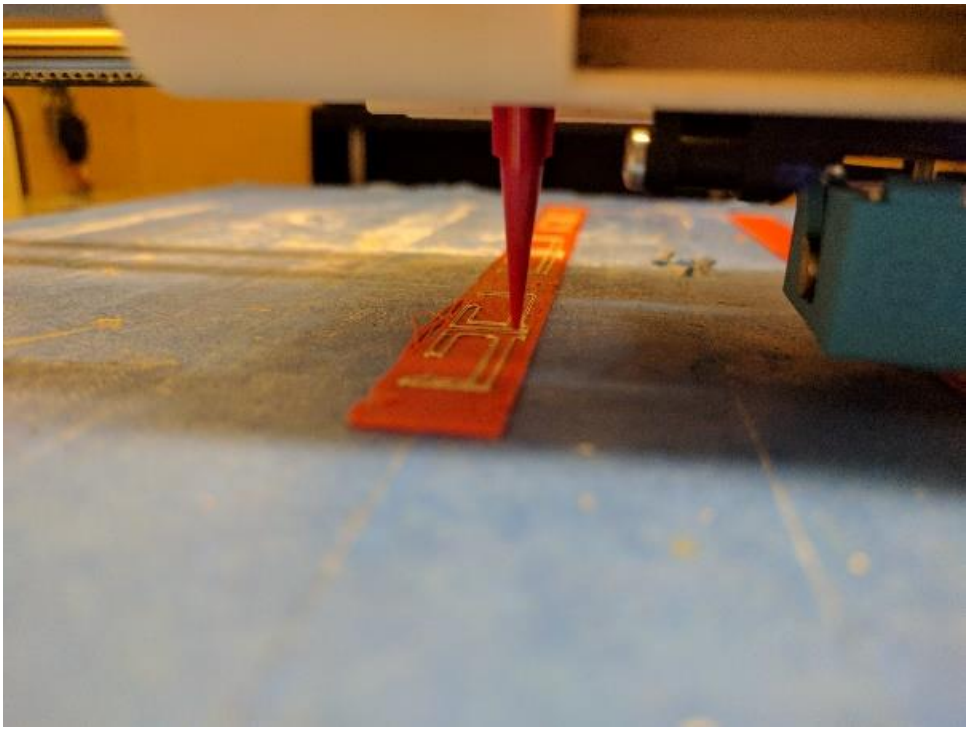

Figure 7-7 The printing of the silver ink on the bracelet antenna

After the two pieces were printed, a thin 100-micron double-sided tape was used to carefully align and stick the two pieces together. The flexible printed part with the antennas was mounted immediately onto the rigid frame of the bracelet before the ink had time to fully cure.

Figure 7-8 Printed bracelet antenna

The bracelet was then checked for any errors in the printing or assembly which included a continuity check on the antennas being as they were moulded onto the bracelet. In the first attempts, there were cracks and open circuits along the antenna.

The next step was to add the connectors, a set of SMA connectors were used. They were connected using some silver glue to connect the pin of the connector to the printed antenna and then using some strong epoxy glue the connector was mounted onto the body of the bracelet.

For comparison, the antenna on the bracelet was also fabricated using the Optomec machine onto a 3D printed substrate. The middle section of the bracelet was printed using a white PLA plastic from 3D FilaPrint with a layer thickness of 100 microns. The antenna design was printed on the surface of the printed PLA and then cured using the PulseForge, this process is discussed in more detail in chapter 8.3. The printed antenna was then electroplated to achieve full conductivity and tested.

Figure 7-9 Optomec printed antenna on an FDM printed bracelet

7.3.1 Surface roughness

The surface roughness was collected to investigate the differences between the surface profile of the printed plastic and the printed ink. The calculation of the surface roughness was done on a TalySurf CCI which provides ultra-high resolution interferometric measurements for non-contact surface roughness. The surface of the printed PLA and the silver ink were tested with the results shown below.

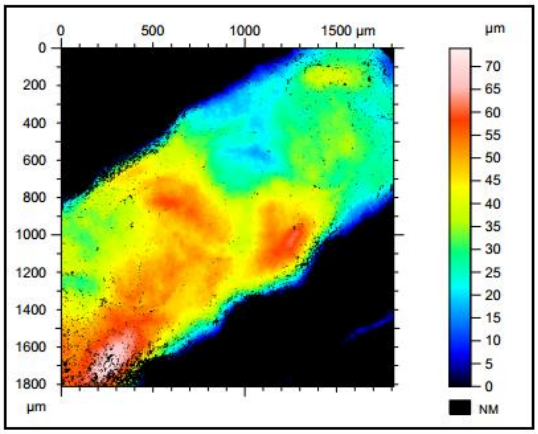

(a)

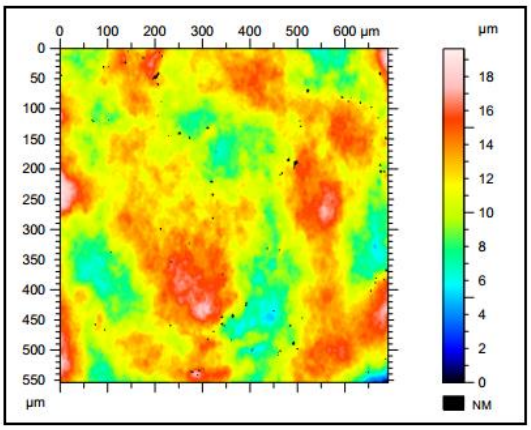

(b)

Parameters calculated on the surface 3ED-Flex antennae S100001 > Zoomed

Sz, Sds and Ssc parameters are defined according to EUR15178N report.

Amplitude Parameters

Sa = 7.585 µm
Sa: Arithmetic Mean Deviation of the Surface.
Sq = 9.366 µm
Sq: Root-Mean-Square (RMS) Deviation of the Surface.
Sp = 18.56 µm
Sp: Maximum height of summits.
Sv = 26.15 µm
Sv: Maximum depth of valleys.
St = 44.71 µm
St: total height of the surface.
Ssk = -0.7126
Ssk: Skewness of the Topography Height Distribution.
Sku = 2.653
Sku: Kurtosis of the Topography Height Distribution.
Sz = 34.9 µm
Sz: Ten Point Height of the Surface.

(c)

Parameters calculated on the surface 3ED-Flex antennae S100001 > ... > Form removed : Polynomial of order 4

Sz, Sds and Ssc parameters are defined according to EUR15178N report.

Amplitude Parameters

Sa = 1.917 µm
Sa: Arithmetic Mean Deviation of the Surface.
Sq = 2.361 µm
Sq: Root-Mean-Square (RMS) Deviation of the Surface.
Sp = 8.046 µm
Sp: Maximum height of summits.
Sv = 11.59 µm
Sv: Maximum depth of valleys.
St = 19.64 µm
St: total height of the surface.
Ssk = -0.1011
Ssk: Skewness of the Topography Height Distribution.
Sku = 2.719
Sku: Kurtosis of the Topography Height Distribution.
Sz = 11.54 µm
Sz: Ten Point Height of the Surface.

(d)

Figure 7-10 The surface roughness results of a 3D printed track and substrate, image (a, b) data (c, d)

The results from figure 7-10 show that the surface of the printed plastic PLA has a surface roughness of 7.585 microns which is understandable because this type printing is not known for its smooth finishes. The surface roughness of the silver ink displayed a roughness of 1.917 microns which is significantly smother than the PLA, this indicates that when the ink is deposited onto the plastic, it levels out, filling in most of the gaps along the surface. It also shows that the lines of ink that is deposited next to each other bond together, without creating any ridges or unleveled surfaces.

7.4 Testing

Throughout the testing stage, one of the issues arose being the tensile strength of the glue connecting the connector to the antenna. As they were connected to the VNA for testing, the stress on the connectors was all focused on the glue holding the connector to the antenna. Over time, the glue could not hold the connector to the bracelet and it broke off.

Figure 7-11 Printed bracelet with a broken off SMA connector

To correct the currents along the transmission line and give more support when testing the antennas, a balun is used to ‘balance’ an unbalanced system, this addition of the balun requires the model to be altered in order to support the extra weight. The rigid section of the bracelet was extended at the location where the feeding of the antenna meets, as to hold the balun connector. This is shown in the figure 7-12.

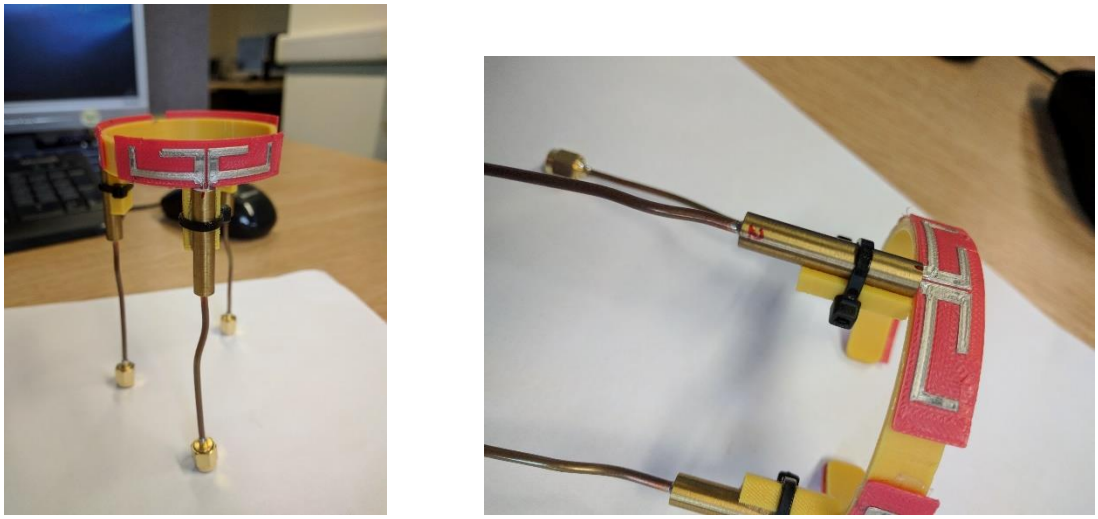

Figure 7-12 The addition of the Balun connector

Used to suppress unbalanced surface currents from the coaxial cable for the radiation measurement purpose. The bracelet was then tested using a VNA to measure the s parameters and using an anechoic chamber for radiation patterns.

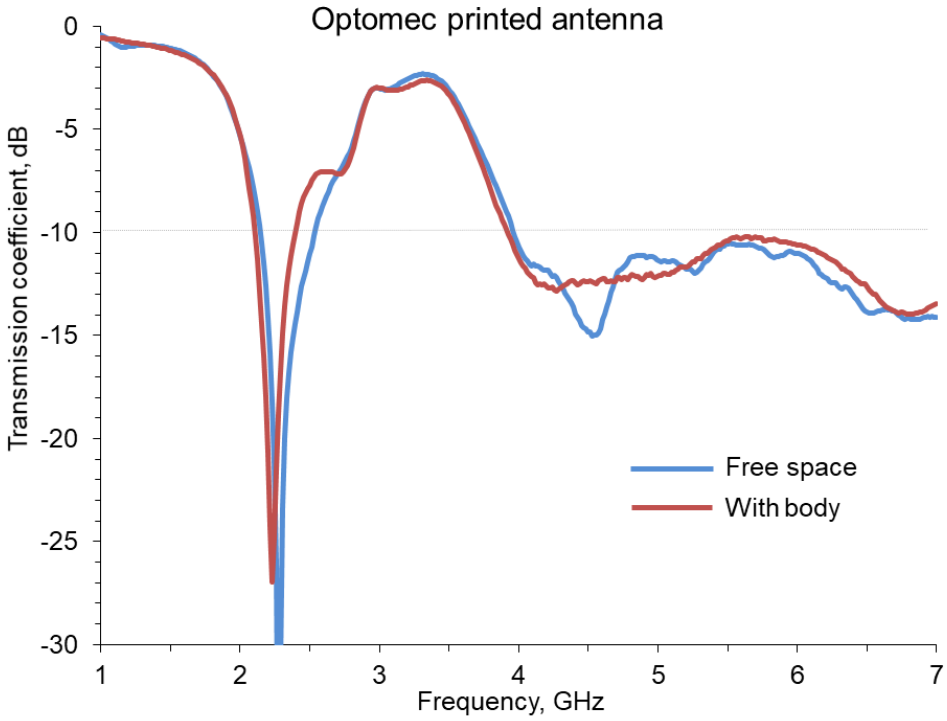

Figure 7-13 Reflection coefficient of the Optomec printed antenna, with and without the body

The reflection coefficient results from figure 7-13 show the differences between the antenna worn on the body and in free space. At the lower 2.4 GHz frequency, both

scenarios show similar performance as the simulations with the free space and on body resonating at about 2.39 GHz at -32 dB and 2.38 GHz at -27 dB respectively. On the other hand, at the higher 5.5 GHz frequency the results are slightly different than the simulations, still covering the 5.5 GHz band, although it seems to be shifted to the left slightly, for the free space resonating at 4.54 GHz with a null of -15 dB.

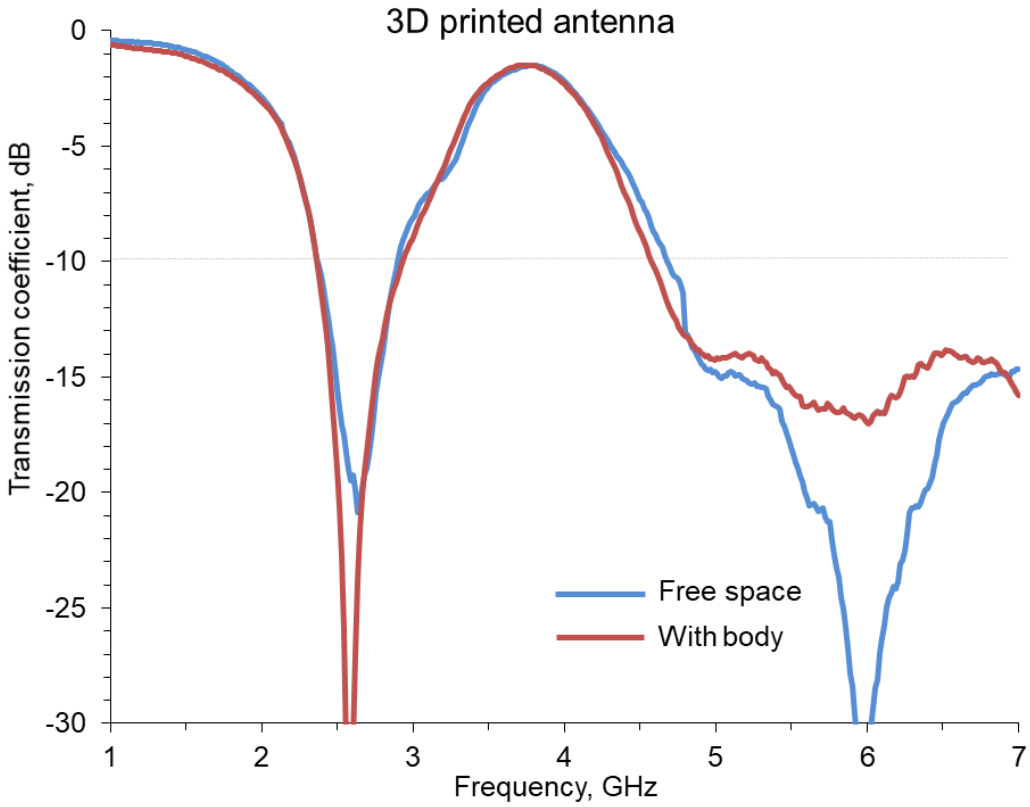

Figure 7-14 Reflection coefficient of the 3D printed antenna, with and without the body

As for the results for the low-cost 3D printed antenna, the results for the free space and on the body in the lower frequency show 2.53 GHz at -21 dB and 2.51 GHz at -37 dB respectively. As for the higher frequency, the results for the free space and on the body show resonating at 5.97 GHz at -40 dB and about 5.5 GHz at -17 dB respectively. There seems to be a shift to the right in both frequencies but they still cover the desired 2.4 and 5.5 GHz bands.

All results obtain the 2.4 and 5.5 GHz wireless LAN band. They have frequency range of from 2.25 to 3.05 GHz at the lower band and from 4.1 GHz to 7 GHz at the higher band.

The radiation patterns of the antennas were measured and normalised at both frequencies 2.4 and 5.5 GHz, this was measured in free space and when worn on the wrist.

(a)

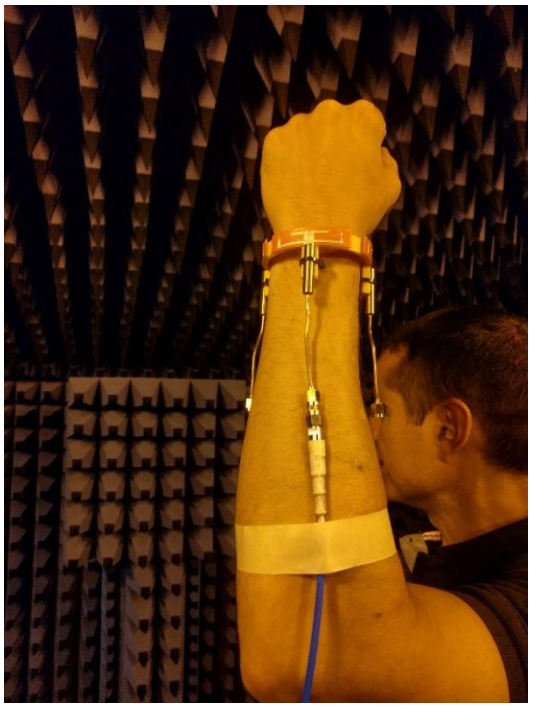

(b)

(c)

Figure 7-15 Measuring the antennas when on the wrist; (a) Measuring S parameters, (b, c) radiation pattern measuring in the anechoic chamber

The radiation patterns for all three of the antennas were measured on the body, the bracelet was worn and then the cables were taped as to not make it move. The tape used was regular masking tape as to not distort the results, the hand was lifted above the head and then measured.

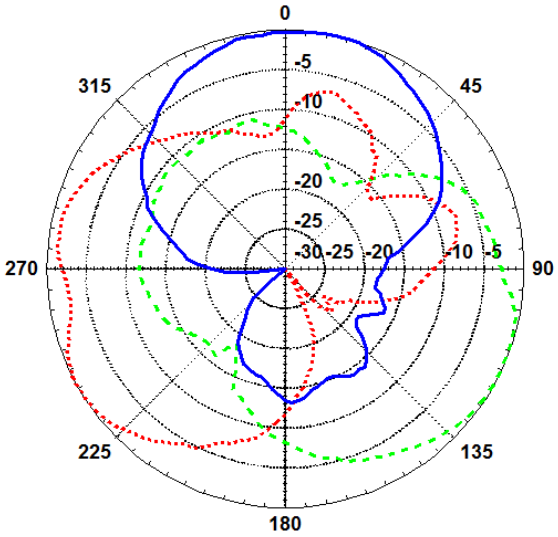

(a)

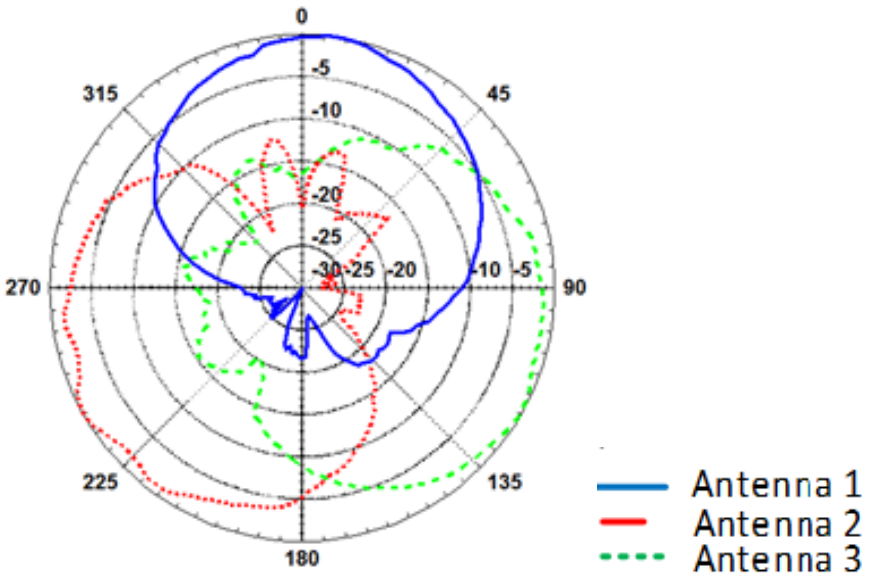

(b)

Figure 7-16 Radiation patterns for the three 3D printed antennas at (a) for 2.4 GHz and (b) for 5.5 GHz with the hand up

Figure 7-16 show the directional radiation patterns when worn on the wrist, the results show it is clear that the human wrist provides the backward attenuation of the radiation patterns. The measured gain with the human wrist at 2.4 and 5.5 GHz are higher than the free space.

7.5 Conclusion

In this chapter, a dipole antenna was designed and printed three times using a modified 3D printer on a substrate that was wrapped around a wrist as a bracelet. The transmission response was compared between on the body and in free space. The results for the 3D printed bracelet were also compared to a different type of fabrication process.

The 3D printed fabrication of this antenna has put the method to the test in several ways, including printing thin layer substrates, and depositing silver ink to form small features within the antennas and finally being able to conform the silver ink along a curved surface without breaking the cured ink. This was a good example to show the advantages of additive manufacturing in a customized conformal structure.

The antenna was designed and optimised with the coverage of 2.4 and 5.5 GHz WLAN band in free space and when worn on a human wrist. Due to the close proximity of the human body along with its movement, the performances of the impedance matching, the radiation patterns and polarization are partially distorted.

References

[1] Hall, P. S., and Hao, Y., “Antennas and Propagation for Body Centric Communications”, European Conference on Antennas and Propagation (EuCAP), November 2006

[2] P. Salonen, L. Sydanheimo, M. Keskilammi and M. Kivikoski, “A small planar inverted-F antenna for wearable applications”. the Wearable Computers, 1999

[3] P. Salonen and J. Rantanen, “A Dual Band and Wide-Band Antenna on Flexible Substrate for Smart Clothing”, 27th Annual Conference of the IEEE, Vol.1, 2001

[4] J.C.G. Matthew, B. Pirollo, A. Tyler and G. Pettitt, “Body wearable antennas for UHF/VHF”, *Antennas and Propagation Conference*, 2008

[5] M. Klemm, I. Locher and G. Troster, "A Novel Circularly Polarized Textile Antenna for Wearable Applications,” the Wireless Technology, 2004

[6] Z. Wang, L. Z. Lee, D. Psychoudakis and J. L. Volakis, "Embroidered Multiband Body-Worn Antenna for GSM/PCS/WLAN Communications," in *IEEE Transactions on Antennas and Propagation*, vol. 62, no. 6, pp. 3321-3329, June 2014

Chapter 8 - Nail Antenna

8.1 Theory

Some believe that in the future, electronics will be a part of our human body [1] and will become a networked integration of various sensors, actuation, computation, storage and communication. It all started with the concept called Internet of Things (IoT), where various devices are connected together through a vast network to a ‘centralised’ cloud that acquires and acts on the data.

One of the main branches of IoT is communication which plays a vital role by sending out and receiving information. Several types of antennas are used depending on the situation and the application.

Antennas on the human body in the form of tattoos have been researched [2], the antenna that was used is a RFID tag placed on the skin. The issue with placing an antenna on the skin is that it is susceptible to a great deal of strain and therefore can break easily. The best alternative is placing it on a solid and flat area on the body where it can be protected and the only part on the human body that is solid and flat is the nail. The nail has a limited space so therefore limits the type of antennas that can be used.

The antenna that is designed is a microstrip patch antenna to be placed onto the finger nail. The idea to this was that the antenna could be connected to a storage device on the body and the antenna allows close electronic devices to access it. Using

higher frequencies, allows for a higher bandwidth and faster transfer speeds to memory devices.

8.2 Antenna design

The design of the microstrip antenna is shown below with the dimensions mentioned below in figure 8-1.

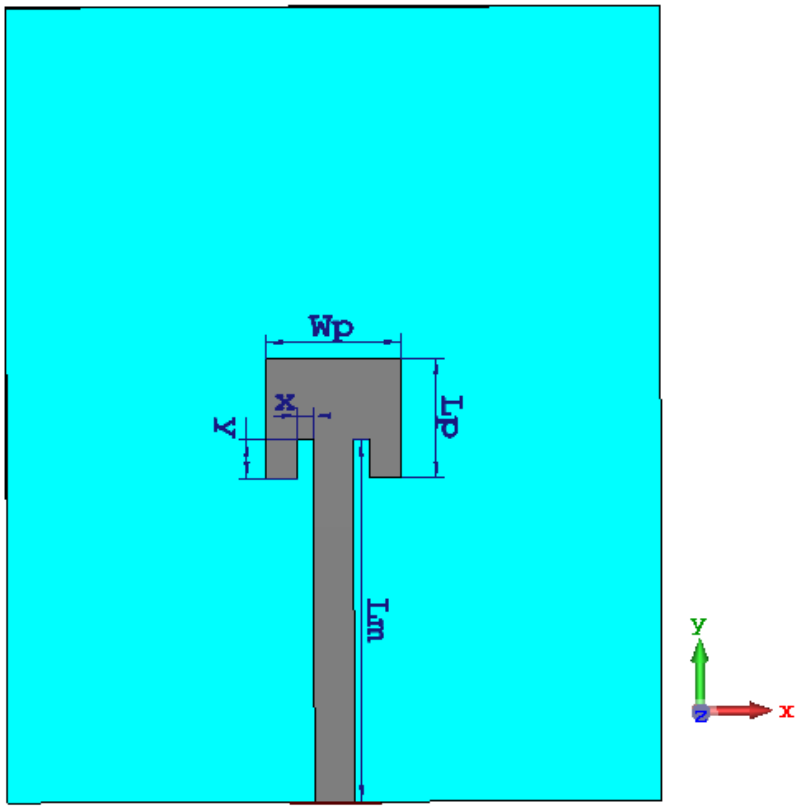

Figure 8-1 Nail patch antenna design

The antenna was matched at the frequency of 28 GHz and at these higher frequencies the feature sizes of the antenna are really small. The dimensions of the patch antenna is shown in table 7

Table 7 Dimensions of the patch antenna

Variable	Wp	Lp	Lm	Wm	x	y
Dimension (mm)	3.72	3.25	10.00	1.10	0.44	1.06

The results for the simulated S11 response and radiation patterns are shown in figure 8-2 and 8-4 respectively. The patch antenna has a resonant frequency of 27.93 GHz with a 4.5% bandwidth at the -10dB level.

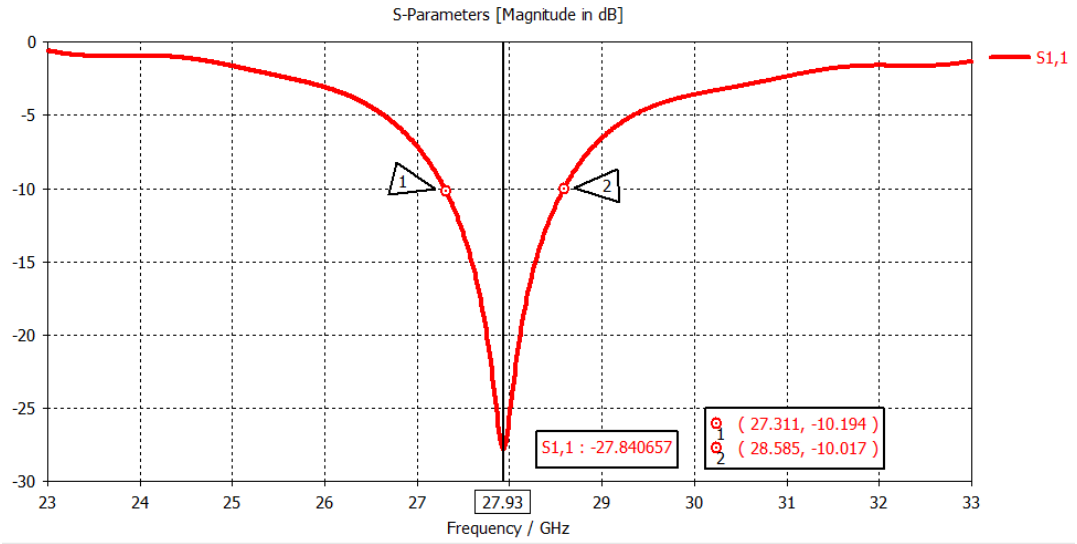

Figure 8-2 S11 of the nail antenna

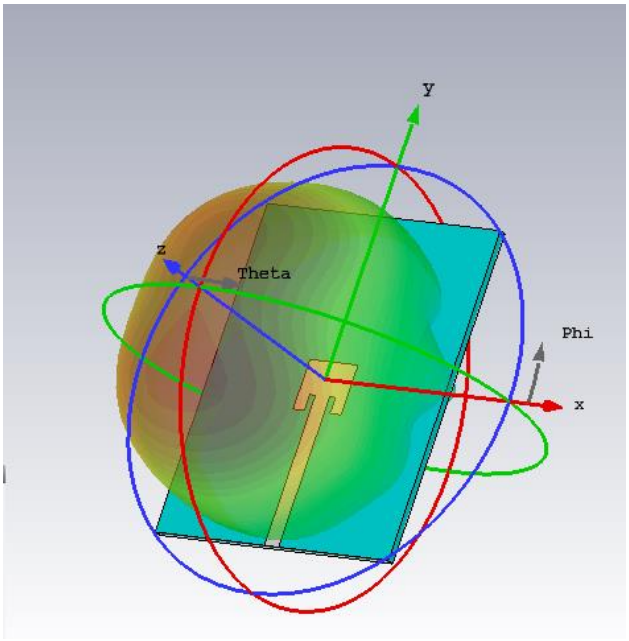

Figure 8-3 3D radiation pattern for the patch antenna

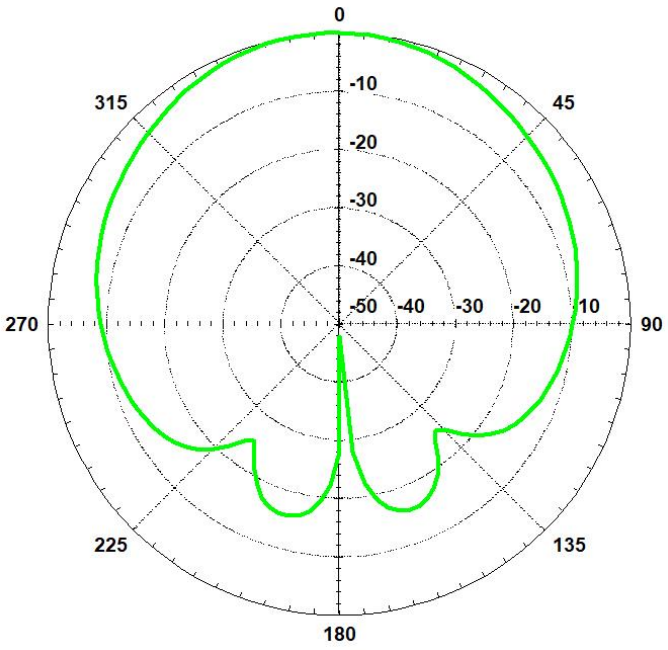

(a)

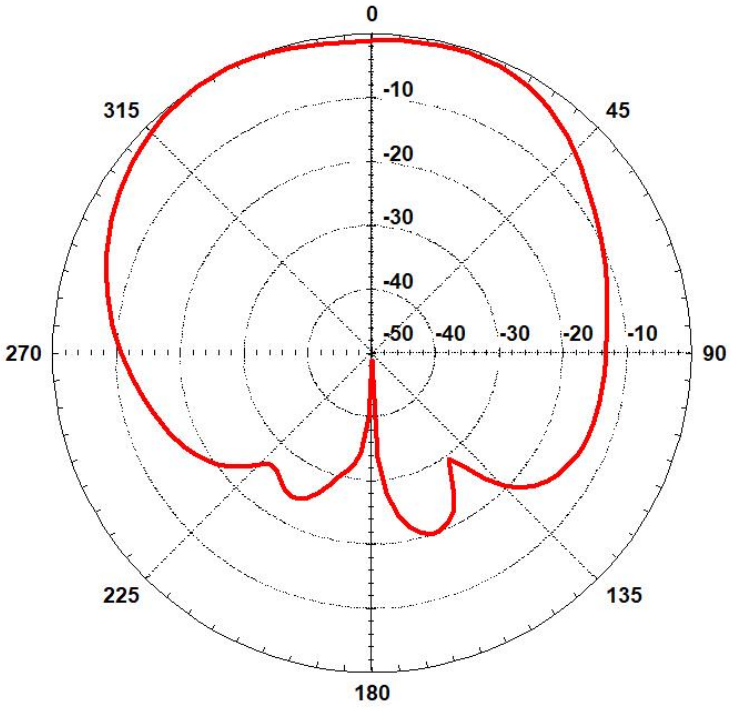

(b)

Figure 8-4 Simulated radiation patterns: (a) *xy* plane, (b) *yz* plane

8.3 Fabrication

Due to the sizes of the features on the antenna, the modified FDM 3D printer with the silver ink dispenser was not able to print to that degree of accuracy. The antenna was therefore fabricated using a variety of machines at CPI, using the Optomec to layer down the silver ink onto the substrate and then cured using the PulseForge machine.

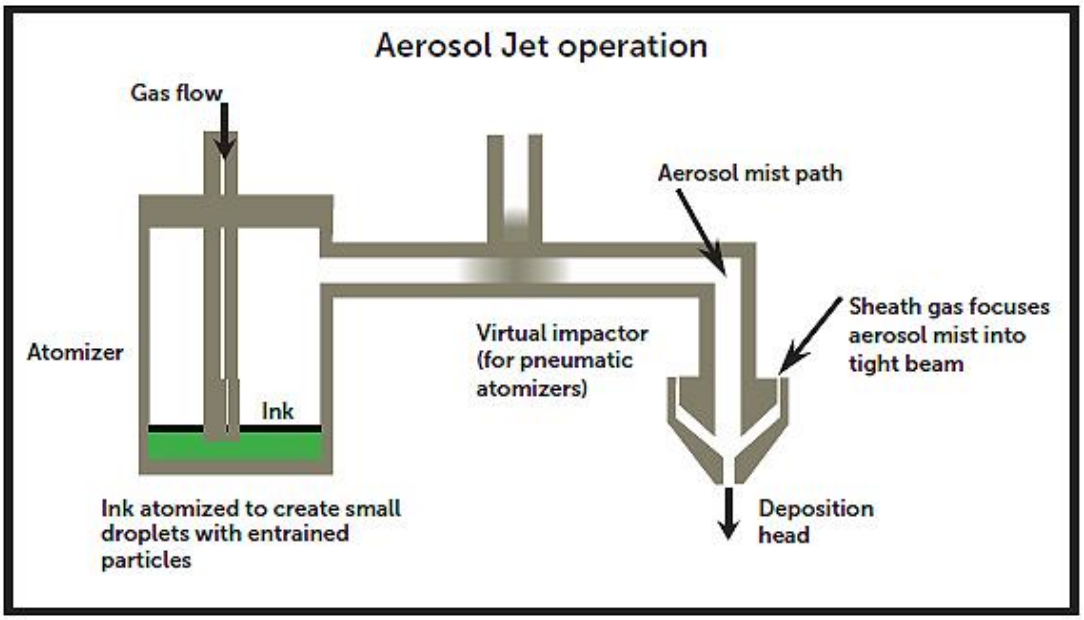

Figure 8-5 Illustration of the operation of an aerosol Jet machine

Due to the type of ink that is used in printed electronics, the pneumatic Atomizer is utilised. The Optomec machine is a reliable and constant manufacturing technique that controls the air pressure at various stages throughout the machine. The first stage is at the atomizer container, which holds the liquid material that will be printed with and then at the impactor, which is the tubing between the Atomizer and the deposition head and finally at the deposition head which is called the Sheath. All three air pressures should be at a specific value for them to work together, they can vary depending on the size of the nozzle on the deposition head and the type of ink that is used.

Within the Atomizer the ink is constantly being jetted onto the side of the container, which therefore creates a mist of ink particles and surrounds the top of the container. The controlled air pressure of the Atomizer then allows these particles to leave the container and through a thin tube, by creating a pressure difference between the two sections the particles travel through the tube and towards the deposition head. The Sheath gas air pressure is controlled to focus the travelling particles through a thinner diameter nozzle.

The formula for calculating the total air pressure within the system is;

$$Total = (\alpha - \beta) + \gamma$$

Where

α = Atomizer pressure

β = Impactor pressure

γ = Sheath pressure

The efficiency of the Optomec machine can vary from slight changes in these values, therefore there is a lot of trial and error. The printing process started with an AutoCAD (dxf) file which had the outline design of the antenna, using a proprietary modelling software, the infill co-ordinates were selected. The infill was designed to create a criss-crossed infill pattern. Once the layout is finalised, it is sent to the Optomec software where it will control the machine and start printing.

As the Optomec can only operate in an enclosed area and due to health and safety reasons, the printing could not be tested on a person's finger nails. Therefore, fake cosmetic nails were used, these had the same size and curvature as a humans' nails. The nails that were chosen is shown in figure 89

Figure 8-6 The fake nails that were used to test the antenna

The Optomec machine does not have the ability to change the Z-axis height whilst printing and has a curved tolerance of 4-5 mm, therefore the nozzle was adjusted to 2 mm above the peak of the nail. Initially there was speculation that the ink will not adhere to the surface of the nail due to the curvature and that the ink requires a longer time to dry. A variety of tests were conducted to change the surface tension of the nails; applying a layer of nail glue to the surface before starting a print and using a nail filer along the top surface of the nail.

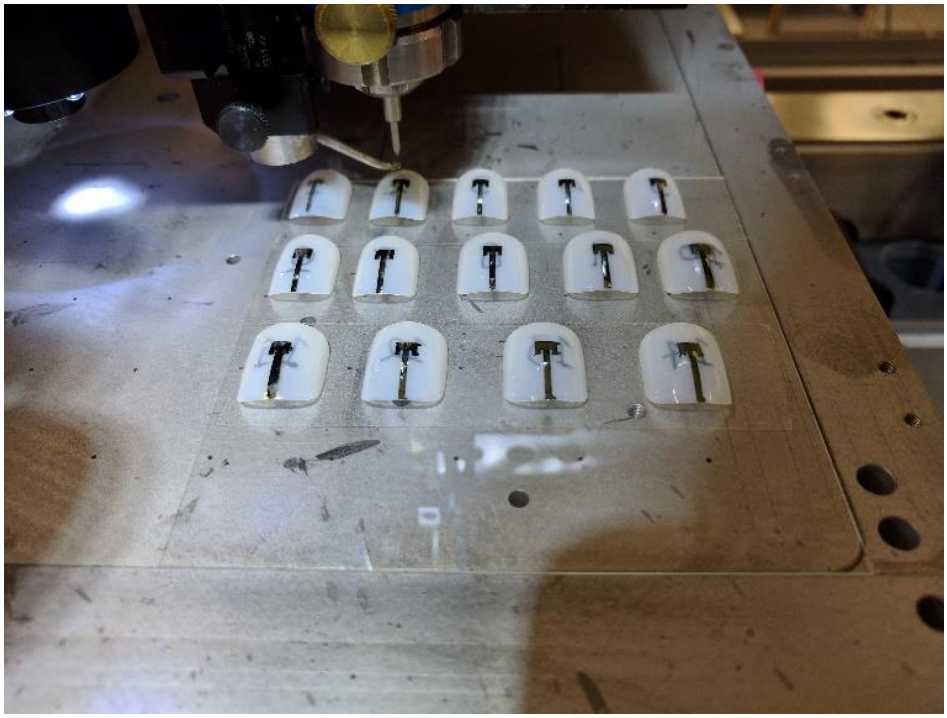

Figure 8-7 Printed antennas using the Optomec machine

After the antennas were printed on the nails using the Optomec, they were left to dry for 24 hours and then were taken to get cured using the PulseForge machine. The PulseForge is another machine that is susceptible to minor changes in the settings, it is controlled using two variables; the voltage and the length of the pulse. As this was a 3D shape and has not been done before, the variables were experimented to see the best values. With the optimum values coming to 310 V at 400 µs, even though these were the best values, not all the nails yielded reliable results. To test if the ink was cured on the nail, a multi metre was used to measure the resistance levels. The aim was to get as low as possible and therefore several pulses were delivered. The issue that arose was that when several pulses were delivered to the nails, there would be a point where the energy was too much and would evaporate the ink off the surface of the nail and therefore destroy it. The margin between fully cured and too much energy is very slim and can vary between nail to nail.

Results

The fabrication of the antenna did not work every time; therefore, several iterations were made with various changes to the surface of the nails, the printing settings and curing parameters in order to achieve acceptable results.

The surface of the nail is very smooth, measurements in the next section indicate that the surface roughness of a plain nail to be 3.77 microns. It was then decided to see if changing the surface of the nail could help the ink adhere to the surface and give a reasonable conductivity. The nail had a layer of nail glue applied to the surface before it was printed on to increase the surface tension. The glue was applied in two different techniques; to be brushed on using the supplied sponge and using a cotton bud, the glue was dotted onto the surface. Another technique to change the surface tension is to use the nail file along the surface of the nail and this was done in a controlled number of scrapes. After the antennas were printed, they were cured in the PulseForge and their resistivity measured. The results are shown in figure 8-8

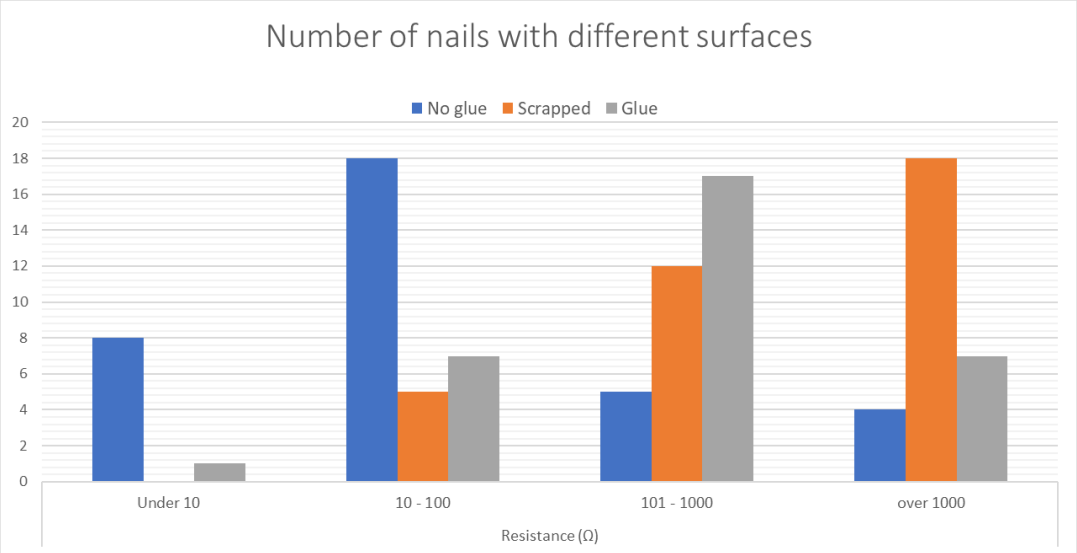

Figure 8-8 Nails with different surfaces

The graph indicated that there was still a major variation within each of the different surfaces of the nails, although it was noted that the filed or scrapped nails did not yield as many reliable results as the nails with and without glue. It was decided to continue focusing by printing on the nails without anything on the surface, the graph

in figure 8-9 shows the range of resistances on the nails without any glue on the surface. It is clear that there isn't a consistent value from the fabrication process.

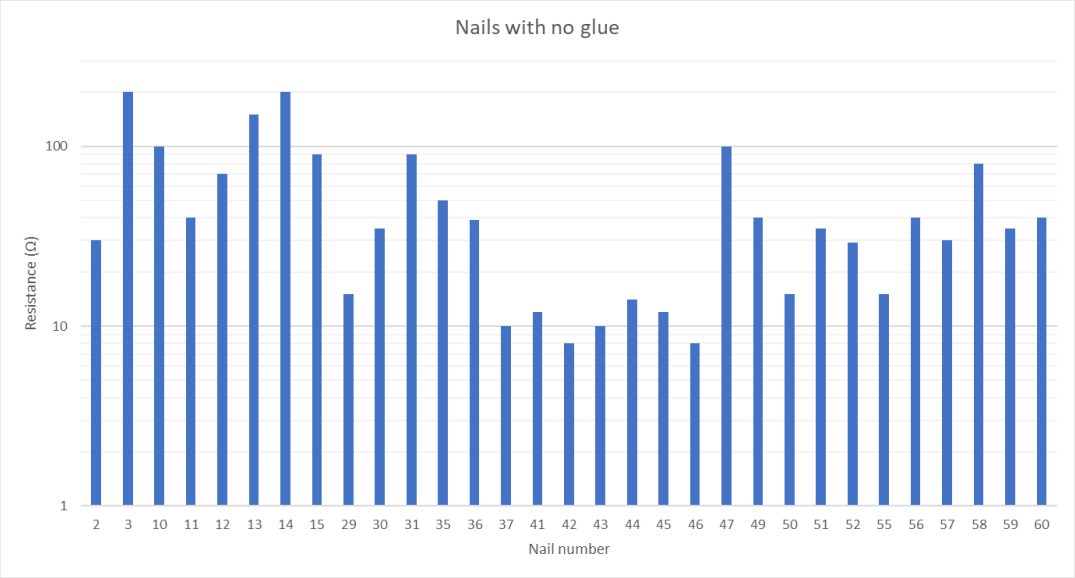

Figure 8-9 Resistance levels on nails without glue

The next change in the fabrication process was the printing settings of the Optomec, the number of layers of ink that was deposited was increased to see if the conductivity would improve. By increasing the number of layers on the surface, the size of the features within the antenna tend to get destroyed. This was fixed by reducing the amount of ink that was deposited onto the surface, in order to deduce the amount of ink, the total amount of air pressure within the system had to be altered.

The pattern of the layering was also a factor, due to the shape of the antenna and the curvature of the nail, the best pattern would be a criss-cross pattern with a single outline perimeter.

Surface roughness

The surface roughness of the nails and the printed ink was collected to see the differences between the stages. One of the nails was tested first without any added material and the surface roughness turned out to be 3.774 µm. The results can be seen in figure 8-10, where there is also a 3D representation of the surface of the nail. The data is focusing on a small section of the nail; measuring 250 x 150 µm, which is the same for all samples collected.

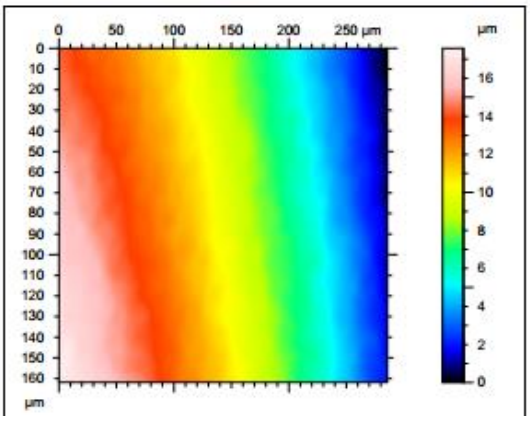

(a)

Parameters calculated on the surface ArtificialNail-00001 > ... > Zoomed

Sz, Sds and Ssc parameters are defined according to EUR15178N report.

Amplitude Parameters

Sa	= 3.774 µm	Sa: Arithmetic Mean Deviation of the Surface.
Sq	= 4.386 µm	Sq: Root-Mean-Square (RMS) Deviation of the Surface.
Sp	= 8.061 µm	Sp: Maximum height of summits.
Sv	= 9.511 µm	Sv: Maximum depth of valleys.
St	= 17.57 µm	St: total height of the surface.
Ssk	= -0.2346	Ssk: Skewness of the Topography Height Distribution.
Sku	= 1.923	Sku: Kurtosis of the Topography Height Distribution.
Sz	= 2.939 µm	Sz: Ten Point Height of the Surface.

(b)

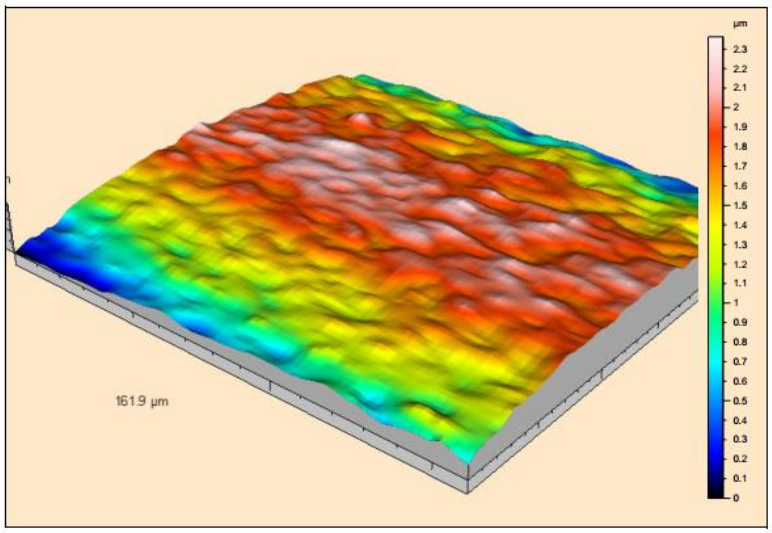

(c)

Figure 8-10 Surface roughness of a plan nail; (a) dimensions of the selected area, (b) data results, (c) 3D representation of the surface

The surface roughness of a printed antenna was also collected, in figure 8-11, the data indicates that the surface roughness of the printed material is 3.163 µm. This result is lower that the plain nail surface and that the material, when printed and cured flows over the rugged surface of the nail and leaves a flat surface of ink. The difference between the values is very miniscule, therefore some of the printed material could be the same as the plain nail.

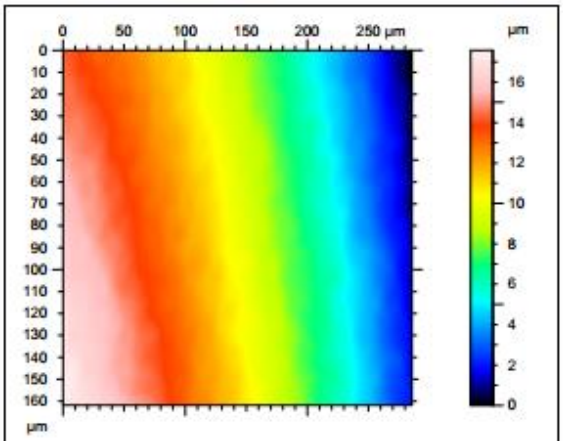

(a)

Parameters calculated on the surface
Printed_ArtificialNail-00001 > ... > Zoomed

```
Sz, Sds and Ssc parameters are defined according to
EUR15178N report.

Amplitude Parameters

   Sa     = 3.163 µm
            Sa: Arithmetic Mean Deviation of the Surface.
   Sq     = 3.655 µm
            Sq: Root-Mean-Square (RMS) Deviation of the
Surface.
   Sp     = 5.969 µm
            Sp: Maximum height of summits.
   Sv     = 7.776 µm
            Sv: Maximum depth of valleys.
   St     = 13.75 µm
            St: total height of the surface.
   Ssk    = -0.1416
            Ssk: Skewness of the Topography Height
Distribution.
   Sku    = 1.837
            Sku: Kurtosis of the Topography Height
Distribution.
   Sz     = *****
            Sz: Ten Point Height of the Surface.
```

(b)

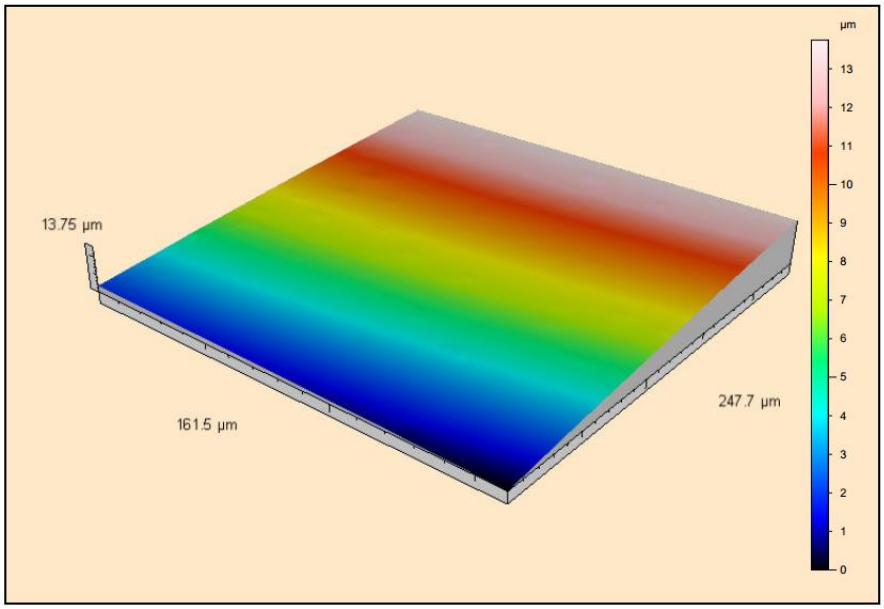

(c)

Figure 8-11 Surface data from a printed nail; (a) dimensions of the selected area, (b) data results, (c) 3D representation of the surface

Printing defects

During the printing and curing process some of the printed nails encountered imperfections in the edge definitions and continuity across the surface of the nails, to investigate the issue, a digital microscope was used to focus on the quality of the top side printing. Some of the samples were examined and pictures were recorded, as shown in figures below. Figure 8-12 shows that one of the samples had an edge definition issue where the ink of the patch antenna would bleed out from the corner. Although the main issue that was observed in a few of the samples were long consistent cracks along the surface of the ink this was observed mostly after the curing stage. In figure 8-14, the cracks along the surface of the ink can be seen, these cracks tend to mainly run vertically which could indicate that they are running along with the curvature of the nails. Due to these cracks, the antenna will not operate because of lack of continuity. The cause of these cracks was not immediately known because it could be linked to several reasons.

One of the reasons for the cracking on the surface of the ink could be from the time between when the nails are printed on the Optomec to when they are cured using the PulseForge. The nails are transported to the PulseForge machine on a glass substrate which means that the nails are exposed to changes in temperature and environment when they are removed from the controlled chamber of the Optomec machine. The results were improved slightly when it was decided to leave the printed nails in the Optomec chamber for about 24 hours before moving them to the PulseForge, this allowed the ink to dry uniformly without intervention.

Figure 8-12 Corner of the patch antenna

Another reason that the ink surface cracks is the power of the curing stage. The intensity of the PulseForge curing might be too strong on the nails, in which, what happens is that as the molecules of the ink is curing, they are trying to get closer and therefore creates ‘pockets’ along the surface of the ink. This could be plausible when looking at figures 8-12 and 8-13 as some of the ‘pockets’ or bubbles join up to their adjacent ones. Although not all turned out the same even though they were printed and cured with the same settings. Some of the nails were seen to have quite substantial cracks measuring a width of at least 30 µm, seen in figure 8-15.

Figure 8-13 Zoomed in photo of the pockets on the surface of the printed material

Figure 8-14 Overview of the level of cracks on the surface of the printed material

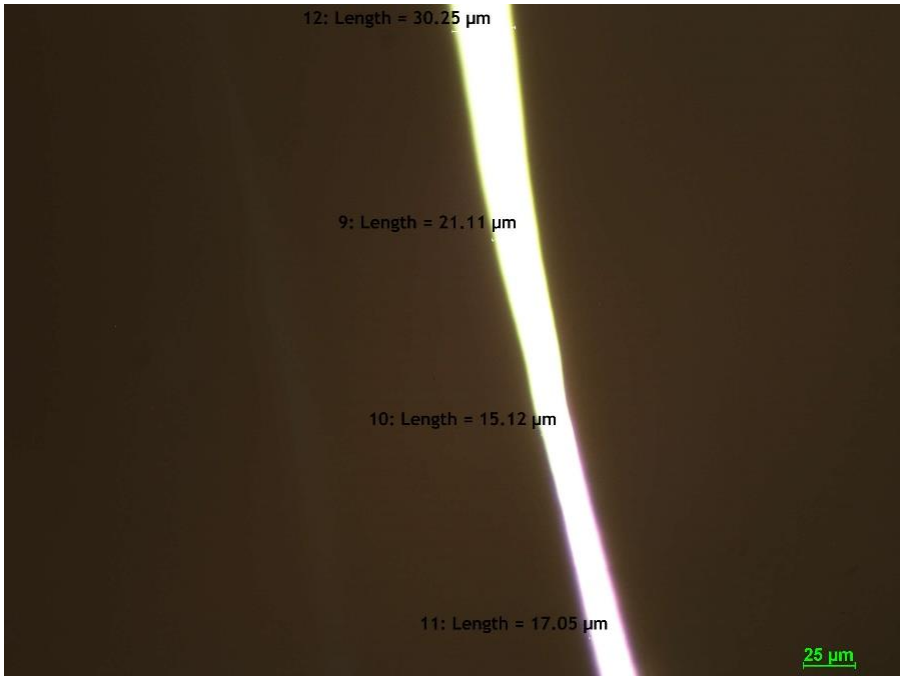

Figure 8-15 Zoomed in photo of one of the cracks seen on the surface of the printed material

The cracks seem to be clean-cut which indicate that the crack was caused from a sudden change, which also could imply that the PulseForge was the cause. The PulseForge machine cures well when the printing of the material is done uniformly without major variations on the height of the material, moreover having a flat surface. As the nails are curved, the ink is not being exposed equally and therefore the top of the antenna could be receiving more power than the sides.

8.4 Testing

After the antennas were printed on the nails and cured, a ground plane was added to the bottom layer of the nail to complete the antenna. For the higher frequency antenna, a high-end connector is required; the connector that was used is the 2.92 mm End launch female connectors from Southwest Microwaves which is designed for high frequencies.

(a)

(b)

Figure 8-16 Nail antenna (a) ground plane attachment, (b) nail surface cut

The connector created issues as to how to be connected to the nails, the connector is made for flat surfaces to be connected to and when the curved nails were inserted, they would fall out. The solution that was implemented was to cut off two pieces from the sides of the nail to allow for the nail to slide into place and the two side screws to close. This was not a perfect solution but there was a sufficient connection to the antenna for the testing. The antenna's transmission response and radiation patterns were measured.

(a)

(b)

Figure 8-17 Attached connector (a) front view, (b) top view

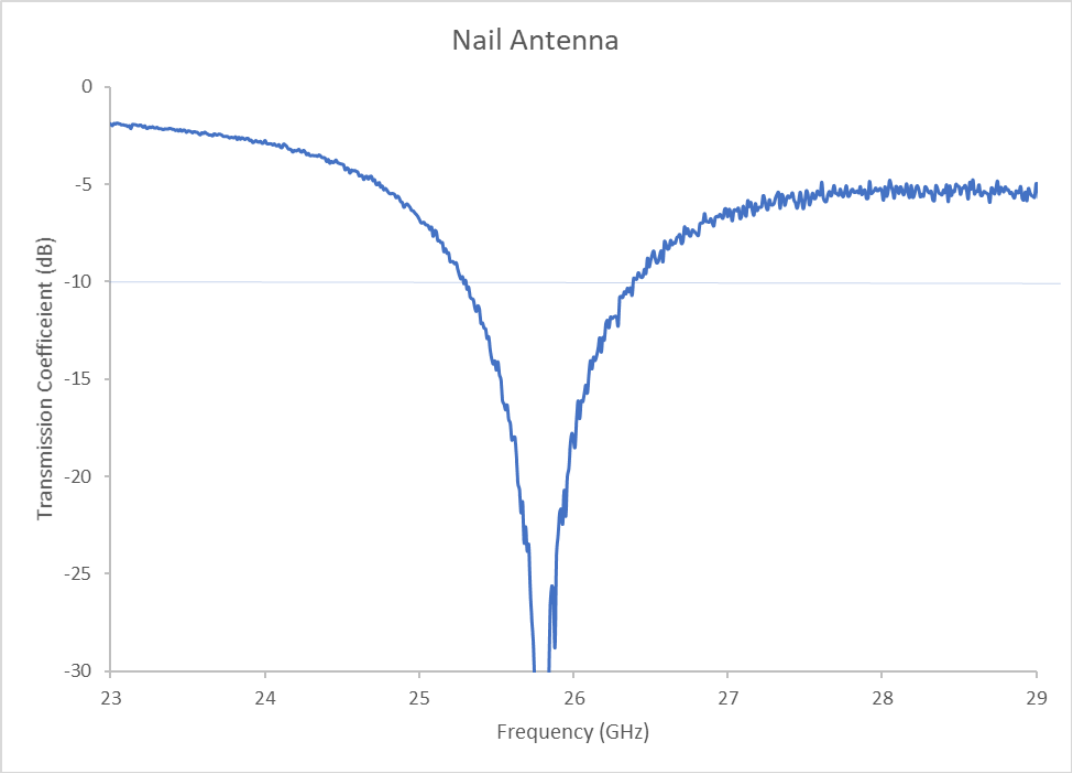

Figure 8-18 Transmission response of the nail antenna

The antenna was tested on a VNA and figure 8-18 shows the S_{11} transmission response, the graph showed that the antenna resonated at 25.9 GHz with a null of -50 dB. The patch antenna was designed to operate at 28 GHz and the result is a big drop shift in frequency. The -10 dB level bandwidth ranges from 25.4 to 26.3 GHz.

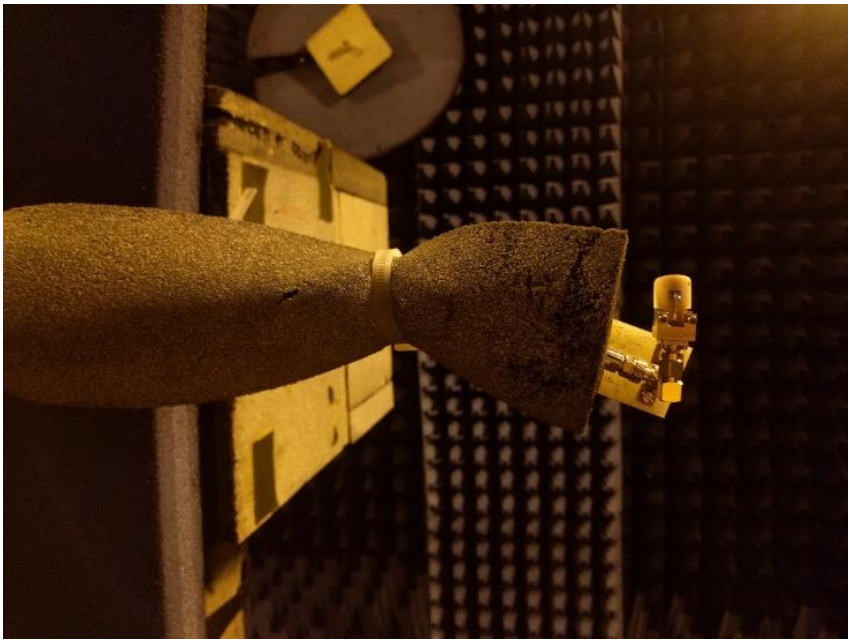

Figure 8-19 Antenna radiation testing rig

The nail antenna was also measured in an anechoic chamber for the radiation patterns. Figure 8-19 shows the test setup of the antenna; the antenna was measured in two orientations; the *yz* and *xy* planes. The results are compared to their simulations which are shown in figure 8-20.

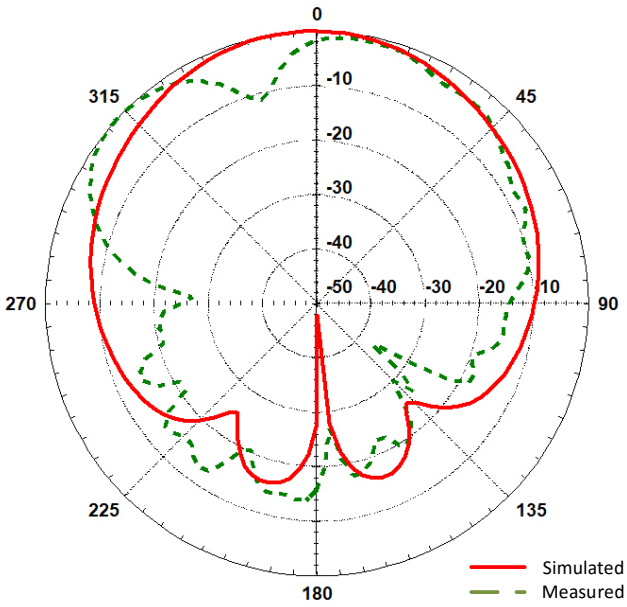

(a)

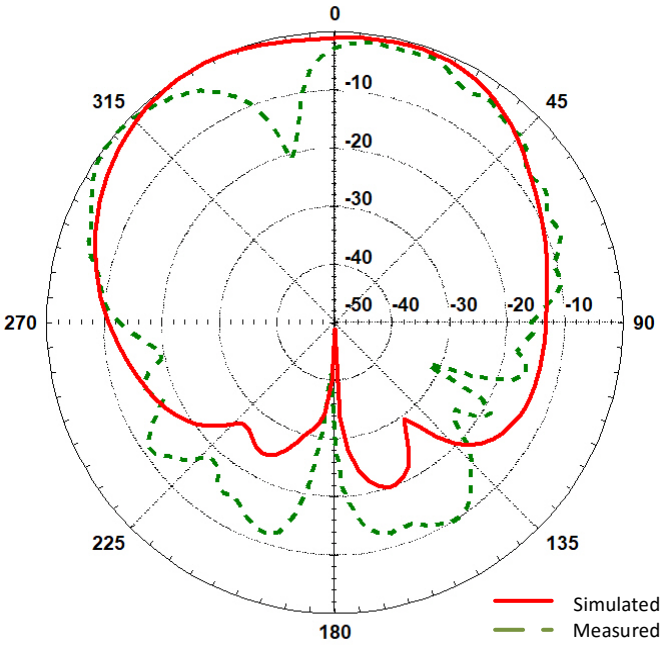

(b)

Figure 8-20 Measured and simulated radiation patterns (a) *xy* plane, (b) *yz* plane

Transmission line losses

To understand the losses within the material, a transmission line was fabricated and measured. The figure 18-21 shows the connectors connected to the printed transmission line, and the transmission response. The graph shows that the material had about a -3 dB loss.

(a)

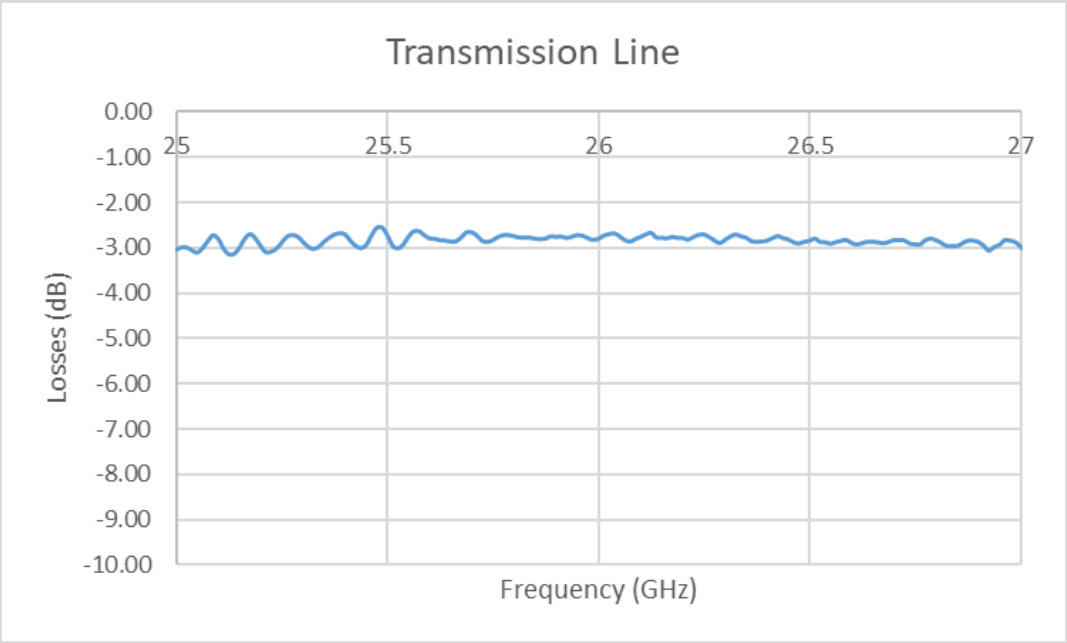

(b)

Figure 8-21 Transmission line (a) printed with the connectors, (b) transmission response

8.5 Conclusion

This chapter discussed the fabrication and measurement of a patch antenna printed on a nail that resonates at about 26 GHz. The antenna was printed using the Optomec machine and cured using the PulseForge, the fabrication results were definitely not constant, resulting in many issues. The optimum results showed that printing on a plain nail with two print passes and leaving it to dry for about 24 hours is the best for the Optomec, as for the PulseForge a setting of 310 V at 400 µs.

The nail antenna was grounded and a connector attached, the nail was tested for its transmission coefficient response and the radiation patterns. The nail was originally designed to resonate at 28 GHz but after testing found out that it resonated at 25.9 GHz, this could have been because of several fabrications and measuring issues and tolerances. The losses in the material were seen to be at the -3 dB level.

References

[1] J. M. Rabaey, "The Human Intranet--Where Swarms and Humans Meet," in *IEEE Pervasive Computing*, vol. 14, no. 1, pp. 78-83, Jan.-Mar. 2015

[2] J. Tribe, D, Oyeka, J. Batchelor et al, (2015) Tattoo Antenna Temporary Transfers Operating On-Skin (TATTOOS). In: Design, User Experience, and Usability: Users and Interactions. Lecture Notes in Computer Science, 9187(1)

Chapter 9 – Summary and Conclusion

Summary

In this thesis, the purpose was to show that a low-cost 3D printer is a viable way to fabricate antennas and RF structures. The description of the research and the steps taken during the work were presented along with the theoretical and literature information to back the assumptions and considerations made. It is hoped that the techniques demonstrated in the thesis will pave the way for the rapid, on-demand low-cost manufacture of high-functioning 3D printed RF devices in a single multi-material machine. A detailed account of the process of the printer was mentioned along with the investigation of a range of antennas and RF structures. The printer was a modified FDM printer with a pneumatic dispenser connected to it, the metallic material used in the project is a silver ink purchased from Voxel8. The simulations along with the experimentations in the designing required were highlighted. The variety of fabricated RF devices discussed in this thesis were two FSS element structures, a CP patch antenna, a dipole antenna and a nail patch antenna, which were all compared to their simulations and their performance discussed. This chapter provides a summary of the conclusions raised from the research.

The research started with a literature background in the variety of additive manufacturing techniques employed by companies and their benefits. The literature review also discusses a plethora of previously fabricated antennas and their performances.

In chapter 3, the various RF devices that will be investigated throughout the thesis are discussed along with the required theoretical calculations needed to design them. In addition, this chapter dives into the background information on antenna analysis and what is required for them to perform.

Chapter 4 discusses the details of the modified 3D printer that is used in this project and the calibration process required to achieve reliable results. The chapter started by introducing the printer and its characteristics from the materials used to the detailed firmware uploaded to its microcontroller. The components chosen were justified to suit this projects application, therefore the printer was modified which was done by designing and printing several sections within the printer. The pieces needed for the printer were printed using another 3D printer to fulfil the aim of keeping it low-cost. The second extruder is setup as an experimental extruder which therefore had to undergo several calibration processes. A couple of improvements were also discussed as a result of the calibration steps.

Chapter 5 discusses the first RF device fabricated using the 3D printer, which is an FSS structure. Two variant elements designs were noted, a loaded cross dipole design and a square looped design where the latter was fully fabricated and tested. The original design of the loaded cross dipole discovered a couple of issues in the fabrication process and therefore the design of the element was modified to a simpler square looped element. The issues in the first design highlighted some of the limitations in the printer and were addressed in the second element. The square looped element was designed to match at 2.7 GHz frequency band. The substrate printed with a height of 0.8 mm and then an array of 5 x 6 elements on top. The FSS structure was measured to show that it operated at 2.73 GHz and nulls deeper than

the required -10 dB level, with a depth of -30 dB. The FSS array also showed good performance stability in the angle of incidence, with a slight shift in both the TE 45 and TM 45. Overall, it was a successful fabrication of a FSS structure.

Chapter 6 discusses the fabrication of a CP patch antenna used for GPS applications. The single fed patch antenna was designed to resonate at the 1.575 GHz frequency band. The 100 x 100 mm substrate was printed with a height of 3 mm and then a single layer of silver ink measuring about 60 x 57 mm was deposited on top using the modified 3D printer. A grounded plane was adhered to the underside and with a SMA connected, the patch was tested. The antenna performed well with a slight shift in frequency to the left, resonating at 1.548 GHz although at the -10 dB level bandwidth covered the desired frequency. The patch antenna also had a second resonance shift at 2.25 GHz where the simulated frequency was at 2.29 GHz. The slight shift in frequency could be due to a combination of fabrication and measuring tolerances, as the simulation gives the optimum values. The axial ratio was also measured to show a slight variation from the simulation, at 3 dB level the measured frequency at 1.582 GHz which is slightly higher which could be linked to the fabrication and measurement tolerances.

Chapter 7 discusses the investigation and fabrication of a wearable bracelet antenna. The antenna chosen was a dipole antenna resonating at 2.4 and 5.5 GHz frequency bands for WLAN communications. The dipole antenna arms were folded as to reduce the antenna footprint, for full radiational directivity the antenna was duplicated around the bracelet to give a total of three antennas. The fabrication process of the bracelet was split into two separate models and then adhered together at the end, one part was printed using rigid material and the other using a flexible variant. The antenna was also fabricated using a more expensive technique; the Optomec jetting technology and the results were compared. The transmission coefficients of both techniques were measured and analysed, the results showed that it compared well with the simulation in both of the frequency bands. The Optomec results showed the free space and on body resonating at about 2.39 GHz at -32 dB and 2.38 GHz at -27 dB respectively for the lower frequency and higher frequency were slightly different at free space resonating at 4.54 GHz with a null of -15 dB. With the 3D printed

bracelet having slightly better results in the higher 5.5 GHz frequency, resonating at 5.97 GHz at -40 dB and about 5.5 GHz at -17 dB for free space and on the body respectively. As for the lower frequency, 2.53 GHz at -21 dB and 2.51 GHz at -37 dB in free space and on the body respectively. The radiational patterns were also measured for the 3D printed bracelet antenna, which showed that the human wrist provides the backward attenuation. The surface roughness of both the 3D printed PLA and the silver ink track were collected, which surprisingly showed that the deposition of the silver ink created a much smoother surface compared to the printed PLA surface. Overall, the antenna fabrication was a success, with a few issues in the fabrication but the final outcome showed favourable results and possibilities into conformal and embedded antennas.

Finally, in chapter 8, is the fabrication of an antenna on the human nail for the full wearable antenna realm. The chosen antenna was a patch antenna printed directly on the nail, due to health and safety reasons a fake French nail was used to replicate the scenario. This experiment was targeting the 5G frequency bands for the world of higher data rates and bandwidth, therefore the target frequency was set at 28 GHz. The antenna was fabricated using the Optomec and the PulseForge, which are a micro-jetting and curing machines for printed electronics. An investigation was conducted to see the best printing and curing conditions of the nails, the nails were then grounded and a connector added. The transmission coefficients and radiation patterns of the antenna measured and compared to the results. The transmission coefficient results showed that there was a shift in the frequency, where it was radiating at around 26 GHz. This major shift in the frequency was most likely due to a collection of factors adding together. Starting with the fabrication process, it did not yield constant results in terms of continuity and print definition. The connector for the nails created issues, as the nails were curved and the connector that was required is usually used for flat surfaces, the connection was not very secure and therefore when testing produced fluctuations. Although the author recons that the main factor that influenced the change in frequency is the value for the dielectric constant of the nail material, where it was assumed to be at 2.4. Where if it was

increased to 2.7 and with the same antenna dimensions, the simulator showed that it would resonate at 26 GHz.

Conclusions and future work

The key conclusions from this thesis are as follows:

- The use of a low-cost 3D printer such as an FDM machine can be easily modified to equip a second experimental extruder. The mechanical design allows for accessible alterations within the structure and the movement of key components such as the extruder motor and the extruder carriage. The fact that it has open-source firmware also allows for easy changes and frequent updates in the operation of the printer. The only drawback in using this technology with this project is the level of accuracy and resolution of the printed models, when striding towards antennas with higher frequencies, the features become significantly smaller and therefore the accuracy is required. Although there are some FDM machines that have demonstrated high quality results but come at a higher price tag.
- The integration of a pneumatic dispenser with the 3D printer has been proven successful, with the printers' microcontroller controlling the operation of the dispenser. The dispenser that was chosen suited this application because of its ease of connection to the microcontroller. The Techcon dispenser was also able to sufficiently dispense the silver ink from the tube with its wide pressure levels.
- The use of the silver ink from Voxel8 was definitely an advantage in this project. The electrical characteristics of the ink suited this application very well, resulting in only requiring a maximum of two layers of ink for acceptable conductivity. With large areas such as the patch antenna for the

GPS, only required one layer of ink to have the antenna operate at the desired frequency.

- The FSS operated well although had a slight shift in the frequency, this was mostly due to the tolerances of the silver ink on the printed substrate. Therefore, to future improve the structure, the upgrade to a more precise pneumatic dispenser could prove beneficial. Also, an investigation into different element shapes and possibly multi-layer elements might be interesting.
- The printed bracelet antenna has proven that the ink can be moulded into a specific shape, an investigation into different shapes may be compelling for complex antenna structures.
- Based on the measurements that were collected, 3D printing of the materials is a viable option for future electronic, RF and microwave devices.

Overall, a low-cost automated multi-layer multi-material printing within one machine is proven possible, the collection of antennas and structures printed using the machine showed similar performance to that of printed using traditional methods.

Appendices

Appendix A

```
int dir=2;

int stp=3;

int en=4;

int state;

unsigned long DIR_SIGNAL;

unsigned long STEP_SIGNAL;

unsigned long EN_SIGNAL;


//output is connected to a 1k2 then base of the NPN transistor

//while the controller is connected to the collector and the ground

void setup() {

  // put your setup code here, to run once:

Serial.begin(9600);

pinMode(dir,INPUT);

pinMode(stp,INPUT);

pinMode(en,INPUT);

pinMode(5,OUTPUT);

}

void loop() {

  // put your main code here, to run repeatedly:

DIR_SIGNAL= digitalRead(dir);

EN_SIGNAL= digitalRead(en);

STEP_SIGNAL=pulseIn(stp,HIGH);

if (STEP_SIGNAL > 1 && STEP_SIGNAL < 21){

  digitalWrite(5,HIGH);

  //delay(10);
```

```
//  digitalWrite(3,LOW);
}
else {
  digitalWrite(5, LOW);
}
state = digitalRead(5);
Serial.print(EN_SIGNAL);
Serial.print(" | ");
Serial.print(DIR_SIGNAL);
Serial.print(" | ");
Serial.print(STEP_SIGNAL);
Serial.print(" | ");
Serial.println(state);

//delay(500);
}
```